

Replacement Sensor Model Tagged Record Extensions Specification for NITF 2.1

APPENDIX C

draft

7/23/04

John Dolloff
Charles Taylor

BAE SYSTEMS
Mission Solutions
San Diego, CA

RSM White Paper

Note that the white paper “Replacement Sensor Models” contained in this appendix utilizes somewhat different notation than the rest of this specification, as summarized below:

Quantity	Specification Representation	Appendix C Representation
Ground position	$X = [x \ y \ z]^T$	$\mathbf{x} = [X \ Y \ Z]^T$
Image position	$I = [r \ c]^T$	$\mathbf{i} = [u \ v]^T$
RSM image support data	Not directly referenced	R
RSM adjustable parameters	R	δ_R
RSM adjustable image-to-ground function	$h(X, R)$	$G(\mathbf{x}, R, \delta_R)$
RSM ground-to-image function	$g(X)$	Not directly referenced
Ground space correction function	$X_adj(X, R)$	$x_adj(\mathbf{x}, R, \delta_R)$
Image space correction function	$I_adj(X, R)$	$i_adj(\mathbf{x}, R, \delta_R)$
RSM error covariance	CR	\mathbf{C}_R

Replacement Sensor Models

Invited Submittal to the 2004 Manual of Photogrammetry*

John Dolloff
BAE SYSTEMS, Mission Solutions
March 5, 2004

*Current draft of an invited section for the 2004 Manual of Photogrammetry; an update to the most recent (2/10/04) submittal. An abstract and detailed table of contents are also included.

Abstract

Replacement sensor models are used to replace sensor-specific original (“rigorous” or “physical”) sensor models. They have become increasingly more important and more available in today’s remote sensing and image exploitation communities. This report provides a general description of replacement sensor models: their general use, benefits, and limitations. It also describes a recent replacement sensor model, RSM, which is more flexible than its predecessors and eliminates their major limitations. In particular, RSM’s use, generation, and performance are thoroughly detailed. In addition, geopositioning based on optimal estimation techniques and multiple images is discussed. Solution algorithms are provided, applicable to both the RSM and the original sensor models it replaces. Other replacement sensor models can not support these optimal estimation techniques, required not only for optimal position estimates, but for reliable accuracy estimates as well. Similarly, RSM also supports the optimal adjustment of image support data (triangulation), where other replacement sensor models can not.

Table of Contents

<u>Section</u>	<u>page</u>
1.0 Introduction to replacement sensor models	5
1.1 replacement sensor model examples	5
1.2 RSM	6
1.3 Limitations of replacement sensor models	7
1.3.1 Substitute sensor model limitations	7
1.3.2 Replacement sensor model limitations	9
1.3.3 RSM limitations	11
2.0 Sensor model functionality	11
2.1 Original sensor model major components	12
2.2 RSM major components	13
2.3 Incomplete sensor models	14
3.0 RSM detailed form	15
3.1 Adjustable ground-to-image function	16
3.1.1 Ground-to-image function polynomial	17
3.1.2 Ground-to-image function grid	19
3.1.3 Adjustments	24
3.2 Error covariance	26
3.2.1 Direct error covariance	26
3.2.2 Indirect error covariance	28
3.2.2.1 Detailed description	28
3.2.2.2 Optional classification of errors	30
3.2.3 Practical considerations	33
3.3 Time and illumination models	34
3.4 Support data format	34
4.0 Geopositioning with RSM	35
4.1 Optimal algorithms	36
4.1.1 Geopositioning	36
4.1.2 Multi-ground point geopositioning and triangulation	42
4.1.3 Optimal versus non-optimal solution comparisons	43
4.2 Adjustable image-to-ground function	51
5.0 RSM generation	52
5.1 Ground-to-image function	52
5.1.1 Ground-to-image function polynomial	52
5.1.1.1 Linear solution for numerator-only coefficients	53
5.1.1.2 Quasi-linear solution for coefficients (Method 1)	55
5.1.1.3 Quasi-linear solution for coefficients (Method 2)	58
5.1.1.4 Recommendations	60
5.1.2 Ground-to-image function grid	60
5.2 Adjustable parameters and error covariance	60
5.2.1 Error covariance generation	60
5.2.2 Adjustment vector selection	64

5.3 Time and illumination models	65
6.0 RSM development status and performance summary	66
6.1 Development status	66
6.2 Performance summary	66
6.2.1 RSM representation error	67
6.2.2 NIMA-sponsored RSM commercial imagery study	68
6.2.2.1 SPOT results	68
6.2.2.2 Sensitivity to adjustment magnitude	71
6.2.2.3 SPOT-IKONOS results	72
7.0 Bibliography	74

Tables

Table 1. Possible approaches to support data error covariance representation by increasing fidelity	33
Table 2. RSM support data groups summary	35
Table 3. Sensor support data error characteristics for Pass 1 images	45
Table 4. Solution performance	48
Table 5. SPOT RSM - original solution maximum normalized differences (%)	70
Table 6. SPOT-IKONOS RSM - original sensor model average differences (meters)	73
Table 7. SPOT-IKONOS original sensor model average error propagation results (meters)	73

Figures

Figure 1. Fit grid for true replacement ground-to-image function	8
Figure 2. Fit points for the ground-to-image function of a substitute sensor model	9
Figure 3. Horizontal discrepancy between the original and substitute sensor models	9
Figure 4. RSM adjustable ground-to-image function	16
Figure 5. Interpolation along the <i>Z</i> -direction	20
Figure 6. Interpolation within a <i>Z</i> -plane	21
Figure 7. Piece-wise linear correlation function example	30
Figure 8. Optimal stereo solution	37
Figure 9. Optimal multi-image solution	37
Figure 10. Optimal Geopositioning Solution Algorithm	38
Figure 11. Imaging geometry	44
Figure 12. Image footprints	45
Figure 13. The effects of RSM representation error on vertical solution accuracy	68

1.0 Introduction to replacement sensor models

A replacement sensor model is a general sensor model that replaces the original, or rigorous, sensor model associated with a specific sensor. It typically represents the rigorous sensor model's ground-to-image relationship as a rational polynomial, mapping a three-dimensional ground point \mathbf{x} to a two-dimensional image point \mathbf{i} .

There are numerous advantages associated with a replacement sensor model. In particular, evaluation of its ground-to-image relationship is typically faster than for its rigorous sensor model counterpart, making it more suitable for real-time photogrammetric operations. Also, a replacement sensor model hides various details associated with a specific sensor that are available in the sensor's rigorous (physical) sensor model. This supports proprietary sensor development. The sensor image provider populates the image support data relative to the replacement sensor model, and the user community requires only the replacement sensor model, along with the imagery and its support data. Also, a replacement sensor model can be applicable to more than one sensor. This commonality reduces sensor model development and maintenance costs to the user. In particular, if a sensor's rigorous sensor model is upgraded, this change is transparent to the user.

1.1 replacement sensor model examples

The concept of a replacement sensor model is not new, and in fact, replacement sensor models are currently utilized operationally by various commercial space-borne image providers. For example, Space Imaging utilizes the Rational Polynomial Coefficient (RPC) model for the Ikonos sensor. RPC is a particular example of a rational function model (RFM), and models the ground-to-image relationship as a third order, rational, ground-to-image polynomial. Another replacement sensor model is the Universal Sensor Model (USM), developed at BAE Systems. It provides a ground-to-image relationship as a variable order, rational, ground-to-image polynomial, although it is usually generated as a numerator-only polynomial. It also allows for optional correction tables and representation of the ground-to-image relationship across an image with multiple polynomials.

Descriptions of various replacement sensor models, including discussions of their history, performance, and limitations, are provided in (OGC, 1999), (Dowman and Dolloff, 2000), and (Tau and Hu, December 2001). However, these replacement sensor models typically supply only a ground-to-image relationship. Adjustability is typically not supplied, and a rigorous error propagation capability is never supplied. Without rigorous error propagation, neither optimal geopositioning solutions, including reliable accuracy estimates, nor optimal image support data adjustments (triangulation) are possible (Dowman and Dolloff, 2000). In addition, many of these replacement sensor models only work for a general class of sensors, such as commercial space-borne imagery. They are not flexible enough to work for a larger class of sensors, and thus can not form a basis for a universal support data format standard.

A more recent replacement sensor model, RSM, has been developed that addresses these various limitations*. Due to its adjustability, rigorous error propagation capabilities, and flexibility, RSM is a significant extension of previous replacement sensor models. However, it does build upon their original concept, including the use of a replacement for the original (or rigorous) sensor model's ground-to-image relationship.

As part of this introduction, an overview of RSM is provided next, followed by a discussion on the limitations of all replacement sensors models. (A further introductory discussion on replacement sensor models can also be found in section Y.Y of this manual.) Following the introduction, RSM is then described in detail, including its use and generation. Because RSM contains the functionality of virtually all other current replacement sensor models as a subset, its description provides a general functional description of others as well.

1.2 RSM

The Replacement Sensor Model (RSM) is a general sensor model that is designed to replace the full functionality of virtually any imaging sensor model. It includes an adjustable ground-to-image function and an error covariance that provides for rigorous error propagation.

RSM image support data for a specific sensor and specific image is generated by any suitably configured "up-stream" process. Inputs to this process are the original sensor model's image support data, and outputs are the RSM image support data. Internally, the process contains and utilizes both the original sensor model and the RSM.

Subsequently, the only resident sensor model required by "down-stream" users is the RSM. Furthermore, in order to exploit any image from any sensor, only the corresponding image and RSM image support data are required as inputs. This capability affords significant user development and maintenance cost savings, as well as provides for a potential standard for all image support data. It also hides details of the original sensor model and its image support data, potentially important to sensor model developers and others.

*The author of this section and designer of RSM, John Dolloff, would like to thank Professor E.M. Mikhail of Purdue University for all the support and expertise he graciously provided during the development and testing of RSM. He would also like to thank Dr. Charles Taylor, of BAE Systems, for his significant contributions in the development and testing of RSM, and Mr. Gregg Kunkel, of BAE Systems, for his work on polynomial ground-to-image functions. Professor Mikhail, Dr. Taylor, Mr. Kunkel, as well as Ms. Michelle Iiyama, of BAE Systems, and Professor J.C. McGlone, of Carnegie Mellon University, also provided insightful critiques of various drafts of this section. Finally, the author would like to thank Mr. Thomas Ager and Mr. Philip Vargas, both from NIMA (now the NGA), for their support in the NIMA sponsored RSM Commercial Imagery Study and RSM Tactical Imagery Study, respectively.

RSM was designed by Dolloff and developed at BAE Systems. It was designed such that multi-image geopositioning, including rigorous error propagation, using RSM and its image support data is virtually identical to results obtained using the corresponding original sensor model and its image support data for all images involved. Images may be from any combination of sensors, including those with different modality (e.g. optical, radar). The RSM is also designed to support optimal adjustment of the RSM sensor model (image support data) for any image. Thus, RSM also supports triangulation of a group of images in a manner analogous to a bundle adjustment using the corresponding original sensor models. Therefore, the RSM design supports all image exploitation processes, ranging from basic image rectification to multiple-image, multiple-sensor triangulation.

1.3 Limitations of replacement sensor models

1.3.1 Substitute sensor model limitations

RSM's replacement of the original sensor model's ground-to-image relationship is a true replacement. Some previous sensor models that are termed "replacement" are not true replacements relative to the original sensor model's ground-to-image relationship, as described below.

A true replacement consists of a general ground-to-image function that maps a three-dimensional ground point (object space) coordinate \mathbf{x} to a corresponding two-dimensional image point (pixel) coordinate \mathbf{i} . This function is usually a rational polynomial. The polynomial coefficients are fit to a dense network of ground point-image point correspondences, $(\mathbf{x}, \mathbf{i})_i, i = 1, \dots, m$, generated using the original sensor model and its image support data. This network of "fit" points usually corresponds to an evenly spaced grid of image points over the entire image and multiple elevation planes covering the expected ground space (object space) domain. After the polynomial is generated, its fit accuracy relative to the original sensor model is confirmed over a different and denser network of ground point-image point correspondences. At a common ground point, the replacement sensor model's corresponding image point typically differs by less than 0.05 pixels from the original sensor model's corresponding image point. This performance is applicable over the entire, expected ground space domain.

Figure 1 illustrates a subset of the fit points, corresponding to one row of the grid in image space and five elevation planes. Of course, the polynomial is generated using the entire network of fit points in a weighted least-squares solution process that simultaneously solves for all the polynomial's coefficients. Thus, the entire ground space domain is covered by the network of fit points. Image-rays (as illustrated for an optical sensor, although the concept is equally valid for SAR and other sensors) associated with the resultant polynomial are virtually identical to their original sensor model counterparts depicted in the figure. This is also true for any image-ray, including those not associated

with fit points. Hence, the polynomial is a true replacement for the original sensor model's ground-to-image relationship.

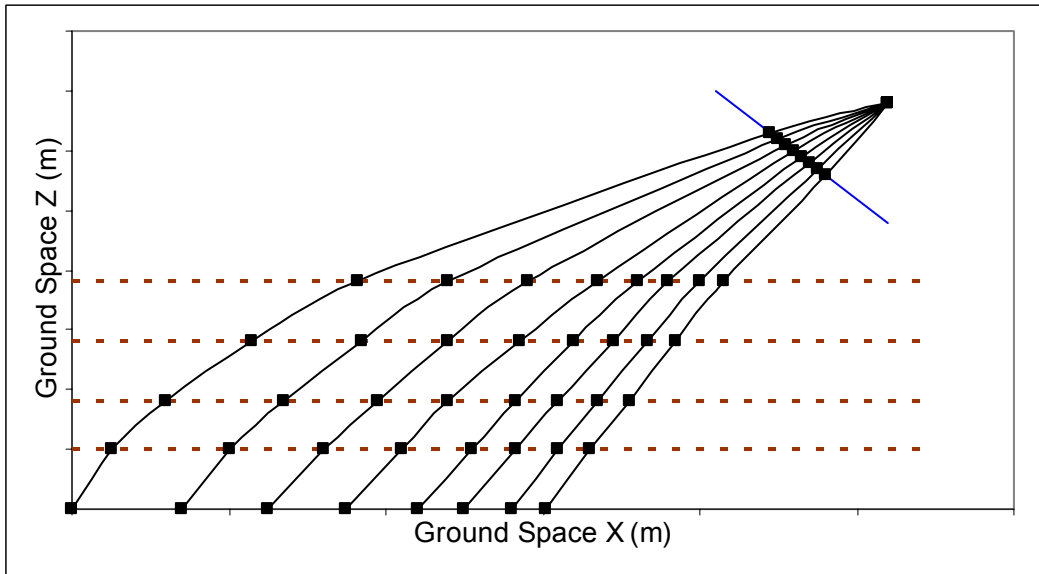


Figure 1. Fit grid for true replacement ground-to-image function.

There are other sensor models that, although of a general form, are not true replacements, and should not be designated as such. Let us term these sensor models “substitute” sensor models. Their generation typically follows the same general fitting procedure described above, but without the use of the original sensor model to generate a dense network of ground point-image point correspondences. Instead, the fit points correspond to a set of ground control point-image point correspondences. These ground control points cover only a limited portion of the possible ground domain. In addition, relative to the original sensor model, their ground point-image point correspondences are in error due to errors in both the ground control and the original sensor model's image support data. Due to both the control's sparse domain and these combined errors, the resultant sensor model is only accurate relative to the control and only at the general vicinity of the ground control points. In general, the substitute sensor model warps the ground-to-image space relationship, and can also be unstable due to the lesser amount of information available for the solution.

Figure 2 illustrates some of these characteristics at the image-rays corresponding to the control points. The triangle points represent control point positions along the terrain surface. The dotted lines are the substitute sensor model's image-rays. In general, their warping will be even more pronounced at image-rays not corresponding to control points. The solid horizontal line in Figure 3 represents the difference between the original and substitute sensor models at the control's elevation, i.e., that is, for the same image point position and same elevation, the difference in their corresponding horizontal ground point positions.

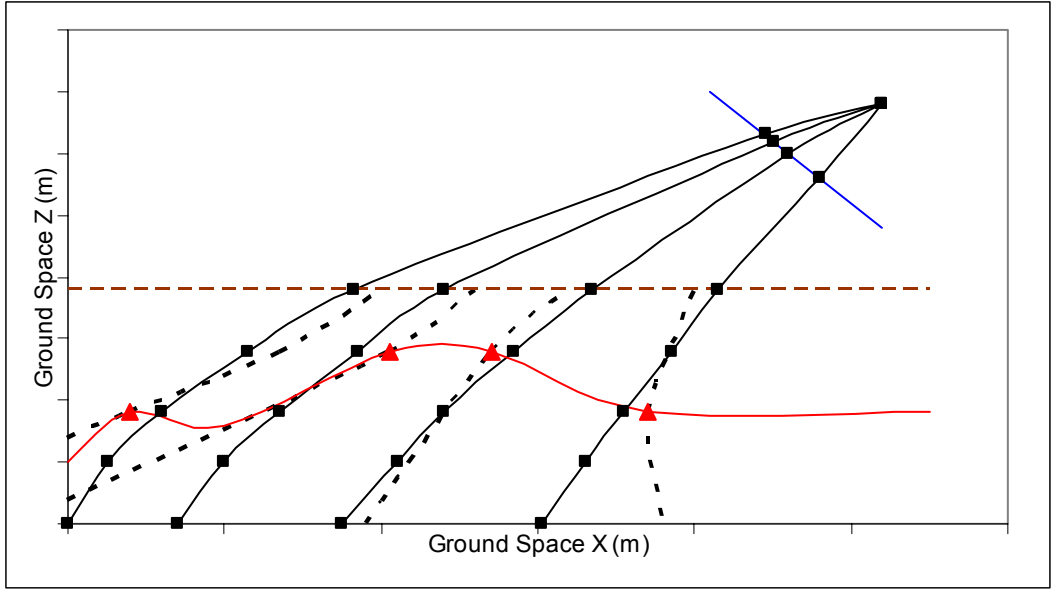


Figure 2. Fit points for the ground-to-image function of a substitute sensor model.

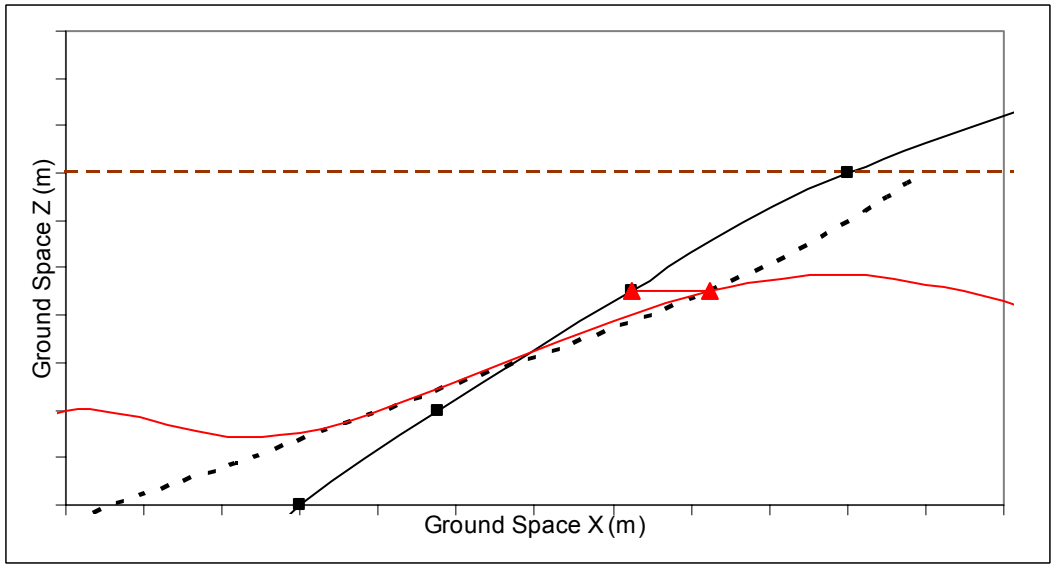


Figure 3. Horizontal discrepancy between the original and substitute sensor models.

1.3.2 Replacement sensor model limitations

By definition, no replacement sensor model and its image support data provide direct details of the original sensor model and its image support data. Thus, for example, an optical sensor's focal length or a particular image's platform position is unknown. The lack of the sensor (platform) position may be a liability in terms of possible ad-hoc analyses. However, in the ground space domain of the ground-to-image function, the

imaging locus is known. (For a given image point, the imaging locus is defined as all possible corresponding ground points.) Thus, the line-of-sight from the ground to the sensor can be approximated for an optical sensor using the ground-to-image function. If required, the nominal sensor position could be included in the replacement sensor model image support data.

In addition, if a particular replacement sensor model has adjustable parameters, they are not directly tied to the physics of the sensor and its imaging process. This can impede various “reasonableness checks” associated with geopositioning and triangulation solutions. For example, the magnitude of parameter adjustments can not be directly compared to a priori (physical) characteristics of the sensor and its image support data. However, such tests are still possible, some just not as intuitive to the human.

No replacement sensor model can directly support an image resection, i.e., the initial generation of a priori support data via control. If it were to do so, its ground-to-image function (support data) would be generated directly from control, and hence, it would be a substitute sensor model by definition. Instead, the recommended procedure is to perform a resection using the original sensor model, and then generate the replacement sensor model’s image support data from the original sensor model and its (resultant) a priori image support data.

All non-RSM replacement sensor models are limited by their lack of adjustability and/or rigorous error propagation, as discussed previously. Let us now briefly discuss limitations with their ground-to-image function. As mentioned previously, this function is usually a rational polynomial, with associated limitations. The denominator of a rational polynomial may contain zeros within the ground space domain which makes it unstable. The process that generates the polynomial should check for zeros, and if encountered, reformulate the solution.

One approach to the reformulation is the use of a numerator-only polynomial. However, in some situations high order terms must be utilized in order to achieve the desired fit accuracy. For example, a polynomial may contain a term $cX^iY^jZ^k$, where c is a coefficient and the combined power $i + j + k$ is significantly larger than 3, say on the order of 10. However, with high order terms, the polynomial solution process itself can become unstable as well as the application of the generated polynomial. Typically, the use of high order terms also corresponds to a solution with a large number of highly correlated parameters (polynomial coefficients), an example of “over parameterization”. On the other hand, there are numerous situations where a numerator-only polynomial will work well without the use of high order terms, but does require a combined power higher than 3. Correspondingly, a limitation of some replacement sensor models is an inflexible polynomial form. They can not generate and disseminate the (higher order) numerator-only polynomial.

Another limitation with all polynomials is their oscillatory or warping behavior near and outside the boundary of the fit grid domain. When generated, the appropriate domain must be selected, and when utilized, the ground point x must reside within the domain.

Finally, there are some situations where no (rational) polynomial will work well. In this case, an interpolated ground space-image space correspondence grid will work, assuming it is dense enough and used with an interpolator of proper order. Linear interpolation in each of the three ground coordinates (tri-linear interpolation) is typically inadequate in terms of fit accuracy with feasible support data bandwidth, and at least second-order interpolation must be used. The use of a grid as the ground-to-image function is discussed further in section 2.2.

1.3.3 RSM limitations

Due to its flexibility and expanded functionality relative to other replacement sensor models, RSM is necessarily more complex.

In terms of the ground-to-image function, RSM contains approaches for any given situation – rational polynomial, numerator-only polynomial, or interpolated grid. Typically the “situation” is dictated by sensor type and general application, since image size and image geometry are usually dependent. However, in order to perform well and provide a stable solution with satisfactory fit accuracy, RSM requires a “smart” up-stream generation process that determines the correct approach. This can range from a priori generation processes tailored to each specific situation, to an automatic process that handles arbitrary situations. Section 5.1 discusses this in more detail.

As mentioned previously, replacement sensor models other than RSM do not provide for adjustability and/or rigorous error propagation. However, in-order for RSM to do so, two conditions must also be satisfied. First, the right set of adjustable parameters must be selected by the RSM “up-stream” generation process for the particular situation. For example, most situations require 6 RSM adjustable parameters per image. In this case, if only two were to be specified, RSM adjustability and error propagation capabilities would not match those of the original sensor model. (See (Dowman and Dolloff, 2000) for a specific example.)

Second, in order for RSM triangulation solutions to match those based on the original sensor model, the original sensor model a priori image support data must be reasonably accurate. This is not a problem for most situations. For example, the a priori position of a space-borne sensor may be in error by five hundred meters and the two solutions will still be virtually identical. Section 6.2.2.2 provides more details.

Section 5.2 discusses both the selection of the appropriate RSM adjustable parameters and generation of the RSM error covariance in detail.

In summary, there are limitations associated with all replacement sensor models. However, in many circumstances, their positive features more than compensate for any limitations, particularly so for RSM.

2.0 Sensor model functionality

This section describes the major functionality and components associated with an original sensor model and their corresponding RSM counterparts.

2.1 Original sensor model major components

An original sensor model is based on the physical details of the sensor. It primarily consists of three major components: (1) a ground-to-image function, (2) adjustable parameters affecting the ground-to-image function, and (3) an error covariance corresponding to errors in the adjustable parameters. Examples of adjustable parameters include adjustments to the a priori sensor position, attitude, and focal length for an optical sensor, and the a priori sensor position and velocity for a SAR sensor. In general, this a priori data is contained in the sensor image support data.

Note that the original sensor model may supply an image-to-ground function (more properly termed an image-and-height-to-ground function) in lieu of a ground-to-image function; however, the ground-to-image function can be obtained (in principle) by inverting the image-to-ground function. Also, the error covariance is relative to the adjustable parameters of the associated image, or more generally, the multi-image error covariance is relative to the combined adjustable parameters for a correlated group of images. The error covariance statistically characterizes the uncertainty in the sensor image support data, i.e., statistically characterizes the errors in sensor position, velocity, etc, contained in the support data. The following expresses mathematically some of the above concepts for an original sensor model:

$$\begin{aligned} \mathbf{i}_{ik} &= F(\mathbf{x}_k, S_i, \boldsymbol{\delta}_{S_i}) \\ \mathbf{C}_{S_{ij}} &= E\left\{\boldsymbol{\varepsilon}_{S_i} \boldsymbol{\varepsilon}_{S_j}^T\right\} \end{aligned} \quad (1)$$

\mathbf{i}_{ik} is the corresponding two-dimensional image point coordinate in image i of the three-dimensional ground point coordinate \mathbf{x}_k . F is the original sensor model's adjustable ground-to-image function. S_i is the corresponding support data for image i , and $\boldsymbol{\delta}_{S_i}$ the n -dimensional support data adjustable parameters for image i . $\boldsymbol{\varepsilon}_{S_i}$ is the n -dimensional error associated with the value of $\boldsymbol{\delta}_{S_i}$ and represents the support data error. Note that prior to an adjustment process, such as triangulation, the adjustment vector $\boldsymbol{\delta}_{S_i}$ typically has a (vector) value of zero corresponding to a priori support data. However, even though the adjustment value is zero, the error in the value is not. In fact, it will typically be larger than when the adjustment value is non-zero.

$E\{\}$ is the statistical expectation operator. $\mathbf{C}_{S_{ij}}$ is the cross-covariance between the errors in the adjustable parameters for image i and the adjustable parameters for image j . It has dimension $n \times n$, and corresponds to image i 's error covariance when $i = j$. Note that all errors are assumed unbiased, i.e., $E\{\boldsymbol{\varepsilon}_{S_i}\} = \mathbf{0}$. This is a reasonable

assumption and consistent with the error covariance as a statistical measure of support data accuracy. (If the errors were biased, the error covariance would become a statistical measure of precision.)

When $i \neq j$, the cross-covariance $C_{S_{ij}}$ will be non-zero for one of two possible reasons. The first is due to a priori modeled, time-correlated, adjustable parameter errors for the sensor. For example, a space-borne sensor typically has highly correlated a priori position errors across time spans less than the orbital period. The second is due to a previous simultaneous adjustment of both sets of adjustable parameters, such as that which occurs during a triangulation involving images i and j . $C_{S_{ij}}$ can be easily generalized to an $n_1 \times n_2$ matrix, corresponding to two images from two different sensors, one with n_1 adjustable parameters, and the other with n_2 adjustable parameters.

2.2 RSM major components

Analogous to the original sensor model, RSM primarily consists of three major components: (1) a ground-to-image function, (2) adjustable parameters affecting the ground-to-image function, and (3) an error covariance corresponding to errors in the adjustable parameters.

The ground-to-image function is either a rational polynomial or an interpolator into a grid of ground point-image point correspondences. The polynomial works well for space-borne sensors and other sensors which do not have a large field-of-view. Also, the polynomial form is compact, i.e., its corresponding support data bandwidth is relatively small. The corresponding RSM image support data consists of the polynomial coefficients and various associated coordinate scale factors and offsets. (Note that an RSM image-to-ground function is also available as an iterative inverse of the RSM ground-to-image function, as described in section 4.2.)

Instead of a polynomial, interpolation into a grid of ground point-image point correspondences may be required to match the original sensor model's ground-to-image function within the desired fit accuracy (typically 0.05 pixels root-mean-square (rms) or less). This can occur when the sensor has a wide field-of-view, on the order of 90 degrees or more. Use of an interpolated grid can also be required if an airborne scanning sensor is flying at low altitude and through turbulence with resultant high frequency fluctuations in image geometry. With the grid approach, the corresponding RSM support data consists of a grid of ground space-image space correspondences. The ground space range corresponds to the image footprint over a reasonable range of height values relative to the ellipsoid. The interpolator is typically second-order in each of the ground space components.

In general, use of a ground-to-image grid with an interpolator provides features unavailable with a polynomial. It will achieve the required fit accuracy for any sensor given a dense enough grid, although with a corresponding penalty in image support data bandwidth. It is also unaffected by potential zero crossings associated with the

denominator of a rational polynomial. The RSM and its support data format are very flexible in that a (rational) polynomial can be specified, a grid specified, or both. If the latter, the interpolated grid supplies corrections to the polynomial's evaluation, providing improved fit accuracy relative to the original sensor model's ground-to-image relationship, and with less bandwidth than for a grid alone.

The RSM adjustable parameters are independent of the particular form selected for the RSM ground-to-image function. They consist of either generic parameters that adjust the RSM ground-to-image function's input \mathbf{x} , or the RSM ground-to-image function's output \mathbf{i} . The RSM (support data) error corresponds to the errors in these adjustable parameters. The following expresses mathematically some of the above concepts for RSM.

$$\begin{aligned} \mathbf{i}_{ik} &= G(\mathbf{x}_k, R_i, \boldsymbol{\delta}_{R_i}) \\ \mathbf{C}_{R_{ij}} &= E\left\{\boldsymbol{\varepsilon}_{R_i} \boldsymbol{\varepsilon}_{R_j}^T\right\} \end{aligned} \quad (2)$$

\mathbf{i}_{ik} is the corresponding two-dimensional image point coordinate in image i of the three-dimensional ground point coordinate \mathbf{x}_k . G is the RSM adjustable ground-to-image function. R_i is the corresponding RSM support data for image i , and $\boldsymbol{\delta}_{R_i}$ the m -dimensional support data adjustable parameters for image i . $\boldsymbol{\varepsilon}_{R_i}$ is the m -dimensional error associated with the value of $\boldsymbol{\delta}_{R_i}$ and represents the support data error. Note that prior to an adjustment process, such as triangulation, the adjustment vector $\boldsymbol{\delta}_{R_i}$ typically has a value of zero corresponding to a priori support data.

$\mathbf{C}_{R_{ij}}$ is the cross-covariance between the errors in the RSM adjustable parameters for image i and the RSM adjustable parameters for image j . It has dimension $m \times m$, and corresponds to image i 's error covariance when $i = j$. (Note that all errors are assumed unbiased, i.e., $E\{\boldsymbol{\varepsilon}_{R_i}\} = \mathbf{0}$.) When $i \neq j$, $\mathbf{C}_{R_{ij}}$ will be non-zero if either the corresponding $\mathbf{C}_{S_{ij}}$ associated with the original sensor model and images i and j is non-zero, or if both sets of RSM adjustable parameters are simultaneously adjusted later by a "down-stream" user, such as that which occurs during a triangulation involving both images i and j . Also, similar to its original sensor model counterparts, $\mathbf{C}_{R_{ij}}$ can be easily generalized to an $m_1 \times m_2$ matrix associated with two different sensors, one with m_1 RSM adjustable parameters, and the other with m_2 RSM adjustable parameters. Again, $\mathbf{C}_{R_{ij}}$ will be non-zero if either the corresponding $\mathbf{C}_{S_{ij}}$ associated with the original sensor models is non-zero, or if both sets of RSM adjustable parameters are simultaneously adjusted later by a down-stream user.

2.3 Incomplete sensor models

The original sensor model and its RSM counterpart described above are complete sensor models. They contain all three major components required to properly perform all relevant geopositioning and triangulation processes. The image provider for a given sensor should have access to this information for the original sensor model, and thus be able to generate and disseminate a complete RSM.

If for some reason they do not have access to the original sensor model adjustable parameter and error covariance information, or choose not to make it available to the user community, either in a form corresponding to the original or RSM model, the corresponding sensor model is not complete. It only contains the ground-to-image relationship. In particular, the RSM support data would only contain the ground-to-image function (see section 3.4). With this data, only monoscopic geopositioning using a single image and a DEM, or stereo geopositioning can be meaningfully performed. However, the latter requires the simultaneous solution of only one ground (object) point and equal weight of both image rays, and neither solution includes error propagation of the support data errors to the ground point solution errors. Subsequent solution accuracy would have to be empirically derived based on comparisons to control. Also, with an incomplete sensor model, an optimal multi-image geopositioning or triangulation solution can not be performed. (See section 4.1 for details on optimal geopositioning and triangulation.)

In some sensor-specific situations, the limited functionality associated with an incomplete sensor model can be mitigated by the user. This presupposes that a nominal set of adjustable parameters and associated error covariance information are found in the literature, usually based on various empirical studies. For optimal triangulation, both the identity of the adjustable parameters (a priori values equal zero) and their error covariance are required. ((Grodecki and Dial, 2003) provide a detailed description of their recommended RPC adjustable parameters and general error covariance information applicable to the Ikonos sensor.) However, if control points are used in the triangulation, a non-optimal solution may be obtained when only the adjustable parameters are identified by setting the adjustable parameter error covariance to values consistent with conservatively large support data errors. The non-optimal solution will approach the optimal solution as the number and accuracy of the control points increase.

The remainder of this report presents the RSM detailed form (section 3), the use of RSM for geopositioning and triangulation (section 4), the generation of RSM (section 5), and a summary of RSM development history, status, and performance (section 6).

3.0 RSM detailed form

This section describes the detailed functional form of RSM. First, the RSM adjustable ground-to-image function is described, followed by a description of the RSM error covariance. Next, a description of the RSM time-of-image and illumination models is provided which are necessary in order for RSM to capture all significant functionality of the original sensor model. Finally, a general description of the RSM support data format is provided.

3.1 Adjustable ground-to-image function

Figure 4 presents the RSM adjustable ground-to-image function $G(\mathbf{x}, R, \delta_R)$. Its inputs are the three-dimensional ground point coordinate (\mathbf{x}), the RSM image support data (R), and any RSM adjustments (δ_R). Its output is the corresponding two-dimensional image point coordinate (\mathbf{i}). (The image subscript i and ground point subscript k are dropped for convenience.) Ground point coordinates $\mathbf{x} = [X \ Y \ Z]^T$ can be relative to either a Rectangular coordinate system or a Geodetic coordinate system, i.e.,

$\mathbf{x} = [X \ Y \ Z]^T = [\lambda \ \phi \ h]^T$, where height (h) is above the WGS-84 ellipsoid. The applicable coordinate system is specified in the RSM image support data. If Rectangular, it is further defined in the RSM image support data as a specified offset and rotation relative to the WGS-84 ECEF (rectangular) coordinate system. For convenience, the remainder of this section assumes that the applicable coordinate system is Geodetic.

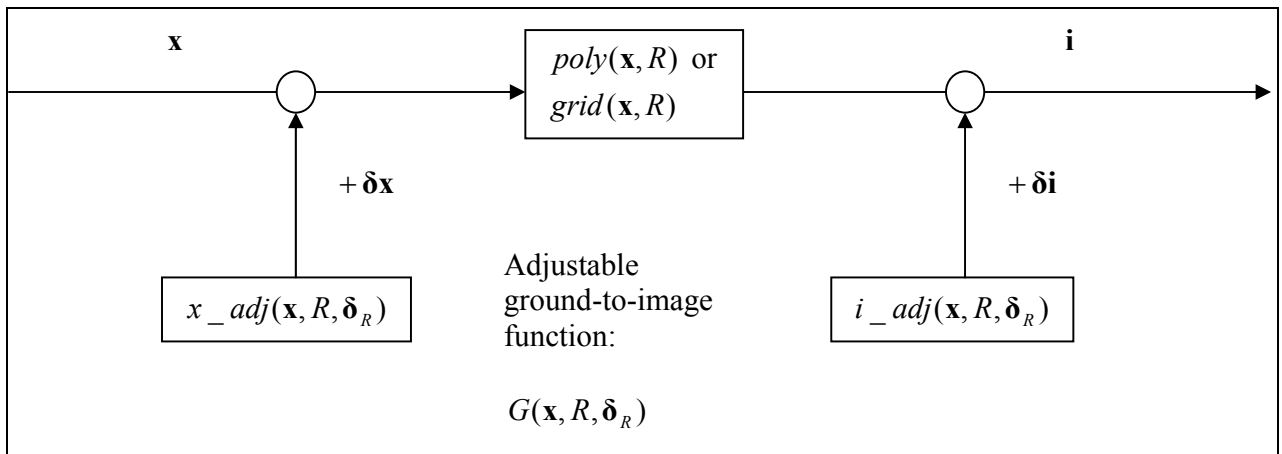


Figure 4. RSM adjustable ground-to-image function.

The RSM adjustable ground-to-image function $G(\mathbf{x}, R, \delta_R)$ consists of three interconnected functions: (1) a ground-to-image function, (2) a ground space adjustment function, and (3) an image space adjustment function. The ground-to-image function is either a rational polynomial ($poly(\mathbf{x}, R)$) or is an interpolator into a ground space-image space correspondence grid ($grid(\mathbf{x}, R)$). Either ground space or image space adjustment functions may be used. All applicable functions and their supporting data, such as polynomial coefficients, are specified in the RSM image support data.

The ground space adjustment function ($x_adj(\mathbf{x}, R, \delta_R)$) modifies the ground point coordinate (\mathbf{x}) prior to its input into the ground-to-image function. It is a function of the unmodified ground point coordinate, the RSM image support data, and the RSM adjustable parameters. The image space adjustment function ($i_adj(\mathbf{x}, R, \delta_R)$) modifies the image point coordinate (\mathbf{i}) following its output from the ground-to-image function. It

is a function of the unmodified ground point coordinate, the RSM image support data, and the RSM adjustable parameters.

The applicable RSM adjustable parameters are specified in the RSM image support data. They consist of up to twenty defined parameters for the image space adjustment or up to sixteen defined parameters for the ground space adjustment. Typically, the number of adjustable parameters specified per image ranges from 5 to 12, reflecting how many RSM adjustable parameters are required to capture the adjustability and error propagation of the original sensor model. Their values are assumed zero unless specified otherwise in the image support data. Their initial values are usually zero, and become non-zero if the RSM is adjusted via a triangulation process. Their values can also become “temporarily” non-zero if the adjustable ground-to-image function is used to compute numerical partial derivatives of the image point with respect to the RSM adjustable parameters during a geopositioning process.

Note that even when the values of the specified RSM adjustable parameters are zero and not explicitly included in the RSM image support data, their identities are still included because the RSM error covariance is relative to errors in the values of the adjustable parameters. Also, when the values of the RSM adjustable parameters are zero, this does not imply that the corresponding original sensor model adjustable parameter values are zero. That is, the RSM ground-to-image function can be generated from an adjusted original sensor model. The RSM ground-to-image function automatically absorbs these previous adjustments.

Although RSM adjustable parameters are typically either image space adjustable parameters or ground space adjustable parameters, in its most general form RSM can support a mixture of both. In addition, both a polynomial and a grid ground-to-image function can be specified in the RSM support data. If the latter, the grid is defined as providing corrections to the polynomial’s output.

3.1.1 Ground-to-image function polynomial

The ground-to-image function polynomial is very general in order to supply a high degree of fit accuracy relative to the original sensor model’s ground-to-image function under a wide variety of sensor types, image sizes, and image geometries. There can be multiple polynomials, each corresponding to a different section of the image, although, only one section is typically required. For a given section, the polynomial is a rational polynomial with variable order. The image support data specifies whether the denominator polynomial is included, and also specifies the order of the numerator polynomial and, if applicable, the denominator polynomial. The functional form of the rational polynomial ($poly(\mathbf{x}, R)$) is as follows (note that there are actually two rational polynomials, one for the image point u coordinate, and one for the image point v coordinate):

$$\text{Define } \mathbf{i} = [u \quad v]^T \text{ and } \mathbf{x} = [X \quad Y \quad Z]^T \text{ (normalized)} \quad (3)$$

$$u = \frac{\sum_{k=0}^{u_{nz}} \sum_{j=0}^{u_{ny}} \sum_{i=0}^{u_{nx}} a_{ijk} X^i Y^j Z^k}{\sum_{k=0}^{u_{dz}} \sum_{j=0}^{u_{dy}} \sum_{i=0}^{u_{dx}} b_{ijk} X^i Y^j Z^k}$$

$$v = \frac{\sum_{k=0}^{v_{nz}} \sum_{j=0}^{v_{ny}} \sum_{i=0}^{v_{nx}} c_{ijk} X^i Y^j Z^k}{\sum_{k=0}^{v_{dz}} \sum_{j=0}^{v_{dy}} \sum_{i=0}^{v_{dx}} d_{ijk} X^i Y^j Z^k}$$

For the u - image point coordinate's rational polynomial, the maximum allowed power for any ground coordinate, for either the numerator or denominator, is 5, i.e., $0 \leq u_{nx}, u_{ny}, u_{nz}, u_{dx}, u_{dy}, u_{dz} \leq 5$. Also, the constant coefficient for the denominator is defined as equal to 1, i.e., $b_{000} \equiv 1$. Corresponding restrictions are also applicable to the v - image point coordinate's rational polynomial.

The polynomials are defined relative to normalized variables, with a range of [-1, 1]. The coordinate offsets and scale factors, stored as part of the support data, define the transformations to and from the normalized variables. There are separate offsets and scale factors for each of the three ground coordinates and for each of the two image coordinates. Thus, the following equation defines the relationship between normalized and un-normalized coordinates for an arbitrary coordinate a :

$$a_{normalized} = \frac{a - offset}{scalefactor}, \quad (4)$$

where the *offset* and *scalefactor* correspond to the arbitrary coordinate a .

Also, normalization of the input \mathbf{x} occurs after any adjustments due to RSM ground-space adjustable parameters, and un-normalization of the output \mathbf{i} occurs prior to any adjustments due to RSM image space adjustable parameters (see section 3.1.3).

The support data also contains two, low order and relatively low fit accuracy numerator-only polynomials – one for u as a function of X, Y, Z , and one for v as a function of X, Y, Z . Their evaluation specifies which section and corresponding rational polynomial to use when the image is divided into multiple sections.

Typically, space-borne sensors and many air-borne sensors require only one section for the entire image. A third order rational polynomial is typical, with 20 active coefficients in both the numerator and the denominator. All coefficients corresponding to a combined power $i + j + k \geq 4$ have a value of zero. This rational polynomial has desirable overall

qualities related to fit accuracy, i.e., small differences in corresponding evaluations of the rational polynomial and underlying original sensor model, continuity, differentiability, and stability. Its ability to successfully replace the original sensor model's ground-to-image relationship for many sensors is due to its inherent similarities to the basic frame-camera projection, which is a linear rational polynomial in rectangular coordinates. However, because it is a rational polynomial, zero-crossings are a concern and must be checked for during its generation. When fit accuracy allows it, a numerator-only polynomial can be specified to avoid potential denominator zero-crossing problems.

3.1.2 Ground-to-image function grid

An image's RSM ground-to-image grid consists of an image point coordinate $\mathbf{i}_j = [u \ v]^T$ associated with each ground point coordinate $\mathbf{x}_j = [X \ Y \ Z]^T$ located within a grid spanning the image's footprint over a range of height. The actual \mathbf{x}_j coordinate values are not included, but are defined by various parameters such as a grid origin, fixed step sizes along each of the X, Y, Z coordinate axes, and the number of points per coordinate axis. These parameters are included in the image's RSM support data.

The ground-to-image function $grid(\mathbf{x}, R)$ outputs an image point $\mathbf{i} = [u \ v]^T$ associated with an arbitrary ground point $\mathbf{x} = [X \ Y \ Z]^T$. The function interpolates the \mathbf{i}_j in a set of \mathbf{x}_j surrounding \mathbf{x} . Piece-wise local interpolation, rather than a global spline interpolation, is recommended for speed. In particular, separable tri-quadratic interpolation is a recommended technique, which uses a $3 \times 3 \times 3$ grid of \mathbf{x}_j surrounding \mathbf{x} . The corresponding interpolating polynomial is of the general form:

$$u = \sum_{k=0}^2 \sum_{j=0}^2 \sum_{i=0}^2 c_{ijk} X^i Y^j Z^k, \quad (5)$$

i.e., all cross-terms associated with the multiplication of three quadratic polynomials, one a function of X , one of Y , and one of Z . Fixed grid spacing in each of the three ground space dimensions is also required. Collectively, these properties allow for an efficient algorithm for the generation and evaluation of the interpolating polynomial, as described below.

Three Z -planes are shown in Figure 5, each with a 3×3 grid in X and Y . A two-dimensional interpolation is first done at the points in the Z -planes indicated by the open circles. Then a one-dimensional interpolation is done along the line indicated for the resultant image coordinate (u) at the desired ground point position (\mathbf{x}) indicated by the filled circle.

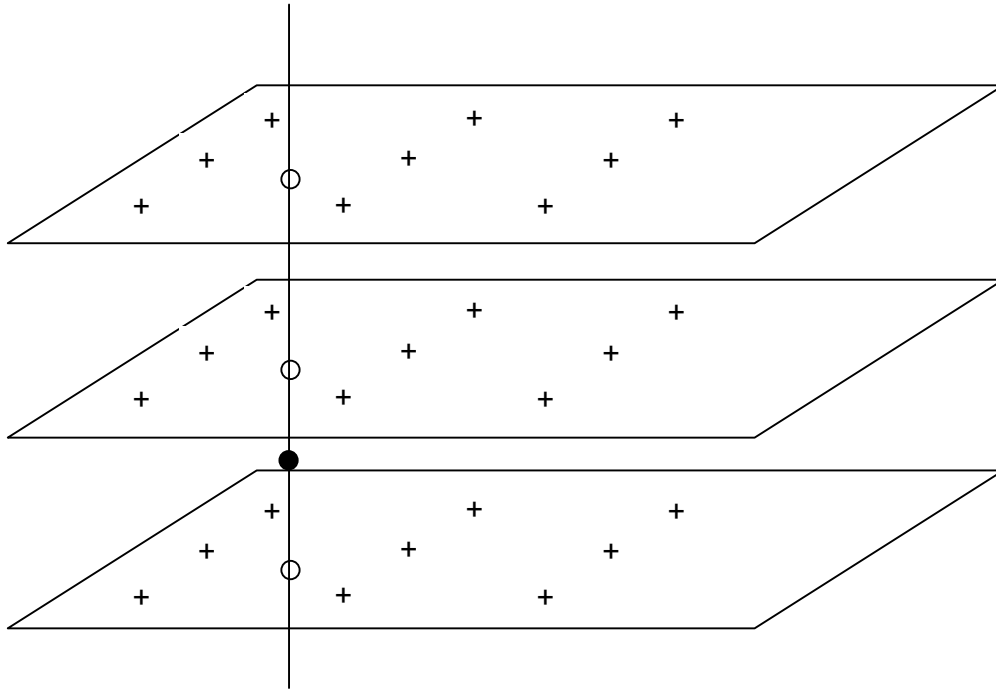


Figure 5. Interpolation along the Z -direction.

Separable interpolation can be done recursively, so that the two-dimensional interpolations in each plane are successively reduced to one-dimensional interpolations, as illustrated in Figure 6. For a given plane, the procedure is as follows. First, a one-dimensional interpolation is done in the X -direction along each horizontal line, generating a value at the diamond (\diamond) using the values at each of the three cross (+) signs. Following these three one-dimensional interpolations, another is done in the Y -direction along the vertical line containing the three diamonds. A value is generated at the desired open circle position using the values at each of the three diamonds.

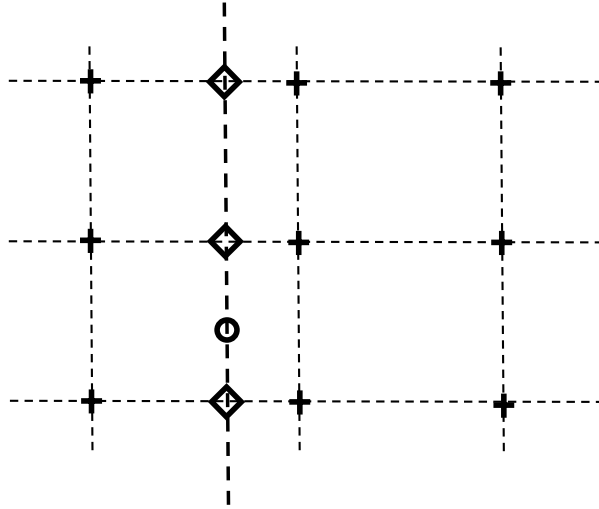


Figure 6. Interpolation within a Z -plane.

There are a total of four one-dimensional interpolations per plane, and a total of thirteen one-dimensional interpolations required for the final value u at the desired three-dimensional ground point position \mathbf{x} . Each one-dimensional interpolation is second-order (quadratic), i.e., based on a quadratic polynomial in one variable. The general (Lagrange) formula for a one-dimensional, second-order interpolation of a value s at position t , using values s_i at three evenly spaced positions t_i (grid spacing d , and $t_{i-1} \leq t \leq t_{i+1}$), can be written as follows:

$$\begin{aligned}
 s = & s_{i-1} \left[-\frac{1}{2d}(t-t_i) + \frac{1}{2d^2}(t-t_i)^2 \right] \\
 & + s_i \left[1 - \frac{1}{d^2}(t-t_i)^2 \right] \\
 & + s_{i+1} \left[\frac{1}{2d}(t-t_i) + \frac{1}{2d^2}(t-t_i)^2 \right]
 \end{aligned} \tag{6}$$

Note that s takes on the value s_{i-1} , s_i , and s_{i+1} at t_{i-1} , t_i , and t_{i+1} , respectively.

In our application, the independent variable t is either X , Y , or Z , and the dependent variable s is u . The values s_i are either u_i at the appropriate grid point position in the $3 \times 3 \times 3$ grid, or a linear combination of u_i generated from previous one-dimensional interpolations. Note that all terms (weights) multiplying s_{i-1}, s_i, s_{i+1} are invariant across all nine one-dimensional interpolations in the X -direction, and all three one-dimensional interpolations in the Y -direction performed in all three planes. Therefore, they need only be computed once per direction. Also, the overall algorithm will yield the same result u for a position \mathbf{x} regardless the order of interpolation. For example, X -

planes could be used instead of Z -planes. And, of course, the entire procedure described above is also applicable to the image point v coordinate, i.e., there are actually two interpolating polynomials for a given \mathbf{x} , one for u and one for v . Terms multiplying the data (s_{i-1}, s_i, s_{i+1}) are identical for their corresponding one-dimensional interpolations.

Analytic partial derivatives of the interpolating polynomial, and hence for the overall RSM ground-to-image function $grid(\mathbf{x}, R)$, can also be generated in an efficient manner when required for geopositioning or triangulation solution algorithms. The above procedure that generates u at \mathbf{x} using (thirteen) one-dimensional interpolations is modified in order to generate the partial derivative of u with respect to the desired ground coordinate component (X , Y , or Z) at the position \mathbf{x} . The modification is minor: if a particular one-dimensional interpolation (of the thirteen) involves the desired ground coordinate component, simply replace Equation 6 with the following equation, otherwise evaluate it as before.

$$\begin{aligned} \frac{\partial s}{\partial t} = & s_{i-1} \left[-\frac{1}{2d} + \frac{1}{d^2}(t-t_i) \right] \\ & + s_i \left[-\frac{2}{d^2}(t-t_i) \right] \\ & + s_{i+1} \left[\frac{1}{2d} + \frac{1}{d^2}(t-t_i) \right] \end{aligned} \quad (7)$$

The above description for interpolating polynomial generation and evaluation is not specific on how the actual $3 \times 3 \times 3$ grid is selected for a given \mathbf{x} . There are two reasonable methods for grid selection, each with different effects on the local (mathematical) topological properties of the interpolating polynomial (Equation 5) and the global topological properties of the RSM ground-to-image function $grid(\mathbf{x}, R)$. The topological properties (continuity and differentiability) are now discussed and the two methods of grid selection defined.

The first method selects the $3 \times 3 \times 3$ grid such that \mathbf{x} always resides in the lower corner $1 \times 1 \times 1$ “cube” of the eight cubes contained within the $3 \times 3 \times 3$ grid. (The cubes are formed by connecting the grid points (+) in the $3 \times 3 \times 3$ grid (see Figure 5) along each direction X, Y, Z .) Correspondingly, the same interpolating polynomial is applicable to all \mathbf{x} within that $1 \times 1 \times 1$ cube. This $1 \times 1 \times 1$ cube is the interpolating polynomial’s domain, and the interpolating polynomial is continuously differentiable over its domain. Also, the RSM ground-to-image grid function $grid(\mathbf{x}, R)$ is continuous across its entire ground domain, since each individual interpolating polynomial replicates its $1 \times 1 \times 1$ cube’s ground space-image space correspondence. The function $grid(\mathbf{x}, R)$ is also continuously differentiable at all ground points in its domain except those within a grid face.

The second method selects the $3 \times 3 \times 3$ grid nearest \mathbf{x} , i.e., \mathbf{x} is always “centered” within the grid. Depending on the value of \mathbf{x} , it will reside in any one of the eight cubes contained in the selected $3 \times 3 \times 3$ grid. Correspondingly, all one-dimensional interpolations (Equation 6) used to evaluate the interpolating polynomial always use the nearest three points for interpolation. This interpolation may be more accurate than interpolation based on the first method. However, with this second method, the corresponding $grid(\mathbf{x}, R)$ is no longer continuous across the entire ground domain. Of course, the interpolating polynomial itself is still continuously differentiable over its (local) ground domain. Let us term the second $3 \times 3 \times 3$ grid selection process “centered”, and the first “cornered”. RSM grid testing to-date (see section 6.1 for RSM development status), has utilized the cornered technique exclusively, with good results.

In addition, regardless the selection technique, a $3 \times 3 \times 3$ grid may not be available for a particular \mathbf{x} , such as that located at the boundary of the supplied RSM ground-to-image grid. In this case, linear interpolation/extrapolation is utilized, i.e., the one-dimensional interpolations are first order (linear).

Note that separable tri-cubic interpolation is also a feasible approach for the RSM ground-to-image function $grid(\mathbf{x}, R)$. The interpolating polynomial generation and evaluation procedure is basically the same as that for separable tri-quadratic interpolation, except that a $4 \times 4 \times 4$ grid is used, and the one-dimensional interpolations are third order (cubic). The one-dimensional interpolations are also set-up such that the point for interpolation is symmetrically located or “centered”, i.e., there are always two data points on either side. Therefore, \mathbf{x} always resides in the center cube of the 27 cubes contained within the selected $4 \times 4 \times 4$ grid. The one-dimensional interpolations are based on four point Lagrange interpolation. The underlying polynomial is a cubic polynomial in one variable that passes through all four fit (data) points. This insures that the interpolating polynomial is continuously differentiable across its local ($1 \times 1 \times 1$ cube) domain, and that the $grid(\mathbf{x}, R)$ function is continuous across its entire (global) ground domain.

Alternatively, the one-dimensional interpolations can instead be formulated to insure that the resultant $grid(\mathbf{x}, R)$ is also continuously differentiable across its entire ground domain. For each one-dimensional interpolation, the coefficients of its underlying cubic polynomial are determined by imposing four constraints. Two constraints are that the polynomial pass through the inner two fit points. The other two constraints require that the derivative be continuous when the set of fit points is shifted forward or backward, e.g., the derivative of the polynomial at fit point 3 must equal the derivative of the polynomial at fit point 2 were it based on four fit points advanced one grid unit. The following presents the corresponding one-dimensional interpolation formula for a value s as a function of t , and its corresponding derivative with respect to t (grid spacing d , and $t_i \leq t \leq t_{i+1}$).

$$\begin{aligned}
s &= s_{i-1} \left[-\frac{1}{2d}(t-t_i) + \frac{1}{d^2}(t-t_i)^2 - \frac{1}{2d^3}(t-t_i)^3 \right] \\
&+ s_i \left[1 - \frac{5}{2d^2}(t-t_i)^2 + \frac{3}{2d^3}(t-t_i)^3 \right] \\
&+ s_{i+1} \left[\frac{1}{2d}(t-t_i) + \frac{2}{d^2}(t-t_i)^2 - \frac{3}{2d^3}(t-t_i)^3 \right] \\
&+ s_{i+2} \left[-\frac{1}{2d^2}(t-t_i)^2 + \frac{1}{2d^3}(t-t_i)^3 \right]
\end{aligned}
\tag{8}$$

, and

$$\begin{aligned}
\frac{ds}{dt} &= s_{i-1} \left[-\frac{1}{2d} + \frac{2}{d^2}(t-t_i) - \frac{3}{2d^3}(t-t_i)^2 \right] \\
&+ s_i \left[-\frac{5}{d^2}(t-t_i) + \frac{9}{2d^3}(t-t_i)^2 \right] \\
&+ s_{i+1} \left[\frac{1}{2d} + \frac{4}{d^2}(t-t_i) - \frac{9}{2d^3}(t-t_i)^2 \right] \\
&+ s_{i+2} \left[-\frac{1}{d^2}(t-t_i) + \frac{3}{2d^3}(t-t_i)^2 \right]
\end{aligned}
\tag{9}$$

3.1.3 Adjustments

The adjustable parameters are specified in an image's RSM support data. They consist of a subset from the adjustable parameter choice set $\tilde{\delta R}$, defined as:

$$\begin{aligned}
\tilde{\delta R} &= \{ \tilde{\delta R}_I \quad \tilde{\delta R}_G \}, \text{ where} \\
\tilde{\delta R}_I &= \{ \delta u_o \quad \delta u_x \quad \delta u_y \quad \delta u_{xx} \quad \delta u_{xy} \quad \delta u_{yy} \quad \delta v_o \quad \delta v_x \quad \delta v_y \quad \delta v_{xx} \quad \delta v_{xy} \quad \delta v_{yy} \quad \cdot \quad \cdot \quad \cdot \} \\
\tilde{\delta R}_G &= \{ \delta x_o \quad \delta y_o \quad \delta z_o \quad \delta \alpha \quad \delta \beta \quad \delta \kappa \quad \delta s \quad \cdot \quad \cdot \quad \cdot \}
\end{aligned}
\tag{10}$$

RSM adjustable parameters specifically identified above are most often specified for RSM image space adjustments and RSM ground space adjustments in the RSM image support data. There are a total of twenty specifiable image space adjustable parameters in $\tilde{\delta R}_I$. Those involved with the Z coordinate, e.g., δu_{xz} , are typically not specified due to the coordinate system they reference, as discussed below. There are a total of sixteen specifiable ground space adjustable parameters in $\tilde{\delta R}_G$. The seven identified above correspond to a seven-parameter transformation, as discussed below. The remaining nine adjustable parameters consist of first-order rate terms in all three ground coordinates, and are typically not specified.

The image space adjustment function ($i_adj(\mathbf{x}, R, \delta_R)$) utilizes a local, rotated tangent plane coordinate system. A ground point coordinate \mathbf{x} represented in this system is indicated with a * superscript, i.e., as $\mathbf{x}^* = [X^* \ Y^* \ Z^*]^T$. The system is defined as follows:

$$\begin{aligned} \mathbf{x}' &= T(\mathbf{x}) \text{ , Geodetic to WGS-84 ECEF coordinate transformation} \\ \mathbf{x}^* &= \mathbf{A}(\mathbf{x}' - \mathbf{b}) \end{aligned} \quad (11)$$

The 3x3 rotation matrix \mathbf{A} and the offset vector \mathbf{b} are specified in the RSM image support data. They typically define a coordinate system that is a local tangent plane coordinate system with an origin centered in the image footprint at a nominal elevation, and then rotated such that the resultant Z^* corresponds to an axis aligned with the imaging locus direction (at the origin), the resultant X^* corresponds to an axis aligned with the image line (sweep) direction (in object space), and the resultant Y^* corresponds to an axis which completes the right-hand rectangular system.

The members of $\delta\tilde{R}_I$ are “rate” terms. The values of the selected $\delta\tilde{R}_I$ members (adjustable parameters) are multiplied by the appropriate \mathbf{x}^* coordinate values corresponding to the associated ground point and the adjustment result $\delta\mathbf{i}$ added to \mathbf{i} . For example, assume that six members $\{\delta u_o \ \delta u_x \ \delta u_y \ \delta v_o \ \delta v_x \ \delta v_y\}$ of the choice set $\delta\tilde{R}_I$ are specified in the RSM support data via “on/off flags” associated with all twenty members of $\delta\tilde{R}_I$. These specified members define the components of the RSM adjustment vector δ_R , whose corresponding value is also specified in the RSM support data. For a given ground point the associated image space corrections ($\delta\mathbf{i}$) are computed as follows:

$$\begin{aligned} \delta_R &= [\delta u_o \ \delta u_x \ \delta u_y \ \delta v_o \ \delta v_x \ \delta v_y]^T \text{ , via RSM image support data} \quad (12) \\ \delta u &= \delta u_o + \delta u_x X^* + \delta u_y Y^* \\ \delta v &= \delta v_o + \delta v_x X^* + \delta v_y Y^* \\ \delta\mathbf{i} &= [\delta u \ \delta v]^T \end{aligned}$$

The ground space adjustment function ($G_adj(\mathbf{x}, R, \delta_R)$) also utilizes the local, rotated tangent plane coordinate system defined above. The first seven members of its adjustable parameter choice set $\delta\tilde{R}_G$ contain adjustable parameters that define a seven-parameter transformation relative to this coordinate system. Thus, if the first seven members in $\delta\tilde{R}_G$ are specified, the adjustment function first transforms the ground point coordinate from an \mathbf{x} to an \mathbf{x}^* representation, applies the seven-parameter transformation using the values of the adjustment parameters contained in the RSM adjustment vector δ_R , converts the resultant \mathbf{x}^* back to an \mathbf{x} representation, and inputs the resultant \mathbf{x} into the ground-to-image function. Specifically:

$\delta_R = [\delta x_0 \quad \delta y_0 \quad \delta z_0 \quad \delta \alpha \quad \delta \beta \quad \delta \kappa \quad \delta s]^T$, via RSM image support data

$$\mathbf{x}' = T(\mathbf{x})$$

$$\mathbf{x}^* = \mathbf{A}(\mathbf{x}' - \mathbf{b})$$

$$\mathbf{x}'' = \begin{bmatrix} \delta x_0 \\ \delta y_0 \\ \delta z_0 \end{bmatrix} + \begin{bmatrix} 1 + \delta s & \delta \kappa & -\delta \beta \\ -\delta \kappa & 1 + \delta s & \delta \alpha \\ \delta \beta & -\delta \alpha & 1 + \delta s \end{bmatrix} \mathbf{x}^* \quad (13)$$

$$\mathbf{x}' = \mathbf{A}^{-1} \mathbf{x}'' + \mathbf{b} = \mathbf{A}^T \mathbf{x}'' + \mathbf{b}$$

$$\mathbf{x} = T^{-1}(\mathbf{x}')$$

3.2 Error covariance

The RSM error covariance statistically describes the image support data errors and supports rigorous error propagation. It is usually generated from the corresponding original sensor model error covariance, and in such a manner that both contain equivalent information. Section 4 describes its fundamental role in optimal geopositioning and triangulation algorithms.

There are two selectable forms for the RSM error covariance information supplied in the RSM image support data, direct and indirect as detailed below. The direct form is relatively straight forward and supports any group of correlated images, regardless the mechanism that induced their correlation. However, at time of generation, it requires knowledge of the specific correlated images, and for a large number of images, requires non-negligible image support data bandwidth. On the other hand, the indirect form requires little image support data bandwidth, and does not require knowledge of the specific correlated images at time of generation. However, the correlation between images must conform to an a priori model, and the indirect form is somewhat complicated.

3.2.1 Direct error covariance

The first form for the RSM error covariance directly supplies a multi-image error covariance that is associated with the image under consideration as well as other identified images that together form a “correlated image group,” i.e., a set of images with correlated support data errors. It is an error covariance relative to p RSM adjustment vectors, associated with the p correlated images ($p \geq 1$). The dimension of the error covariance is $(m_1 + \dots + m_p) \times (m_1 + \dots + m_p)$, assuming m_i RSM adjustable parameters per image i . For each image, the errors in its adjustment vector are assumed constant over all pixel positions (image points) within the image (although their effect does vary with pixel position via imaging geometry effects). Also, if there are multiple images ($p > 1$), the mechanism for their correlation of errors is arbitrary, ranging from known a priori correlation mechanisms for images from the same sensor during a reasonably short time

period (e.g., an orbit's period for a space-borne sensor), to a triangulation process involving images from different sensors.

Specifically, the upper triangular portion of the following symmetric multi-image error covariance is directly provided in the RSM support data for an image:

$$\mathbf{C}_R = \begin{bmatrix} \mathbf{C}_{R_{11}} & \mathbf{C}_{R_{12}} & \cdot & \cdot & \mathbf{C}_{R_{1p}} \\ \cdot & \mathbf{C}_{R_{22}} & \cdot & \cdot & \cdot \\ \cdot & \cdot & \cdot & \mathbf{C}_{R_{ij}} & \cdot \\ \cdot & \cdot & \cdot & \cdot & \cdot \\ \cdot & \cdot & \cdot & \cdot & \mathbf{C}_{R_{pp}} \end{bmatrix}, \text{ where } \mathbf{C}_{R_{ij}} = E \left\{ \boldsymbol{\epsilon}_{R_i} \boldsymbol{\epsilon}_{R_j}^T \right\}, m_i \times m_j. \quad (14)$$

The number of images, their id's, and their number of RSM adjustable parameters per image are also identified in the RSM image support data. Images need not correspond to the same sensor nor have the same number of adjustable parameters, i.e., in general, $\mathbf{C}_{R_{ij}}$ has dimension $m_i \times m_j$. In addition, the identities of the applicable RSM adjustable parameters for the current image are also included.

Recall that RSM image support data for a specific sensor and specific image is generated by any suitably configured "up-stream" process, as described in section 1.2. If the RSM image support data is not being generated in near real-time by this process, \mathbf{C}_R may be redundantly supplied by this process in each of the p -image's RSM support data. If the "down-stream" user is working with all p -images, he will utilize the entire \mathbf{C}_R , which is available in the support data for any of these images. If he is working with only one image, he will extract from that image's RSM support data the appropriate single-image block from the p -image \mathbf{C}_R .

On the other hand, if the "upstream" process generates RSM image support data in near real time, p (and \mathbf{C}_R) may grow in the support data for each successive correlated image. For example, assume that there are two, time-ordered, correlated images. When the RSM support data is generated for the first image, the error covariance \mathbf{C}_R only references this image ($p = 1$). When the RSM support data is next generated for the second image, the error covariance \mathbf{C}_R references both images ($p = 2$). In this case, the "one-image" \mathbf{C}_R provided in the first image's RSM support data will be duplicated in the relevant portion of the larger "two-image" \mathbf{C}_R contained in the second image's RSM support data. A "down-stream" user working with both the first and second images will utilize the larger \mathbf{C}_R that is available in the second image's support data.

When the RSM error covariance \mathbf{C}_R is of the direct form as described above, it is also termed the RSM direct error covariance. If it corresponds to the triangulation of RSM adjustable parameters, it is automatically generated by the triangulation process and

available for direct insertion into the RSM support data. Otherwise, it is first generated from its original sensor model counterpart \mathbf{C}_s (see section 5.2) and then inserted into the RSM support data. Section 4.1.3, Equation 27, provides a specific example of an original sensor model error covariance, and Equation 28, the corresponding RSM direct error covariance computed from it.

3.2.2 Indirect error covariance

The second form for the RSM error covariance is applicable to the image under consideration as well as any number of other initially unidentified (possibly future) images associated with the same sensor. This form for the error covariance is indirect in the following sense. The sensor identification and time-of-image data contained in an image's RSM support data is sufficient for the user to identify any other collected images that are also from the same sensor and have correlated errors. The images' collective RSM support data contains error covariance data sufficient for the user to build a multi-image error covariance relative to the errors in the adjustment vectors for these images. The resultant multi-image error covariance is based on an assumed piece-wise linear decay time correlation model for errors. The correlation time is defined as the time between image center pixel positions.

3.2.2.1 Detailed description

The key to this general and flexible approach is to supply error covariance and time correlation data applicable to the original sensor model, where errors are associated with true physical parameters, and the time correlation structure is actually applicable. A "mapping matrix" is also supplied that transforms original sensor model adjustable parameters (errors) to RSM adjustable parameters (errors). With this data, the user can build the appropriate multi-image joint error covariance relative to the RSM adjustable parameters. Note, however, that this approach does not explicitly identify the original sensor model adjustable parameters to the user, nor does it require his use of the original sensor model in any way. Specifically, the following is supplied in an image i 's RSM support data:

- Φ_i , the $m \times n$ mapping matrix for image i (15)
- $\mathbf{C}_{S_{ii}}$, the original sensor model's $n \times n$ error covariance for image i
- $\rho_{S_i}(\tau)$, the original sensor model's time correlation function for image i , where τ is defined as the time between images ($\tau \geq 0$)

In addition, the identities of the actual RSM adjustable parameters for the image are included. Using the above data from all images of interest, the user computes the block entries of the multi-image error covariance (\mathbf{C}_R , see Equation 14) as follows:

$$\begin{aligned} \mathbf{C}_{R_{ii}} &= \Phi_i \mathbf{C}_{S_{ii}} \Phi_i^T, \text{ or more generally for the } m \times m \text{ cross-covariance,} & (16) \\ \mathbf{C}_{R_{ij}} &= \Phi_i \rho_{S_i}(\tau_{ij}) \mathbf{C}_{S_{ii}} \Phi_j^T, \text{ where } i, j \leq p \end{aligned}$$

Note that in the last equation, $\rho_{S_i}(\tau_{ij})\mathbf{C}_{S_{ii}}$ corresponds to the original sensor model's cross-covariance $\mathbf{C}_{S_{ij}}$. This is based on the assumption that $\mathbf{C}_{S_{ii}}$ and the function $\rho_{S_i}(\tau)$ are invariant across the correlated images $i = 1, \dots, p$, i.e., errors are modeled as a wide sense stationary stochastic process (Papoulis, 1991). This is the typical case. However, the RSM support data also supports the case when these values do change across correlated images. In this case, the $\rho_{S_i}(\tau)$ and $\mathbf{C}_{S_{ii}}$ used to generate $\mathbf{C}_{R_{ij}}$ in Equation 16 are replaced with "averages" taken over the variable values of $\rho_{S_i}(\tau)$ and $\mathbf{C}_{S_{ii}}$, respectively, $i = 1, \dots, p$, to insure the resultant \mathbf{C}_R is a legitimate error covariance, i.e. at least positive semi-definite. That is, for the original sensor model, a general stochastic error process is approximated using p separate wide sense stationary models - the values of $\rho_{S_i}(\tau)$ and $\mathbf{C}_{S_{ii}}$ are allowed to change across images. Further details on the "averaging" algorithm are not provided in this section, since this approach to error modeling is not necessary for most geopositioning applications.

The following details the forms of $\mathbf{C}_{S_{ii}}$ and $\rho_{S_i}(\tau)$, of Equations 15 and 16. Assuming that the original sensor model errors are associated with n adjustable parameters, these n errors are further sub-divided into w subgroups, each containing n_k errors, where

$k = 1, \dots, w$ and $\sum_{k=1}^w n_k = n$. The errors in each of these subgroups are assumed

uncorrelated with errors in the other subgroups. Each of these subgroups has its own $n_k \times n_k$ positive definite error covariance matrix, $\mathbf{C}_{S_{ik}}$, and scalar correlation function, $\rho_{S_{ik}}(\tau)$, provided in the support data. (Examples of typical subgroups for an optical sensor with $n = 7$ adjustable parameters (errors) are a 3-element sensor position subgroup, a 3-element attitude subgroup, and a 1-element focal length subgroup.) Thus, assuming the n adjustable parameters are ordered in concert with subgroup ordering, $\rho_{S_i}(\tau)\mathbf{C}_{S_{ii}}$ becomes the $n \times n$ symmetric block diagonal matrix:

$$\rho_{S_i}(\tau)\mathbf{C}_{S_{ii}} = \begin{bmatrix} \rho_{S_{i1}}(\tau)\mathbf{C}_{S_{i1}} & 0 & \cdot & \cdot & 0 \\ \cdot & \cdot & \cdot & \cdot & \cdot \\ \cdot & \cdot & \rho_{S_{ik}}(\tau)\mathbf{C}_{S_{ik}} & \cdot & \cdot \\ \cdot & \cdot & \cdot & \cdot & 0 \\ \cdot & \cdot & \cdot & \cdot & \rho_{S_{iw}}(\tau)\mathbf{C}_{S_{iw}} \end{bmatrix} \quad (17)$$

The individual functions $\rho_{S_{ik}}(\tau)$, where τ is the time between images, are specified in the RSM image support data. As mentioned earlier, the correlation functions $\rho_{S_{ik}}(\tau)$ are specified as piece-wise linear decay functions. Figure 7 presents an example of a three "piece", piece-wise linear decay function. For a particular function $\rho_{S_{ik}}(\tau)$, up to nine sets of (ρ, τ) correspondences, used to define the individual linear segments, can be

specified in the RSM support data. Note also that by using multiple linear segments, an exponential correlation function, $e^{-\tau/T}$, where T is the time constant, may be accurately approximated. The piece-wise linear decay model is more general than the exponential decay model, the former can represent the latter, but not vice versa.

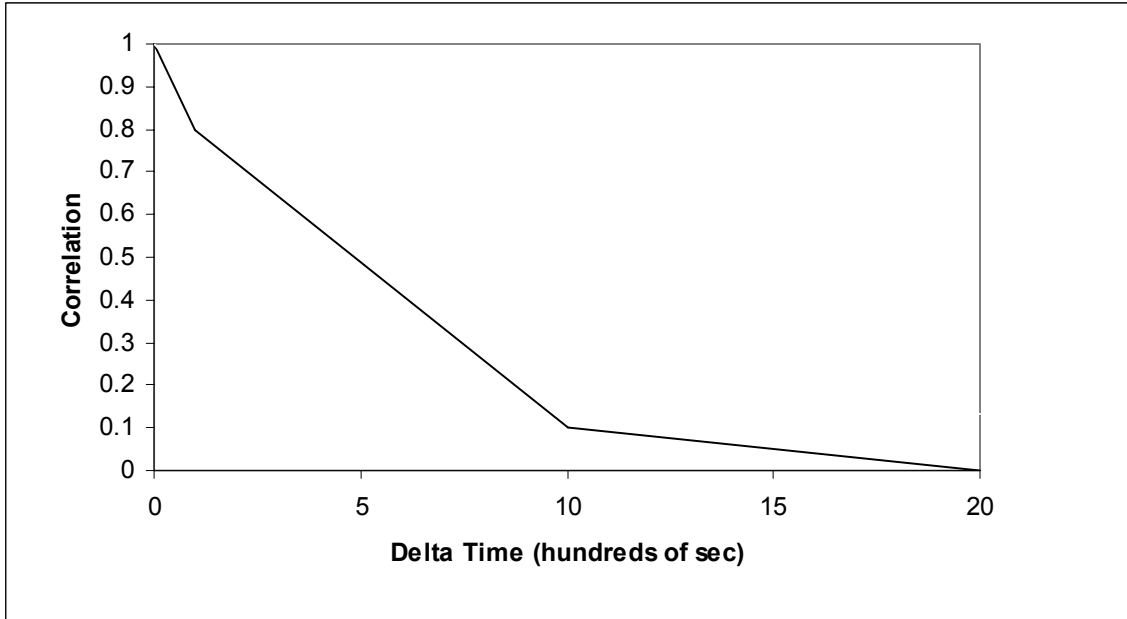


Figure 7. Piece-wise linear correlation function example.

The properties of $\rho_{S_{ik}}(\tau)$, $\mathbf{C}_{S_{ik}}$, and Φ_i , insure that \mathbf{C}_R will be a legitimate error covariance matrix once assembled. To that end, the RSM format requires the piece-wise linear correlation function $\rho_{S_{ik}}(\tau)$ to be a non-negative, non-increasing, convex function of time (τ) between images. It also has a “floor” value of zero, i.e., $\rho_{S_{ik}}(\tau) = 0$, for all $\tau > \tau_{\max}$, where τ_{\max} is associated with the last linear segment.

When the RSM error covariance \mathbf{C}_R is of the indirect form as described above, it is also termed the RSM indirect error covariance. It is generated from its original sensor model counterpart \mathbf{C}_S (see section 5.2) and then inserted into the RSM support data. Section 4.1.3, Equation 27, provides a specific example of an original sensor model error covariance, and in the latter part of the section (near Equation 28), describes its corresponding RSM indirect error covariance.

3.2.2.2 Optional classification of errors

This subsection describes various optional classifications and statistical representations of errors that are supported by RSM. They are not required for most geopositioning (and triangulation) applications.

The multi-image error covariance \mathbf{C}_R associated with the direct form (Equation 14), and associated with the indirect form (Equations 15 - 17) is applicable to errors assumed constant over all pixels in an image. However, these errors do vary from image to image in a correlated manner when they are from the same sensor. They can also be correlated with errors from different sensors when \mathbf{C}_R is represented by the direct form.

Let us term these types of errors as “image” errors. Historically, the use of an “image” error model is the standard approach for both geopositioning and triangulation processes. It is required for triangulation, since a set of image-wide adjustments (corrections) are solved for each image in a multi-image solution process. However, it is not required for geopositioning - the optimal solution of object position(s) using multiple images, where corrections to the image support data are not solved for, but image support data errors are correctly accounted for in the measurement weighting process.

In the most general case of geopositioning, the image support data errors can also be modeled as “image element” errors where an image element is defined as that portion of an image associated with a unique time (see section 3.3). The “image element” error model corresponds to a (wide sense) stationary stochastic error process, where time is associated with an image element, not an entire image. Typically, for scanning sensors, an image element corresponds to an image line, i.e., all v coordinates associated with a specific u coordinate.

For a given realization of the stationary stochastic error process, a different error value is associated with each image element (time). Thus, support data errors associated with two elements in either the same or two different images from the same sensor can be specified as two different, but correlated, error values. The “restricted image element” error model adds the restriction that the errors are uncorrelated between elements from different images. Thus, only support data errors associated with two elements in the same image can be specified as correlated.

The RSM indirect approach for error covariance supports this generality, when the appropriate flags are set in the RSM image support data. In fact, all the individual adjustable parameters (errors) associated with a subgroup can be specified as “image”, “image element”, or “restricted image element.” For both the “image element” error model and “restricted image element” error model, the subscripts i and j utilized in Equations 14 and 16, correspond to support data errors at element i and element j of two (possibly the same) images. In addition, τ in Equations 15 and 16 is defined as the time between element i and element j . However, the mapping matrix Φ_{i^*} , the error covariance $\mathbf{C}_{S_{i^*}}$, and the correlation function $\rho_{S_{i^*}}$ are now indexed by the image i^* containing the element. The RSM direct approach for error covariance is applicable to “image” errors only; hence, the RSM direct approach does not support this generality.

Typically, “image element” error modeling in support of geopositioning can utilize a smaller number of corresponding adjustable parameters (errors) than does “image” error

modeling in support of triangulation. For example, for an optical push-broom sensor, both position and velocity adjustable parameters may be included for triangulation, but only position may be needed for geopositioning. Assuming wide sense stationary stochastic error processes, the “velocity effect” is captured by time correlation between position errors associated with different times (elements within the same or different images). This more general case of error modeling for geopositioning is most applicable to scanning sensors, such as push-broom sensors, when image scan time is relatively long.

Further details on “image element” and “restricted image element” error modeling are not provided here, since this “fine-grain” approach to error modeling is not necessary for most geopositioning applications.

The RSM support data associated with the indirect specification of error covariance contains one final, optional set of data. This data defines the “un-modeled error” covariance. This error covariance (\mathbf{C}_U) can be used to represent the summed effects in image space of all (high frequency) errors that can not be represented as errors in the original sensor model adjustable parameters, and hence, RSM adjustable parameters via its error covariance \mathbf{C}_R . Un-modeled errors are assumed “restricted image element” errors, where the element is defined as an image point, or image pixel (u, v) , and “time” between elements is defined as two-dimension pixel distance between pixel positions within the same image. Thus, these errors are modeled as wide sense stationary fields, i.e., their correlation function is a product of two correlation functions, one a function of image u distance and the other a function of image v distance. Also, there is no “mapping matrix” involved, as the errors are represented directly in image space. Other than these exceptions, specification of un-modeled error characteristics is done using the same approach as done for \mathbf{C}_R . In particular, the RSM image support data for image k supplies a 2×2 error covariance \mathbf{C}_{U_k} corresponding to un-modeled image line and sample errors at an arbitrary pixel position within the image. It also supplies the scalar correlation functions, ρ_u and ρ_v , that specify the correlation between arbitrary image pixel position pairs within the same image. If we assume there are m image measurements $(u, v)_i$ of interest in the image, the corresponding $2m \times 2m$ multi-measurement error covariance, expressed directly in image space, equals:

$$\mathbf{C}_U = \begin{bmatrix} \mathbf{C}_{U_{11}} & \mathbf{C}_{U_{12}} & \cdot & \cdot & \mathbf{C}_{U_{1m}} \\ \cdot & \mathbf{C}_{U_{22}} & \cdot & \cdot & \cdot \\ \cdot & \cdot & \cdot & \cdot & \cdot \\ \cdot & \cdot & \cdot & \cdot & \cdot \\ \cdot & \cdot & \cdot & \cdot & \mathbf{C}_{U_{mm}} \end{bmatrix}, \text{ where} \quad (18)$$

$$\mathbf{C}_{U_{ii}} = \mathbf{C}_{U_k} \quad \text{and} \quad \mathbf{C}_{U_{ij}} = \rho_u(\Delta u_{ij})\rho_v(\Delta v_{ij})\mathbf{C}_{U_k}.$$

If a geopositioning application involves more than one image, there can be multiple C_U 's, one for each image. However, the associated errors are uncorrelated between images. C_U is not needed for most applications. A simple example of its use, and independent of the original sensor model and RSM adjustable parameters, is the statistical characterization of excessive RSM ground-to-image fit errors, if they were to occur. (Note that for a geopositioning solution process, C_U is added directly to the mensuration error covariance Σ_M - see Equation 21 of section 4.1.1.)

3.2.3 Practical Considerations

It is recognized that in some applications, it may not be practical to generate an RSM error covariance with full fidelity. The RSM support data has the flexibility to provide error covariance information at any level, as summarized in Table 1 for cases ordered by increasing fidelity (Case 1 lowest fidelity).

Case	Description	Direct Error Covariance	Indirect Error Covariance
1	No information available and/or down-stream users do not require error covariance	Do not generate	Do not generate
2	Empirically derived diagonal covariance directly referencing the RSM adjustable parameters; no time correlation	Place directly into one-image Direct Error Covariance	An equivalent formulation possible; not described because Direct Error Covariance simpler
3	Like 2, but empirically derived time correlation between images from same sensor also applicable and available and described as piece-wise linear decay per uncorrelated subgroup (Typically a one-segment correlation decay to zero at time T and one uncorrelated subgroup)	An equivalent formulation possible for a set of known, correlated images; not described because Indirect Error Covariance more straightforward	Place covariance into original sensor model covariance portion of Indirect Error Covariance, place piece-wise linear decay function per uncorrelated subgroup into corresponding function, and set mapping matrix to the identity matrix.
4	Covariance referencing the original sensor model adjustable parameters is available; no time correlation (Covariance typically diagonal)	Place into one-image Direct Error Covariance; first transform to RSM adjustable parameter equivalent (sections 3.2.1 and 5.2 - resultant covariance is non-diagonal and image dependent)	An equivalent formulation possible; not described because Direct Error Covariance simpler
5	Like 4, but time correlation between images from same sensor also applicable and available and described as piece-wise linear decay per uncorrelated subgroup	An equivalent formulation possible for a set of known, correlated images; not described because Indirect Error Covariance more straightforward	Place into Indirect Error Covariance; first transform to RSM adjustable parameter equivalent (sections 3.2.2 and 5.2)
6	A correlated group of images from a triangulation. The triangulation's multi-image (full) error covariance is available	If from an RSM triangulation, place directly into multi-image Direct Error Covariance; if from an original sensor model triangulation, first transform to RSM adjustable parameter equivalent (sections 3.2.1 and 5.2) - resultant multi-image covariance is full (non-diagonal with non-zero cross-image blocks)	n/a

Table 1. Possible approaches to support data error covariance representation by increasing fidelity.

3.3 Time and illumination models

RSM includes a time-of-image model and an optional image illumination model in order to supply virtually all of the functionality associated with an original sensor model.

The detailed relationship between time and pixel position (image point coordinates) is embedded in the original sensor model's ground-to-image relationship, and hence, implicit in the RSM ground-to-image relationship. However, an explicit relationship between time and pixel position is still required for ancillary RSM applications, such as time interval calculations associated with the RSM indirect error covariance. The RSM time-of-image model is as follows:

$$t = t_0 + \left[\frac{u}{n_{ug}} \right] \cdot t_{ug} + \left[\frac{v}{n_{vg}} \right] \cdot t_{vg} , \text{ where} \quad (19)$$

t_0 is image acquisition time, n_{ug} is number of adjacent u positions acquired simultaneously, t_{ug} is time between adjacent u groups, n_{vg} is number of adjacent v positions acquired simultaneously, and t_{vg} is time between adjacent v groups. These various parameters are contained in the image's RSM support data. For a frame camera, t_{ug} and t_{vg} are typically set to 0, corresponding to one time applicable for the entire image. For a pushbroom sensor, there is typically a unique time for each image line, thus $n_{ug} = 1$, t_{ug} equals image line acquisition time, and $t_{vg} = 0$.

An image illumination model provides the direction of illumination associated with each pixel position within the image. For an optical sensor, it is the direction of the sun's illumination, while for a SAR sensor, it is the direction of incident radiation. Illumination direction information supports various image mensuration functions, such as height by shadow measurement. The RSM illumination model provides the azimuth angle (λ) and elevation angle (ψ) as a function of pixel position (u, v) for the associated ground point position (at a nominal elevation) as follows:

$$\begin{aligned} \lambda &= a_1 + a_2u + a_3v + a_4u^2 + a_5uv + a_6v^2 \\ \psi &= b_1 + b_2u + b_3v + b_4u^2 + b_5uv + b_6v^2 \end{aligned} \quad (20)$$

The various parameters defining these equations are contained in the image's RSM support data.

3.4 Support data format

A subset of eight possible groups of RSM image support data is associated with an image (see Table 2). Group 1 is always provided. It contains various identifiers and a time of image model and an optional illumination model. The RSM ground-to-image function is either a polynomial (Groups 2 and 3) or a grid (Groups 4 and 5). Either groups associated with a polynomial or groups associated with a grid must be provided. Group 6 contains the identity of the RSM adjustable parameters and their values, and is only required when their values are non-zero (adjusted). Group 7 contains the direct form of the support data error covariance (RSM direct error covariance), and Group 8 the indirect form (RSM indirect error covariance). Note that the identity of the RSM adjustable parameters corresponding to errors referenced by the error covariance are also contained in Groups 7 and 8. Although neither Group 7 nor Group 8 is explicitly required, one or the other must be included for a complete sensor model. Also, if the RSM ground-to-image function is a polynomial and there is only one image section, Group 2 need not be supplied. Similarly, if the RSM ground-to-image function is a grid and there is only one image section, Group 4 need not be supplied.

Group Number	Group Name	Summary of Contents
1	RSM Identification	Various id's, image footprint, time model, illumination model
2	Polynomial Identification	Ground-to-image polynomial image section information
3	Polynomial	Rational polynomial coefficients, offsets, and scale factors for a particular image section
4	Grid Identification	Ground-to-image grid image section information
5	Grid	Ground-to-image grid for a particular image section
6	Adjustments	RSM adjustable parameters selected and their values
7	Error covariance (direct)	RSM direct error covariance, including image id's and the number of RSM adjustable parameters per image
8	Error covariance (indirect)	Data for building RSM indirect error covariance, including current image's mapping matrix

Table 2. RSM support data groups summary.

The above groups and their contents reflect the current design for the RSM support data. (Each of the eight groups is associated with a planned NITF Tagged Record Extension, see section 6.1 for RSM development status.) Note that a typical image requires only one polynomial (section) and a direct error covariance. Therefore, only three groups would be required: 1, 3, and 7.

4.0 Geopositioning with RSM

Any geopositioning or triangulation solution technique, used in conjunction with an original sensor model and its image support data, can also be used in conjunction with RSM and its image support data, by simply substituting the original sensor model's adjustable ground-to-image function F , adjustable parameters δ_S , and associated error covariance C_S , with RSM's adjustable ground-to-image function G , adjustable parameters δ_R , and associated error covariance C_R , respectively.

Optimal geopositioning provides an optimal solution of an object's position using one or more images, where corrections to the image support data are not solved for, but image support data errors are correctly accounted for in the measurement weighting process. In particular, we define an optimal solution as the "Best Linear Unbiased Estimate" (B.L.U.E.). It is an unbiased estimate and a linear function of the measurement data. Of all unbiased and linear estimates, it has the minimum error variance or, equivalently, the minimum mean square error. Let us subsequently equate an "object" with a "ground point", and its corresponding three-dimensional ground point coordinate values with its "position", for convenience. An example of an optimal geopositioning algorithm using RSM follows.

4.1 Optimal algorithms

4.1.1 Geopositioning

An optimal solution for a ground point's position using $p \geq 1$ images requires optimal weighting of the multiple (conjugate) image measurements corresponding to the ground point. Weighting is primarily dependent on the multi-image (support data) error covariance \mathbf{C}_R . This weighting also significantly affects the solution's a posteriori error covariance, which can be used to generate reliable solution accuracy estimates.

The error covariance \mathbf{C}_R statistically describes the major error source affecting the ground point solution. The other error source is mensuration error, i.e., the errors in the identification and measurement of the ground point's conjugate image points (pixels). Its error covariance is represented as Σ_M .

Figures 8 and 9 graphically depict the optimal solution for a two-image (stereo) case and a general, multiple image case, respectively. For the two-image case, the optimal solution can be represented graphically as lying along the minimum separation vector between the two rays associated with the image measurements. It is midway along the vector only if the images have equal weight, e.g., the imaging geometry is symmetric, and \mathbf{C}_R 's diagonal blocks, $\mathbf{C}_{R_{11}}$ and $\mathbf{C}_{R_{22}}$, are equal. If one image has more accurate support data, the solution is closer to its ray. This typically occurs when either the images are from different sensors, or from the same sensor but acquired at significantly different times, e.g., from two different orbital passes for a space-borne sensor.

Because support data errors are most often the dominant error source, weighting is essentially inversely related to \mathbf{C}_R . Both the degree of correlation between errors associated with different adjustable parameters from the same image and between adjustable parameters from different images (characterized by the $\mathbf{C}_{R_{ij}}$ image cross-blocks) also significantly affect the weighting and subsequent solution. Proper weighting is only possible using the appropriate error covariance, \mathbf{C}_R if using RSM and \mathbf{C}_S if using the original sensor model. See section 4.1.3 (an expansion of details presented in

(Dowman and Dolloff, 2000)) for further discussion and examples on the importance of proper weighting. In general, the only solution unaffected by the use (or non-use) of the error covariance is the single-image (monoscopic) solution, since there is no redundant information (additional image measurements) available. However, without proper use of the error covariance, the solution's a posteriori error covariance is non-representative of the true solution errors.

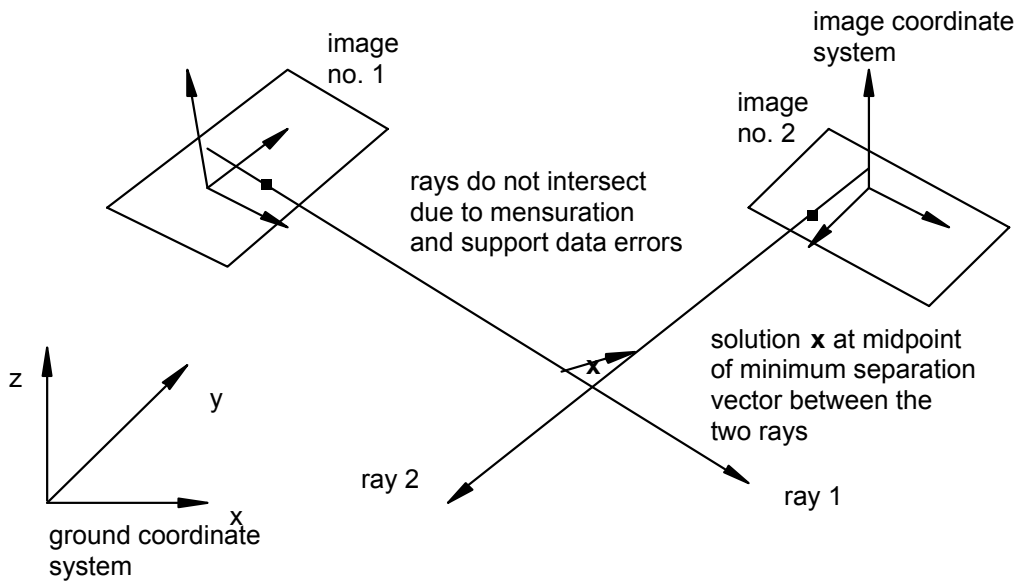


Figure 8. Optimal stereo solution.

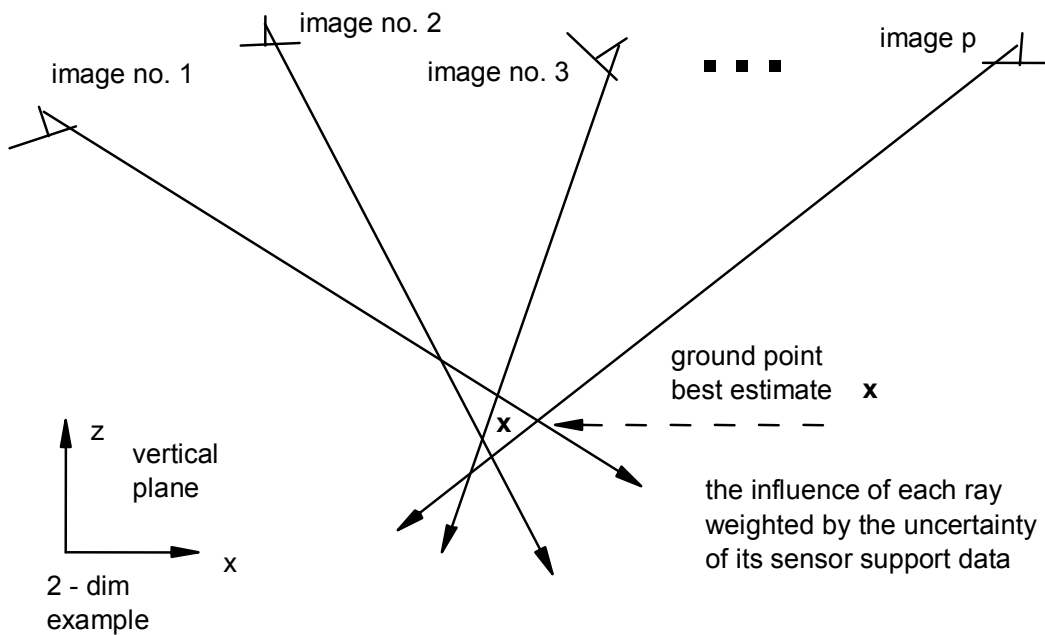


Figure 9. Optimal multi-image solution.

The following presents the equations defining the optimal solution for a ground point's three-dimensional position \mathbf{x} when using RSM. The general solution approach is weighted least squares with a priori estimate – [Sorrenson, 1980; Gelb, 1974; Bar-Shalom and Fortmann, 1988]. The solution is based on the linearization of a non-linear problem. The optimal solution is $\mathbf{x} = \mathbf{x}_0 + \delta_x$, where δ_x is a correction to an a priori position estimate \mathbf{x}_0 and computed as follows:

$$\delta_x = C_x \mathbf{B}^T \mathbf{W} \mathbf{z}, \text{ where} \tag{21}$$

$\mathbf{z} = (\mathbf{m} - \mathbf{m}_0)$ is the a priori measurement residual (misclosure) vector,
 $\mathbf{W} = (\Sigma_M + \mathbf{B}_R C_R \mathbf{B}_R^T)^{-1}$ the weight matrix, and
 $C_x = (C_{x_0}^{-1} + \mathbf{B}^T \mathbf{W} \mathbf{B})^{-1}$ the solution's a posteriori error covariance.

The algorithm iterates (sum δ_x into \mathbf{x}_0 , re-compute predicted measurements and partial derivatives) until convergence. Figure 10 summarizes the iterative solution process. Convergence of the solution typically occurs within two iterations when reasonably accurate a priori position estimates are utilized (on the order of a few hundred meters). Convergence occurs when image residuals stabilize between iterations and $\delta_x \rightarrow 0$.

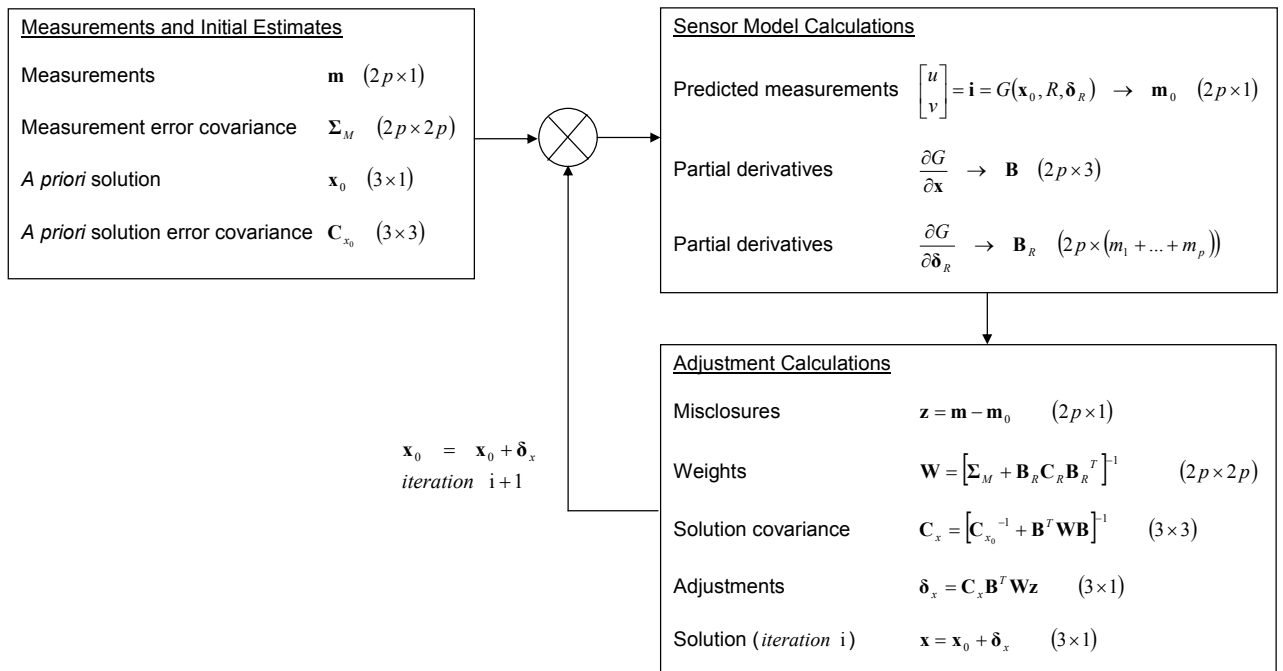


Figure 10. Optimal Geopositioning Solution Algorithm.

The following presents the detailed definitions associated with equation 21:

$\mathbf{x}_0 = [X \ Y \ Z]_0^T$ is 3×1 a priori ground point position,

$\mathbf{C}_{x_0} = E\{\boldsymbol{\varepsilon}_{x_0} \boldsymbol{\varepsilon}_{x_0}^T\}$ is 3×3 error covariance of a priori position \mathbf{x}_0 ,

$\boldsymbol{\delta}_x$ is 3×1 correction to a priori position,

$\mathbf{m} = [\mathbf{i}_1^T \ \dots \ \mathbf{i}_p^T]^T$ is $2p \times 1$ measurement vector containing a 2×1 image measurement of the ground position from each of p images,

$\mathbf{m}_0 = [G(\mathbf{x}_0, R_1, \boldsymbol{\delta}_{R_1})^T \ \dots \ G(\mathbf{x}_0, R_p, \boldsymbol{\delta}_{R_p})^T]^T$ is $2p \times 1$ predicted (a priori) measurements,

$\mathbf{B} = \partial \mathbf{m} / \partial \mathbf{x}$ is $2p \times 3$ partial derivatives of the measurements with respect to position and evaluated using predicted measurements at the a priori operating point (\mathbf{x}_0),

$\boldsymbol{\delta}_R = [\boldsymbol{\delta}_{R_1}^T \ \dots \ \boldsymbol{\delta}_{R_m}^T]^T$ is $m^* \times 1$ vector of RSM adjustable parameters from p images

($m^* = (m_1 + m_2 + \dots + m_p)$),

$\mathbf{B}_R = \partial \mathbf{m} / \partial \boldsymbol{\delta}_R$ is $2p \times m^*$ partial derivatives of measurements with respect to RSM adjustable parameters and evaluated using predicted measurements at the a priori operating point (\mathbf{x}_0),

$\boldsymbol{\Sigma}_M$ is $2p \times 2p$ error covariance for mensuration (image measurement) errors,

$\mathbf{C}_R = E\{\boldsymbol{\varepsilon}_R \boldsymbol{\varepsilon}_R^T\}$ is $m^* \times m^*$ error covariance for RSM adjustable parameters $\boldsymbol{\delta}_R$,

\mathbf{z} is $2p \times 1$ a priori measurement residual vector,

\mathbf{W} is $2p \times 2p$ image measurement weight matrix,

$\mathbf{x} = \mathbf{x}_0 + \boldsymbol{\delta}_x$ is 3×1 a posteriori solution - best estimate of position,

$\mathbf{C}_x = E\{\boldsymbol{\varepsilon}_x \boldsymbol{\varepsilon}_x^T\} = (\mathbf{C}_{x_0}^{-1} + \mathbf{B}^T \mathbf{W} \mathbf{B})^{-1}$ is 3×3 a posteriori solution error covariance.

Note that G is the RSM adjustable ground-to-image function, $\boldsymbol{\delta}_{R_i}$ the RSM adjustable parameter (values) for image i , and \mathbf{C}_R is the error covariance for the p sets of RSM adjustable parameters from p correlated images (see equations 14 and 15 through 17).

Note that if all images (support data errors) are not from a single correlated image group, \mathbf{C}_R contains cross-blocks of zero between independent groups of correlated images. For example, assume there are 5 images, 6 RSM adjustable parameters per image, 2 images in correlated group one with corresponding 12×12 error covariance \mathbf{C}_{R1} , and 3 images in correlated group two with corresponding 18×18 error covariance \mathbf{C}_{R2} . The 30×30 error

covariance \mathbf{C}_R would then be assembled as follows: $\mathbf{C}_R = \begin{bmatrix} \mathbf{C}_{R1} & \mathbf{0} \\ \mathbf{0} & \mathbf{C}_{R2} \end{bmatrix}$. Both \mathbf{C}_{R1} and

\mathbf{C}_{R2} are full (non-diagonal) matrices, and in general, the individual image blocks they contain are full as well. Further note that, in general, the weight matrix \mathbf{W} is a full matrix due to the projection of \mathbf{C}_R to image space via the partial derivative \mathbf{B}_R . Also, \mathbf{W} is inversely related to the sum of the projected support data error covariance (\mathbf{C}_R)

and the mensuration error covariance (Σ_M). Although it can be non-diagonal, the mensuration error covariance is typically a diagonal matrix with variances on the order of 1 pixel-squared down the diagonal.

The partial derivatives can be computed either analytically or numerically. For example, the 2×3 block of \mathbf{B} beginning in row $(i-1) \cdot 2 + 1$ and column 1 can be approximated with 2×3 numerical partial derivatives, represented symbolically as:

$$\Delta \mathbf{i}_i / \Delta \mathbf{x} = [G(\mathbf{x}_0 + \Delta \mathbf{x}, R_i, \delta_{R_i}) - G(\mathbf{x}_0, R_i, \delta_{R_i})] / \Delta \mathbf{x}, \quad (22)$$

where $\Delta \mathbf{x}$ is the appropriate step size. Note that δ_{R_i} is the current value (zero if unadjusted) of the RSM adjustment vector for image i .

Similarly, the $2 \times m_i$ block of \mathbf{B}_R beginning in row $(i-1) \cdot 2 + 1$ and column $(m_1 + \dots + m_{i-1}) + 1$ can be approximated with $2 \times m_i$ numerical partial derivatives, represented symbolically as:

$$\Delta \mathbf{i}_i / \Delta(\delta_{R_i}) = [G(\mathbf{x}_0, R_i, \delta_{R_i} + \Delta(\delta_{R_i})) - G(\mathbf{x}_0, R_i, \delta_{R_i})] / \Delta(\delta_{R_i}), \quad (23)$$

where $\Delta(\delta_{R_i})$ is the appropriate step size.

Of course, the three-dimensional $\Delta \mathbf{x}$ and the m_i -dimensional δ_{R_i} are perturbed one component at a time. Also, the numerical derivative technique outlined above is based on only one step (perturbation) per component, and is the fastest technique. Other techniques, such as the average of results from a step forward and a step back can be more accurate, and should be considered (See (Press, and Teukolsky, Vetterling, Flannery, 2002), chapter 5, for various numerical differentiation algorithms). In addition, when numerical partial derivatives are incorporated, and if the adjustable ground-to image function (G) utilizes multiple polynomials (*poly*) corresponding to different sections of the image, it is recommended that the same section be used during calculations corresponding to the same ground point.

Analytic partial derivatives involve the partial derivatives of the functions making up G , i.e., *poly* or *grid*, and i_adj or x_adj (see Figure 4). The following is a specific example assuming the use of *poly* and i_adj , and the nominal 6 RSM image space adjustable parameters (see Equation 12). Partial derivatives are computed for a two-dimensional image measurement from image i , with corresponding blocks of \mathbf{B} and \mathbf{B}_R designated by the subscript i :

$$\begin{aligned}
\mathbf{B}_i &= \frac{\partial G(\mathbf{x}, R_i, \delta_{R_i})}{\partial \mathbf{x}} \Big|_{\mathbf{x}=\mathbf{x}_0} \quad (2 \times 3 \text{ matrix}) \\
&= \frac{\partial poly(\mathbf{x}, R_i)}{\partial \mathbf{x}} \Big|_{\mathbf{x}=\mathbf{x}_0} + \frac{\partial i_adj(\mathbf{x}, R_i, \delta_{R_i})}{\partial \mathbf{x}} \Big|_{\mathbf{x}=\mathbf{x}_0} \\
&= \frac{\partial poly(\mathbf{x}, R_i)}{\partial \mathbf{x}} \Big|_{\mathbf{x}=\mathbf{x}_0} + \begin{bmatrix} \delta u_x \frac{\partial X^*}{\partial X} + \delta u_y \frac{\partial Y^*}{\partial X}, & \delta u_x \frac{\partial X^*}{\partial Y} + \delta u_y \frac{\partial Y^*}{\partial Y}, & \delta u_x \frac{\partial X^*}{\partial Z} + \delta u_y \frac{\partial Y^*}{\partial Z} \\ \delta v_x \frac{\partial X^*}{\partial X} + \delta v_y \frac{\partial Y^*}{\partial X}, & \delta v_x \frac{\partial X^*}{\partial Y} + \delta v_y \frac{\partial Y^*}{\partial Y}, & \delta v_x \frac{\partial X^*}{\partial Z} + \delta v_y \frac{\partial Y^*}{\partial Z} \end{bmatrix} \Big|_{\mathbf{x}=\mathbf{x}_0} \quad (24) \\
&= \frac{\partial poly(\mathbf{x}, R_i)}{\partial \mathbf{x}} \Big|_{\mathbf{x}=\mathbf{x}_0}, \quad \text{if } \delta_{R_i} = 0 \text{ (unadjusted)}.
\end{aligned}$$

$$\mathbf{B}_{R_i} = \frac{\partial G(\mathbf{x}, R_i, \delta_{R_i})}{\partial \delta_{R_i}} \Big|_{\mathbf{x}=\mathbf{x}_0} = \frac{\partial i_adj(\mathbf{x}, R_i, \delta_{R_i})}{\partial \delta_{R_i}} \Big|_{\mathbf{x}=\mathbf{x}_0} = \begin{bmatrix} 1 & X^* & Y^* & 0 & 0 & 0 \\ 0 & 0 & 0 & 1 & X^* & Y^* \end{bmatrix} \quad (2 \times 6 \text{ matrix})$$

The entries X^* and Y^* correspond to the horizontal coordinates of \mathbf{x}_0 expressed in the local system for image i as described in section 3.1.3. In general, analytic partial derivatives associated with x_adj and RSM ground space adjustable parameters will be somewhat more complex than above because x_adj actually involves more than an additive correction to \mathbf{x} , and \mathbf{x} is an input, not an output, of the ground-to-image function.

The a priori position estimate \mathbf{x}_0 used in Equation 21, and in its various ancillary calculations, such as partial derivatives, can be initialized with the RSM adjustable image-to-ground function for any image i selected from the p images (or the averaged results from all the images). This function is an iterative inverse of the RSM adjustable ground-to-image function, and represented symbolically as $\mathbf{h} = G^{-1}(\mathbf{i}_i, Z_0, R_i, \delta_{R_i})$, where \mathbf{h} is two-dimensional horizontal position. Both the two-dimensional image measurement \mathbf{i}_i and an a priori estimate of height Z_0 are input, and the a priori position estimate set equal to the a priori height and resultant horizontal position, i.e., $\mathbf{x}_0 = [\mathbf{h}^T \quad Z_0]^T$. Also, the corresponding a priori error covariance \mathbf{C}_{x_0} is set to a diagonal matrix with large variance (typically $1 \times 10^8 \text{ m}^2$) down the diagonals. Because the values are large, little weight is given to the a priori estimate (nor should it be, since the estimate is actually correlated with the sensor support data via this practical initialization process). However, the use of \mathbf{C}_{x_0} insures a stable solution, particularly in the case of poor imaging geometry. Regarding the values of \mathbf{C}_{x_0} , a monoscopic solution ($p = 1$) is an exception. The a priori height comes from the intersection of an imaging locus with a Digital Elevation Model (DEM), and the (3,3) element of \mathbf{C}_{x_0} is set to the DEM's variance of elevation error. Further details on the RSM adjustable image-to-ground function are presented in section 4.2.

Note that if the coordinate system for \mathbf{x} is any other than the Geodetic coordinate system (or Rectangular) used by the RSM adjustable ground-to-image function G , \mathbf{x} is simply converted to Geodetic coordinates prior to calling G . Similarly, the output \mathbf{x} from the RSM adjustable image-to-ground function can be converted from Geodetic coordinates to the other coordinate system.

4.1.2 Multi-ground point geopositioning and triangulation

Equation 21 also provides a simultaneous best estimate for multiple ground points by simply augmenting the defined variables in the appropriate manner. In particular, δ_x (and \mathbf{x}_0, \mathbf{x}) is augmented with the additional ground points for solution, \mathbf{m} is augmented with additional measurements to the additional ground points, \mathbf{B} is expanded in accordance with the additional image measurements and ground points, \mathbf{B}_R and \mathbf{W} are expanded in accordance with the additional image measurements, and \mathbf{C}_{x_0} is expanded in accordance with the additional ground points for solution. In particular, assuming k ground points, δ_x becomes a $3k \times 1$ vector, \mathbf{m} a $2q \times 1$ vector, where q is the total number of image measurements from p images to k ground points, \mathbf{B} a $2q \times 3k$ matrix, \mathbf{B}_R a $2q \times m^*$ matrix, \mathbf{W} a $2q \times 2q$ matrix, and \mathbf{C}_{x_0} a $3k \times 3k$ matrix.

Equation 21 is also directly related to triangulation. In particular, if Equation 21 is further augmented to solve for δ_R for all relevant (p) images, as well as to solve for numerous (k) tie and ground control points measured in the images, i.e.,

$$\delta_x \rightarrow \begin{bmatrix} \delta_R \\ \delta_x \end{bmatrix} = \begin{bmatrix} \delta_R^T & \delta_x^T \end{bmatrix}^T = \begin{bmatrix} \delta_{R_1}^T & \dots & \delta_{R_p}^T & \delta_{x_1}^T & \dots & \delta_{x_k}^T \end{bmatrix}^T, \text{ it becomes a triangulation}$$

solution:

$$\begin{bmatrix} \delta_R \\ \delta_x \end{bmatrix} = \left(\begin{bmatrix} \mathbf{C}_R^{-1} & 0 \\ 0 & \mathbf{C}_{x_0}^{-1} \end{bmatrix} + \begin{bmatrix} \mathbf{B}_R^T \\ \mathbf{B}^T \end{bmatrix} \Sigma_M^{-1} \begin{bmatrix} \mathbf{B}_R & \mathbf{B} \end{bmatrix} \right)^{-1} \begin{bmatrix} \mathbf{B}_R^T \\ \mathbf{B}^T \end{bmatrix} \Sigma_M^{-1} (\mathbf{m} - \mathbf{m}_0), \quad (25)$$

where δ_R is dimension $m^* \times 1$, the weight matrix \mathbf{W} becomes Σ_M^{-1} , and the elements of \mathbf{C}_{x_0} corresponding to the control points contain their improved (smaller) accuracies relative to the tie points (Consistent with the assumptions for support data and mensuration errors, control point errors are assumed unbiased; hence, their error covariance is a statistical measure of accuracy.) Like the geopositioning solution process, the triangulation solution process is also iterative (sum δ_x into \mathbf{x}_0 and δ_R into a δ_{R0} between iterations and re-compute predicted measurements and partial derivatives). Note that all vectors and matrices in Equation 25 are expanded and augmented in accordance with the previous paragraphs describing a multiple ground point geopositioning solution.

Equation 25 is based on a direct solution (matrix inversion) of the corresponding normal equations. The normal equations may be written as:

$$\left(\begin{bmatrix} \mathbf{C}_R^{-1} & 0 \\ 0 & \mathbf{C}_{x_0}^{-1} \end{bmatrix} + \begin{bmatrix} \mathbf{B}_R^T \\ \mathbf{B}^T \end{bmatrix} \Sigma_M^{-1} \begin{bmatrix} \mathbf{B}_R & \mathbf{B} \end{bmatrix} \right) \begin{bmatrix} \delta_R \\ \delta_x \end{bmatrix} = \begin{bmatrix} \mathbf{B}_R^T \\ \mathbf{B}^T \end{bmatrix} \Sigma_M^{-1} (\mathbf{m} - \mathbf{m}_0) \quad (26)$$

In some scenarios the number of parameters for solution may become very large. Therefore, Equation 26 is usually solved for by means other than direct matrix inversion. (See (Mikhail, 1976; Mikhail and Bethel and McGlone, 2001) for solution techniques as well as a general description of triangulation.)

Similar to its role in a geopositioning solution, \mathbf{C}_R also plays an important role in a triangulation solution. It represents the a priori accuracy of the support data to be adjusted, i.e., $\mathbf{C}_R = E\{\boldsymbol{\varepsilon}_R \boldsymbol{\varepsilon}_R^T\}$, where the a priori value of δ_R is zero. The larger the value of \mathbf{C}_R , the larger the statistically permitted adjustment to the RSM support data. Its influence on the solution increases as the number of control points and/or their accuracy decreases. In fact, there are many triangulations that involve no ground control points; thus, \mathbf{C}_R is a dominating factor. They occur for relative orientations and for absolute orientations involving overlapping groups of images from different sensors. The images from the more accurate sensor are used to control the images from the other via the tie points.

Note that, strictly interpreted, a triangulation based on RSM is not a bundle adjustment, i.e., directly tied to the effects of the sensor's physical parameters on the "bundle of rays". Also, analogous to \mathbf{C}_S , \mathbf{C}_R is required to be positive definite (hence, invertible) for the triangulation solution, but only positive semi-definite for the geopositioning solution, since Σ_M is assumed positive definite. In addition, when the augmentation of Equation 21 corresponds to a multi-ground point and multi-image geopositioning solution and not a triangulation solution (it does not include δ_R for solution), it can still be considered a triangulation's partitioned solution for ground points; analogous to the solution of the reduced normal equations, but for the ground point adjustments instead of sensor parameter adjustments.

Finally, if a downstream user adjusts the RSM image support data by a triangulation, the RSM image support data format supports the inclusion of the corresponding adjustable parameter values and related error covariance. (Note that the initial RSM ground-to-image function does not change.) Thus, the user need only modify the applicable RSM image support data accordingly and disseminate it to others, if so desired.

4.1.3 Optimal versus non-optimal solution comparisons

A simulation was performed to illustrate the advantages of an optimal geopositioning algorithm. A set of two-ground point, multi-image geopositioning solutions were first performed using the original sensor model to illustrate the effects of additional images

and proper weighing on the solution. An additional solution was then performed using an RSM counterpart to illustrate its virtually identical results. The sensor simulated was relatively simple, as described below, but adequate to demonstrate the principals of optimal geopositioning.

A space-born sensor was emulated using a simulated frame camera with seven sensor error (adjustable) parameters consisting of position, attitude, and focal length errors. A focal length of 3 meters and a vertical ground sample distance of 3 m were assumed. Images were 10k×10k pixels. Six images were simulated, three from each of two passes. The sensor support data errors were modeled as time correlated errors for images from the same pass. Figure 11 illustrates the imaging geometry for this scenario and Figure 12 the corresponding image footprints and horizontal position for the two ground points for solution. The elevations above the local tangent plane for the two ground points were 1000 m and 300 m, respectively. The imaging geometry was relatively poor, with object-to-image elevation angles ranging from about 35 to 45 degrees relative to the local ground tangent plane, and convergence angles between pairs of same pass images ranging from about 8 to 35 degrees.

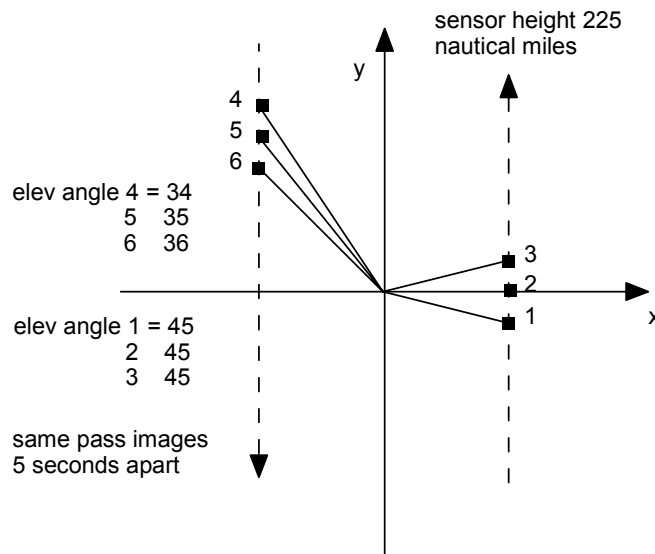


Figure 11. Imaging geometry.

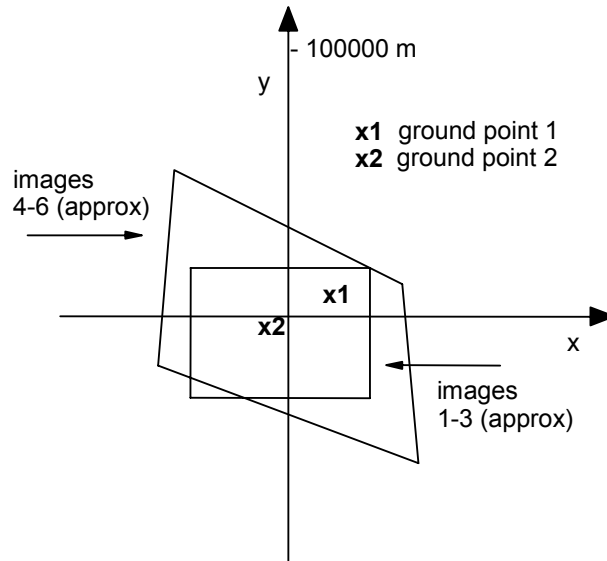


Figure 12. Image footprints.

Table 3 presents the original sensor model's support data error characteristics for images 1-3. Support data error standard deviations ("sigma's") were ten times larger for images 4-6. Let us term images 1-3 as coming from "Pass 1", and images 4-6 as coming from "Pass 2". Images within the same pass have correlated support data errors, and images from different passes are uncorrelated. Support data errors were modeled as wide-sense stationary, Gauss-Markov, stochastic processes, a commonly used error model.

Error parameter	Sigma	Time Const
Along track position	4 m	2000 s
Cross track position	8 m	3000 s
Radial position	2 m	1000 s
Rotation ω	.00001 rad	200 s
Rotation ϕ	.00001 rad	100 s
Rotation κ	.0002 rad	300 s
Focal	.001 m	5000 s

Table 3. Sensor support data error characteristics for Pass 1 images.

The original sensor model's adjustable parameters for image i from Pass 1 consist of a 7×1 vector δ_{S_i} with adjustments to along track position, .., focal length, with corresponding error covariance $C_{S_{ii}}$, consisting of a diagonal matrix with the square of the corresponding sigma's from Table 3 down the diagonal. The value of δ_{S_i} is zero, with the covariance of the value's error represented by $C_{S_{ii}}$. The cross covariance $C_{S_{ij}}$ between images i and j from pass 1 is a diagonal matrix with diagonal elements equal to the corresponding diagonal elements in $C_{S_{ii}}$ multiplied by the applicable correlations. The time constants of Table 3 specify the correlations. For example, the time constant for rotation (attitude) error ω about the focal plane axis x equals 200 seconds; thus, the correlation between rotation ω errors from images i and j equal $e^{-\tau_{ij}/T}$, where $T = 200$ seconds, and τ_{ij} is the absolute value of the time difference between the images. For images 1 and 3, $\tau_{ij} = 10$ seconds, and the correlation equals $e^{-\tau_{ij}/T} = e^{-.05} = 0.95$. The $C_{S_{ii}}$ and $C_{S_{ij}}$ corresponding to images from Pass 2 are identical in form to those of Pass 1, except that they are 100 times larger.

In particular, if we designate C_S as the 42×42 error covariance corresponding to the collective support data adjustable parameters for images one through six (Pass 1 and Pass 2):

$$C_S = \begin{bmatrix} C_{S11} & C_{S12} & C_{S13} & 0 & 0 & 0 \\ C_{S12}^T & C_{S22} & C_{S23} & 0 & 0 & 0 \\ C_{S13}^T & C_{S23}^T & C_{S33} & 0 & 0 & 0 \\ 0 & 0 & 0 & C_{S44} & C_{S45} & C_{S46} \\ 0 & 0 & 0 & C_{S45}^T & C_{S55} & C_{S56} \\ 0 & 0 & 0 & C_{S46}^T & C_{S56}^T & C_{S66} \end{bmatrix}_{42 \times 42}, \text{ and where, for example, } \quad (27)$$

$$C_{S11} = \begin{bmatrix} 4^2 & 0 & 0 & 0 & 0 & 0 & 0 \\ 0 & 8^2 & 0 & 0 & 0 & 0 & 0 \\ 0 & 0 & 2^2 & 0 & 0 & 0 & 0 \\ 0 & 0 & 0 & .00001^2 & 0 & 0 & 0 \\ 0 & 0 & 0 & 0 & .00001^2 & 0 & 0 \\ 0 & 0 & 0 & 0 & 0 & .0002^2 & 0 \\ 0 & 0 & 0 & 0 & 0 & 0 & .001^2 \end{bmatrix}_{7 \times 7} \quad \text{and}$$

$$\mathbf{C}_{S13} = \begin{bmatrix} e^{\frac{-10}{2000}} 4^2 & 0 & 0 & 0 & 0 & 0 & 0 \\ 0 & e^{\frac{-10}{3000}} 8^2 & 0 & 0 & 0 & 0 & 0 \\ 0 & 0 & e^{\frac{-10}{1000}} 2^2 & 0 & 0 & 0 & 0 \\ 0 & 0 & 0 & e^{\frac{-10}{200}} .00001^2 & 0 & 0 & 0 \\ 0 & 0 & 0 & 0 & e^{\frac{-10}{100}} .00001^2 & 0 & 0 \\ 0 & 0 & 0 & 0 & 0 & e^{\frac{-10}{300}} .0002^2 & 0 \\ 0 & 0 & 0 & 0 & 0 & 0 & e^{\frac{-10}{5000}} .001^2 \end{bmatrix}_{7 \times 7}$$

(Note that if the six images had also been adjusted simultaneously in a triangulation process prior to the geopositioning solution, in general, all the adjustable parameter (errors) would be correlated and all the zeros replaced with non-zero values in the above matrices.)

A simulation was performed 100 times, with a different set of random numbers utilized each time consistent with all error sources, their standard deviations, and their correlations. In addition to sensor support data errors, mensuration errors (0.5 pixel, one-sigma) and errors in the a priori estimates of the two ground points (1000 m, one-sigma, for all three ground components) were generated. At the end of each simulation run, a number of different original solutions were performed using the same measurements and a priori ground point estimates: (1) an optimal solution “Original 1”, (2) an optimal solution “Original 2”, (3) a non-optimal solution “Original 2 No Correlation”, and (4) a non-optimal solution “Original 2 Equal Weight”. “1” indicates that a solution utilized measurements from Pass One, images 1-3, and “2” indicates that a solution utilized measurement from both Pass One and Pass Two, images 1-6. “Original” indicates an optimal solution using the original sensor model and Equation 21 (with F, δ_S, C_S substituted for G, δ_R, C_R , respectively). “Original No Correlation” indicates that the solution incorrectly ignores the correlation between sensor support data errors between different images, i.e., assumes all are uncorrelated ($C_{S_{ij}} = 0$). “Original Equal Weight” indicates all image measurements from all images are incorrectly given an equal weight of 1.0, i.e., the sensor support error covariance C_S is not used for weighting.

Table 4 presents the simulation and solution results. The solutions’ actual position errors (“rms”) are presented as well as their corresponding error propagation or accuracy estimates (“sigmas”). Absolute statistics (“abs”) refer to ground point 1, relative statistics (“rel”) refer to the ground point 1-ground point 2 pair; units are meters.

Solution position error was calculated as the root-mean-square (rms) error over the 100 runs in each ground coordinate ($X-Y-Z$). The absolute position error for each individual run was computed by differencing the solution’s ground point position from the true ground point position for both ground points 1 and 2, and also subtracting the

two differences for their relative position error, i.e., the ground point 1 absolute position error is $(\mathbf{x}_1 - \mathbf{x}_{T1})$ and the ground point 1-ground point 2 relative position error is $((\mathbf{x}_1 - \mathbf{x}_{T1}) - (\mathbf{x}_2 - \mathbf{x}_{T2}))$, where the subscript T represents the true position. Solution error propagation results were represented as $(X - Y - Z)$ standard deviations computed from the solution a posteriori error covariance averaged over the 100 runs. The a posteriori error covariance was virtually invariant over the 100 runs.

In addition to absolute accuracy, relative accuracy is an important solution metric in most geopositioning and triangulation applications. (Here, the term “accuracy” represents both the statistical characterization of a solution’s actual ground point position error as well as its corresponding estimated or predicted characterization, i.e., error propagation.) In a properly modeled solution, relative accuracy is almost always less than $\sqrt{2}$ times the absolute accuracy, due to the positive correlation of solution position errors between the various ground points which use the same images (support data errors) for measurements. In many cases, relative accuracy is significantly better (less than) the absolute accuracy. (Thus, when comparing a candidate replacement sensor model’s solution to an original solution, relative accuracy should always be considered explicitly. Similar absolute accuracy between the two solutions does not automatically insure similar relative accuracy.)

Solution	abs rms X-Y-Z (m)	abs sigma X-Y-Z (m)	rel rms X-Y-Z (m)	rel sigma X-Y-Z (m)
original_1	38 32 34	40 37 37	40 39 39	42 41 41
original_2	29 24 26	30 27 28	19 18 17	18 16 16
original_2_no_cor	45 41 44	28 26 27	21 21 19	13 12 12
original_2_eq_wt	55 58 53	n/a	29 27 29	n/a
replacement_1	38 32 34	40 37 37	40 39 39	42 41 41
replacement_2	29 24 26	30 27 28	19 18 17	18 16 16

Table 4. Solution performance.

Original 1 is the optimal solution using measurements from images 1-3. Note that its actual position errors (“rms”) are in close agreement with its estimated position errors from the solution’s error propagation (“sigma”), indicative of a well-modeled solution. Original 2 utilizes additional measurements from images 4-6. The solution improves significantly relative to Original 1, even though the additional images’ support data errors are much larger, corresponding to standard deviations ten times as large. This illustrates the benefits of using images from different passes or different sensors. Even if their support data errors are significantly larger, their improvement in overall image-to-object geometry can make them well worthwhile. And, of course, if the additional images’

support data errors are of the same statistical magnitude as those of the initial images, solution results will improve even more. In particular, Original 2 absolute accuracy would be on the order of 10 meters, or about three times as accurate as the Original 1 solution. In addition, using more simultaneous measurements (images) allows for more meaningful blunder detection and editing processes, when included in the solution process.

The degradation in Original 2 No Correlation solution results relative to Original 2 illustrates the importance of accounting for correlated support data errors in the solution process. Also, note the unreliability of the solution's estimated accuracy relative to the true solution accuracy ("sigma" vs. "rms").

The degradation in Original 2 Equal Weight solution results relative to Original 2 is even more pronounced, illustrating the general importance of (inversely) weighting the image measurements by their support data error covariance. Also, with artificial equal weighting, there are no meaningful accuracy estimates provided by the solution. This is a significant loss. In many geopositioning applications, timely and reliable accuracy estimates are as critical as the solution's ground point position.

Note that, although the simulation implemented a geopositioning solution, all of the above general observations regarding the advantages of using many measurements (images), and the need to utilize the appropriate sensor support data (adjustable parameter) error covariance and error cross-covariance (time correlations), are equally applicable to triangulation solutions. Triangulation solutions based on artificially equal, or simplistic, weighting should be avoided if at all possible.

Of course, it must be mentioned that all the advantages described previously with an optimal geopositioning (or triangulation) solution are predicated on the availability of a support data error covariance that is reasonably consistent with actual support data errors. In the real-world, this can be somewhat problematic for some sensors.

In addition to the various original solutions discussed above, RSM geopositioning counterparts to Original 1 and Original 2, termed Replacement 1 and Replacement 2, respectively, were also performed for each of the same 100 runs. For each RSM solution, the RSM adjustable parameter vector δ_{R_i} for an image i consisted of the nominal 6 image space adjustable parameters (see Equation 12), and the corresponding multi-image direct error covariance C_R was generated from its C_S counterpart, as described in sections 3.2.1 and 5.2. C_R corresponds to 3 images (18 adjustable parameters) for Replacement 1, and 6 images (36 adjustable parameters) for Replacement 2. (An actual RSM ground-to-image polynomial was not generated for simplicity. Thus, fit error was assumed zero; not overly optimistic considering actual fit error is expected to be less than 0.01 pixels (rms), see section 6.2). The RSM solutions used the same general algorithm (Equation 21) as did the Original 1 and Original 2 solutions.

Table 4 also presents the Replacement 1 and Replacement 2 results. They are virtually identical to the Original 1 and Original 2 results, respectively. In addition, section 6.2.2

presents RSM to original solution comparisons, using real (non-simulated) data corresponding to push-broom sensors, and full RSM generation.

Finally, let us discuss \mathbf{C}_R in a little more detail. The following is the form for the three-image direct error covariance \mathbf{C}_R utilized in the Replacement 1 solution. \mathbf{C}_R is provided directly in the RSM support data, and is generated as described in section 5.2. An entry \mathbf{C}_{Rij} corresponds to images i and j and is computed, prior to its placement in the RSM support data, using its original sensor model counterpart \mathbf{C}_{Sij} , the image i mapping matrices Φ_i , and the image j mapping matrix Φ_j . Since there are 6 RSM adjustable parameters and 7 original sensor model adjustable parameters per image, \mathbf{C}_{Sij} is a 7×7 matrix, Φ_i a 6×7 matrix, and \mathbf{C}_{Rij} a 6×6 matrix.

$$\mathbf{C}_R = \begin{bmatrix} \mathbf{C}_{R11} & \mathbf{C}_{R12} & \mathbf{C}_{R13} \\ \mathbf{C}_{R12}^T & \mathbf{C}_{R22} & \mathbf{C}_{R23} \\ \mathbf{C}_{R12}^T & \mathbf{C}_{R12}^T & \mathbf{C}_{R33} \end{bmatrix}_{18 \times 18}, \text{ and in more detail,} \quad (28)$$

$$\mathbf{C}_R = \begin{bmatrix} \Phi_1 \mathbf{C}_{S11} \Phi_1^T & \Phi_1 \mathbf{C}_{S12} \Phi_2^T & \Phi_1 \mathbf{C}_{S13} \Phi_3^T \\ \Phi_2 \mathbf{C}_{S12}^T \Phi_1^T & \Phi_2 \mathbf{C}_{S22} \Phi_2^T & \Phi_2 \mathbf{C}_{S23} \Phi_3^T \\ \Phi_3 \mathbf{C}_{S13}^T \Phi_1^T & \Phi_3 \mathbf{C}_{S23}^T \Phi_2^T & \Phi_3 \mathbf{C}_{S33} \Phi_3^T \end{bmatrix}_{18 \times 18}$$

Note that in this particular example, the structure of \mathbf{C}_S is also consistent with three images $\{1,2,3\}$ from the same sensor and with errors corresponding to a wide sense stationary stochastic error process with an a priori time correlation model, i.e., \mathbf{C}_{Sii} and image i 's time correlation model are identical for all three images, and \mathbf{C}_{Sij} can be computed for any i and j using them. Thus, \mathbf{C}_R can also be represented as an indirect error covariance, if so desired. In this case, each image i would supply its own unique Φ_i , the (common) data representing \mathbf{C}_{Sii} , and the (common) a priori time correlation model, and hence, \mathbf{C}_{Sij} for any j . The RSM user would then compute \mathbf{C}_R exactly as specified in Equation 28. Regarding the data representing \mathbf{C}_{Sii} and \mathbf{C}_{Sij} , for this particular example there are 7 uncorrelated error subgroups, each corresponding to one adjustable parameter. Thus, for each entry in Table 3, the corresponding variance ("Sigma" squared) is supplied in the RSM support data as well as the parameters defining a piece-wise linear decay time correlation model (Figure 7) that closely models the effect of the time constant ("Time const"). (Note that in practice, the original sensor model would actually be modeled using the piece-wise linear decay time correlation model directly, and the parameters for that model directly available for the RSM support data.)

4.2 Adjustable image-to-ground function

The RSM adjustable image-to-ground function is an iterative inverse of the RSM adjustable ground-to-image function. Given a two-dimensional image point coordinate \mathbf{i} and a priori ground point height above the ellipsoid Z_0 , it provides the corresponding two-dimensional horizontal ground point coordinate $\mathbf{h} \equiv [X \ Y]^T$. The resultant three-dimensional ground point coordinate is represented as $\mathbf{x} = [\mathbf{h}^T \ Z_0]^T = [X \ Y \ Z_0]^T$. The RSM adjustable image-to-ground function is represented symbolically as follows:

$$\mathbf{h} = G^{-1}(\mathbf{i}, Z_0, R, \delta_R), \quad (29)$$

where $\mathbf{h} = [X \ Y]^T$, Z_0 is the desired (a priori) height above the ellipsoid, $\mathbf{i} = [u \ v]^T$, R the RSM sensor support data for the associated image, and δ_R is the corresponding RSM adjustable parameter value.

An algorithm for computing $G^{-1}(\mathbf{i}, Z_0, R, \delta_R)$ is as follows:

set \mathbf{h}_1 to a corresponding a priori estimate of \mathbf{h} inside the image footprint (30)

set estimate of 3×1 ground point coordinate $\mathbf{x}_1 = [\mathbf{h}_1^T \ Z_0]^T$

set loop index $i = 1$

compute 2×1 $\mathbf{i}_i = G(\mathbf{x}_i, R, \delta_R)$

compute 2×1 $\Delta \mathbf{i}_i = \mathbf{i} - \mathbf{i}_i$

compute 2×2 partial derivative matrix $(\partial \mathbf{h} / \partial \mathbf{i})_i$

compute 2×1 $\Delta \mathbf{h}_i = (\partial \mathbf{h} / \partial \mathbf{i})_i \Delta \mathbf{i}_i$

set new estimate of ground point coordinate $\mathbf{x}_{i+1} = [(\mathbf{h}_{i+1})^T \ Z_0]^T = [(\mathbf{h}_i + \Delta \mathbf{h}_i)^T \ Z_0]^T$

set output $\mathbf{h} = \mathbf{h}_{i+1}$

check magnitude of $\Delta \mathbf{i}_i$ for convergence

increment i and repeat loop if non-convergence

The a priori estimate of \mathbf{h} required to seed the above algorithm can be set to the horizontal coordinates of a “reference ground point” that is provided in the RSM support data for the image. However, to insure convergence when the image geometry varies significantly over the corresponding ground footprint, it can also be set to the horizontal ground point coordinates computed by the interpolation, at height Z_0 and image point coordinate \mathbf{i} , of eight ground point-image point correspondences also provided in the RSM support data. The individual ground points correspond to an image corner position at either the maximum or minimum height from an a priori height range (typically corresponding to the height range used to generate the image’s RSM ground-to-image function).

The partial derivatives used above are usually computed numerically and as follows:

$$\begin{aligned} \text{compute } [\delta u / \delta X \quad \delta v / \delta X] &= (1 / \delta X) \left[G(\mathbf{x}_i + [\delta X \quad 0 \quad 0]^T, R, \delta_R) - G(\mathbf{x}_i, R, \delta_R) \right]^T \quad (31) \\ \text{compute } [\delta u / \delta Y \quad \delta v / \delta Y] &= (1 / \delta Y) \left[G(\mathbf{x}_i + [0 \quad \delta Y \quad 0]^T, R, \delta_R) - G(\mathbf{x}_i, R, \delta_R) \right]^T \\ \text{set } (\partial \mathbf{h} / \partial \mathbf{i})_i &= \begin{bmatrix} \delta X / \delta u & \delta X / \delta v \\ \delta Y / \delta u & \delta Y / \delta v \end{bmatrix} = \begin{bmatrix} \delta u / \delta X & \delta u / \delta Y \\ \delta v / \delta X & \delta v / \delta Y \end{bmatrix}^{-1} \end{aligned}$$

Typical step sizes for δX and δY are on the order of $10 \cdot GSD$, and typical convergence criteria for the magnitude of $\Delta \mathbf{i}_i$ is 0.001 pixels for both the u and v components. GSD is the ground sample distance, preferably computed at the reference ground point and relative to the ground plane perpendicular to the imaging locus at the reference ground point, with units of meters/pixel. Note that the RSM adjustable image-to-ground function (G^{-1}) is independent of whether the RSM adjustable ground-to-image function (G) is based on a polynomial or a grid.

5.0 RSM Generation

This section describes how to generate the RSM (image support data).

5.1 Ground-to-image function

5.1.1 Ground-to-image function polynomial

The RSM ground-to-image function polynomial ($poly(\mathbf{x}, R)$) can be generated manually, semi-automatically, or automatically. If generated manually, the number of image sections and their locations are specified, and a polynomial generated for each. Each polynomial is also specified as a numerator-only polynomial or a rational polynomial. The polynomial order is specified as well prior to its generation.

The other extreme is automatic generation, where various candidate polynomials are automatically generated and their fit accuracy relative to the original sensor model's ground-to-image relationship automatically assessed. The process stops when the pre-defined fit accuracy is met. The overall process has an outer loop over image sectioning and an inner loop over polynomial order (pre-defined minimum and maximum). The image can be divided into 1 to 256 sections in the image row direction, and from 1 to 256 sections in the image column direction, with a constraint of no more than a total of 256 rectangular sections. Either numerator-only polynomials, rational polynomials, or both types are pre-definable as candidates. Parameters affecting the overall process, such as fit accuracy requirements, allowed polynomial order, and maximum number of image sections allowed can be predefined by sensor type. Typically, for either a geodetic or a local tangent plane ground coordinate system, the polynomial's X and Y orders are the same, but the Z order may be less. If the above process does not provide a polynomial with sufficient fit accuracy, an interpolated grid may be selected as the RSM ground-to-image function.

Typical fit accuracy requirements are less than 0.05 pixels (rms). This requirement is typically met with only one section per image. The actual polynomial generation process for a pre-determined image section is now defined. The polynomial is assumed applicable to the line image coordinate u , since the process is identical for the polynomial for the sample image coordinate v .

In general, there are three practical approaches to the polynomial generation process. They are represented symbolically as follows:

$$\begin{array}{ll}
 (1) \mathbf{c} = \mathbf{D}\mathbf{m} & \text{Linear} \\
 (2) \mathbf{c} = \mathbf{D}(\mathbf{m})\mathbf{m} & \text{Quasi-linear-1} \\
 (3) \Delta\mathbf{c} = \mathbf{D}(\mathbf{c}_0)\Delta\mathbf{m} \ , \ \mathbf{c} = \mathbf{c}_0 + \Delta\mathbf{c} & \text{Quasi-linear-2}
 \end{array} \tag{32}$$

The first approach solves for the vector of polynomial coefficients \mathbf{c} as a true linear function of the vector of image measurements \mathbf{m} associated with the fit grid. \mathbf{D} is a measurement-to-coefficient mapping matrix, whose values are independent of the measurements \mathbf{m} and any a priori estimate \mathbf{c}_0 of the coefficients. This approach is only applicable to a numerator-only polynomial, and is termed “Linear”.

The second and third approaches solve for the vector of polynomial coefficients \mathbf{c} associated with a rational polynomial, i.e., coefficients pertaining to both numerator and denominator. Because of the denominator, this problem is inherently non-linear. Both of these approaches represent “quasi-linear” solutions. In particular, the solution for the coefficients \mathbf{c} in the second approach is a linear function of the measurements \mathbf{m} , however, the matrix \mathbf{D} is also a function of the measurements \mathbf{m} . This approach is termed the “Quasi-linear-1”.

The third approach is based on a first-order Taylor series expansion of a non-linear problem. Corrections $\Delta\mathbf{c}$ to a priori coefficient values \mathbf{c}_0 are solved for as a linear function of corresponding delta measurements $\Delta\mathbf{m}$. The matrix \mathbf{D} is also a function of \mathbf{c}_0 . This approach is termed the “Quasi-linear-2”.

In general, for each approach, the matrix \mathbf{D} represents a weighted least squares solution process, as detailed below.

5.1.1.1 Linear solution for numerator-only coefficients

Assume the u image space coordinate polynomial coefficients are ordered as follows:

$$\begin{array}{l}
 u = a_1 + a_2X + a_3Y + a_4Z + a_5X^2 + \dots \ , \ \text{with a corresponding} \\
 n \times 1 \ \text{vector of coefficients for solution } \mathbf{c} = [a_1 \ a_2 \ \dots \ a_n]^T.
 \end{array} \tag{33}$$

Generate an m -point ground-to-image fit grid using the original sensor model (see Figure 1). That is, a u_i is associated with each grid ground point \mathbf{x}_i , in Geodetic coordinates, for $i = 1, \dots, m$. Both the image space coordinates and ground space coordinates are also normalized, with a range of $[-1, 1]$. The corresponding offsets and scale factors are included in the RSM support data in order to convert to and from normalized coordinates, when implementing the polynomial.

Typically, the ground-to-image fit grid is generated using the original sensor model's adjustable image-to-ground function, evaluated over an evenly spaced horizontal grid of image points within the image section, and over a set of evenly spaced height planes. Symbolically, this function is represented as $\mathbf{h} = [X \ Y]^T = F^{-1}(\mathbf{i}, Z_0, S, \delta_S)$. An original sensor model adjustable function is utilized so that the RSM ground-to-image polynomial will automatically absorb any previous adjustments made to the original sensor model's image support data. Also, if there is more than one image section making up the image, the fit grid for the current section may be defined to partially overlap any adjacent section to insure continuity.

Assume that there are n_z evenly spaced height planes about a nominal height, n_u image points along the image u -axis, and n_v image points along the image v -axis. Assume that the polynomial's maximum X , Y , and Z orders are u_{nx} , u_{ny} , and u_{nz} , respectively. Furthermore, assume that the Z coordinate is approximately aligned in the direction of increasing height. Define $xy_pwr_{\max} = \max(u_{nx}, u_{ny})$, and $uv_num_{\min} = \min(n_u, n_v)$. It is required that $uv_num_{\min} > xy_pwr_{\max}$, and that $n_z > u_{nz}$. For a reasonable amount of redundancy (degrees of freedom), $uv_num_{\min} \cong 2.5(xy_pwr_{\max} + 1)$, and $n_z \cong 1.5(u_{nz} + 1)$. A typical fit grid is $n_u \times n_v \times n_z = 11 \times 11 \times 6$. Let the total number of grid points equal m .

Associate with each \mathbf{x}_i , a scalar measurement $m_i = u_i$, with basic measurement (observation) equation:

$$m_i = \mathbf{b}_i \mathbf{c} + \varepsilon_i, \quad (34)$$

where $\mathbf{b}_i = [1 \ X_i \ Y_i \ Z_i \ X_i^2 \ \dots] = \partial m_i / \partial \mathbf{c}$, a $1 \times n$ row vector. The error ε_i typically corresponds to the summed effects of modeling error and random noise, if applicable.

$$\text{Define the } m \times 1 \text{ measurement vector } \mathbf{m} = [m_1 \ m_2 \ \dots \ m_m]^T, \quad (35)$$

$$\text{and the } m \times n \text{ partial derivative matrix } \mathbf{B} = \begin{bmatrix} \mathbf{b}_1 \\ \mathbf{b}_2 \\ \dots \\ \mathbf{b}_m \end{bmatrix} = [\mathbf{b}_1^T \ \mathbf{b}_2^T \ \dots \ \mathbf{b}_m^T]^T.$$

The linear, (equal) weighted least squares solution for the coefficients \mathbf{c} is the (unique) solution to the following normal equations:

$$(\mathbf{B}^T \mathbf{W} \mathbf{B}) \mathbf{c} = \mathbf{B}^T \mathbf{W} \mathbf{m}, \text{ with equal weights } \mathbf{W} = \mathbf{I}_{m \times m}. \quad (36)$$

Symbolically, the solution can be represented as:

$$\mathbf{c} = \mathbf{D} \mathbf{m}, \text{ where } \mathbf{D} = (\mathbf{B}^T \mathbf{W} \mathbf{B})^{-1} \mathbf{B}^T \mathbf{W} \quad (37)$$

The solution \mathbf{c} minimizes the weighted sum of the square of the a posteriori measurement residuals, i.e., the quadratic cost function:

$$(\mathbf{m} - \mathbf{B} \mathbf{c})^T \mathbf{W} (\mathbf{m} - \mathbf{B} \mathbf{c}). \quad (38)$$

Identical weight for all measurements ($\mathbf{W} = \mathbf{I}$) is used because there is no reason to weight one measurement more than another, i.e., there is no a priori statistical description of the error.

The solution for the image v coordinate polynomial is as above for the u image coordinate polynomial, and uses the same ground-to-image correspondence grid.

Once the polynomial is computed, its fit accuracy is assessed. Another ground-to-image (evaluation) grid is generated using the original sensor model. It typically has twice the density as the fit grid in each of the grid's three dimensions. The polynomial is then evaluated at each ground point in the evaluation grid, and its corresponding u image coordinate output is differenced from the evaluation grid's corresponding u image coordinate value. Statistics, including the root-mean-square (rms), are then taken over the differences associated with all evaluation grid points. Note that if RSM image support data is being generated in near-real time, the above process may be bypassed. Instead, assuming enough redundancy, the a posteriori measurement residuals associated with the fit grid can be computed and statistics taken, or for even faster results, an a priori fit accuracy contained in a data base may be utilized, indexed as a function of sensor type, etc.

5.1.1.2 Quasi-linear solution for coefficients (Method 1)

The problem set-up is basically the same as in the Linear approach (section 5.1.1.1) in that a grid of redundant data is generated. However, the vector for solution is expanded ($n = n_1 + n_2$) to include the coefficients from both a numerator polynomial and a denominator polynomial. The number of fit points m may also require modification in order to maintain the desired degrees of freedom (redundancy):

$$u = (a_1 + a_2 X + a_3 Y + a_4 Z + a_5 X^2 + \dots) / (1 + b_1 X + b_2 Y + b_3 Z + b_4 X^2 + \dots), \quad (39)$$

with a corresponding $n \times 1$ vector of coefficients for solution

$$\mathbf{c} = \begin{bmatrix} \mathbf{c}_a^T & \mathbf{c}_b^T \end{bmatrix}^T = \begin{bmatrix} a_1 & \dots & a_{n_1} & b_1 & \dots & b_{n_2} \end{bmatrix}^T.$$

For a given fit point i , consider u_i as a measurement m_i , with measurement equation:

$$m_i = (\mathbf{b}_{a_i} \mathbf{c}_a) / (1 + \mathbf{b}_{b_i} \mathbf{c}_b) + \varepsilon_i, \text{ where} \quad (40)$$

$\mathbf{b}_{a_i} = [1 \quad X_i \quad Y_i \quad Z_i \quad X_i^2 \quad \dots]$, is a $1 \times n_1$ row vector,

$\mathbf{b}_{b_i} = [X_i \quad Y_i \quad Z_i \quad X_i^2 \quad \dots]$, a $1 \times n_2$ row vector, and ε_i the error.

Note that \mathbf{b}_{a_i} is the partial derivative of the numerator polynomial with respect to the coefficients \mathbf{c}_a , and \mathbf{b}_{b_i} is the partial derivative of the denominator polynomial with respect to the coefficients \mathbf{c}_b .

Cross-multiplying by the denominator and rearranging terms, the basic scalar measurement equation becomes:

$$m_i = \mathbf{b}_{a_i} \mathbf{c}_a - m_i \mathbf{b}_{b_i} \mathbf{c}_b + (1 + \mathbf{b}_{b_i} \mathbf{c}_b) \varepsilon_i = \mathbf{b}_{a_i} \mathbf{c}_a - m_i \mathbf{b}_{b_i} \mathbf{c}_b + \varepsilon_i^*, \quad (41)$$

where ε_i^* is the error associated with the new measurement equation.

In order to linearize the problem, we consider the m_i on the right side of Equation (41) as a fixed parameter. The measurement m_i can then be considered a linear function of the coefficients for solution:

$$m_i = \mathbf{b}_i \begin{bmatrix} \mathbf{c}_a \\ \mathbf{c}_b \end{bmatrix} + \varepsilon_i^* = \mathbf{b}_i \mathbf{c} + \varepsilon_i^*, \quad (42)$$

where $\mathbf{b}_i = [\mathbf{b}_{a_i} \quad -m_i \mathbf{b}_{b_i}]$, a $1 \times (n_1 + n_2)$, or equivalently $1 \times n$, row vector. Note that \mathbf{b}_i can be considered the partial derivative of the measurement m_i with respect to the coefficients \mathbf{c} .

Again, define the $m \times 1$ measurement vector $\mathbf{m} = [m_1 \quad \dots \quad m_m]^T$ and the $m \times n$ partial derivative matrix $\mathbf{B} = [\mathbf{b}_1^T \quad \dots \quad \mathbf{b}_m^T]^T$. The weighted least squares solution for the coefficients \mathbf{c} is the solution to the normal equations:

$$(\mathbf{B}^T \mathbf{W} \mathbf{B}) \mathbf{c} = \mathbf{B}^T \mathbf{W} \mathbf{m}, \text{ with equal weights } \mathbf{W} = \mathbf{I}_{m \times m}. \quad (43)$$

Symbolically, the solution can be represented as:

$$\mathbf{c} = \mathbf{D}(\mathbf{m}) \mathbf{m}, \text{ where } \mathbf{D}(\mathbf{m}) = (\mathbf{B}^T \mathbf{W} \mathbf{B})^{-1} \mathbf{B}^T \mathbf{W}. \quad (44)$$

Note that the image measurements-to-coefficients mapping matrix \mathbf{D} is a function of the measurements, represented as $\mathbf{D}(\mathbf{m})$, due to the inclusion of the scalar m_i in the computation of \mathbf{b}_i , or equivalently, the measurement vector \mathbf{m} in the matrix \mathbf{B} .

The solution \mathbf{c} minimizes the quadratic cost function:

$$(\mathbf{m} - \mathbf{Bc})^T \mathbf{W}(\mathbf{m} - \mathbf{Bc}). \quad (45)$$

Because the matrix \mathbf{B} is an explicit function of the measurements \mathbf{m} , the above cost function does not give equal weight to each measurement m_i 's a posteriori residual, even though $\mathbf{W} = \mathbf{I}$. However, this can be compensated for as follows. Let the solution become iterative, where only the weight matrix changes between iterations, and use a weight matrix in Equation 43 after the first iteration equal to:

$$\mathbf{W} = \begin{bmatrix} W_1 & 0 & \dots & 0 \\ 0 & \dots & \dots & 0 \\ \dots & \dots & \dots & \dots \\ 0 & \dots & 0 & W_m \end{bmatrix}, \text{ where} \quad (46)$$

the scalar $W_i = (1 + \mathbf{b}_{b_i} \mathbf{c}_b)^{-2}$, and \mathbf{c}_b is from the last iteration's solution. (Note that $W_i = (1 + \mathbf{b}_{b_i} \mathbf{c}_b)^{-2}$ corresponds to the error relationship $\varepsilon_i^* = (1 + \mathbf{b}_{b_i} \mathbf{c}_b) \varepsilon_i$, and an identity $m \times m$ error covariance (inverse weight matrix) assigned to $\boldsymbol{\varepsilon} = [\varepsilon_1 \quad \varepsilon_2 \quad \dots \quad \varepsilon_m]^T$.)

Using this \mathbf{W} , the corresponding cost function approximates the desired:

$$\left(\begin{bmatrix} m_1 \\ \dots \\ m_m \end{bmatrix} - \begin{bmatrix} \mathbf{b}_{a_1} \mathbf{c}_a / (1 + \mathbf{b}_{b_1} \mathbf{c}_b) \\ \dots \\ \mathbf{b}_{a_m} \mathbf{c}_a / (1 + \mathbf{b}_{b_m} \mathbf{c}_b) \end{bmatrix} \right)^T \left(\begin{bmatrix} m_1 \\ \dots \\ m_m \end{bmatrix} - \begin{bmatrix} \mathbf{b}_{a_1} \mathbf{c}_a / (1 + \mathbf{b}_{b_1} \mathbf{c}_b) \\ \dots \\ \mathbf{b}_{a_m} \mathbf{c}_a / (1 + \mathbf{b}_{b_m} \mathbf{c}_b) \end{bmatrix} \right). \quad (47)$$

Regardless of the weight \mathbf{W} used in the solution (Equation 43), it is also recommended that a priori constraints on the coefficients be included for solution stability:

$$\begin{aligned} a_i &= 0 \quad \text{with error variance } \sigma_{a_i}^2, \quad \text{for } i = 1, \dots, n_1; \\ b_i &= 0 \quad \text{with error variance } \sigma_{b_i}^2, \quad \text{for } i = 1, \dots, n_2; \end{aligned} \quad (48)$$

A nominal value for both $\sigma_{a_i}^2$ and $\sigma_{b_i}^2$ is 1×10^{10} . Application of the constraints into the solution process is straightforward, simply modify $\mathbf{B}^T \mathbf{W} \mathbf{B}$ in Equation 43 as follows:

$$\mathbf{B}^T \mathbf{W} \mathbf{B} \rightarrow \left(\mathbf{B}^T \mathbf{W} \mathbf{B} + \begin{bmatrix} \sigma_{a_i}^{-2} \mathbf{I}_{n_1 \times n_1} & 0 \\ 0 & \sigma_{b_i}^{-2} \mathbf{I}_{n_2 \times n_2} \end{bmatrix} \right) \quad (49)$$

Because the solution (Equation 43) corresponds to a rational polynomial, zero checks must be performed for the denominator when solving for the coefficients and/or post-solution. A simple, sufficient condition for the lack of zeros is that the sum of the absolute value of all denominator coefficients for solution be less than 1.0, since the ground coordinate variables are normalized. This condition can be sharpened by excluding all positive coefficients associated with even powers of all variables involved, e.g., X^2 or $X^2 Y^2 Z^2$, if present. If this condition is not satisfied, then the denominator is checked for sign changes over a grid of ground points. If a zero (sign change) is detected, then the order of the rational polynomial must be changed, a numerator-only polynomial selected, or an interpolated ground-to-image grid selected for the ground-to-image function. If the solution is successful in that it has no zeros, fit statistics are generated following the solution as is done in the Linear approach.

5.1.1.3 Quasi-linear solution for coefficients (Method 2)

The problem set-up is basically the same as in the Linear approach (section 5.1.1.1) in that a grid of redundant data is generated. And again, as in the Quasi-linear-1 approach (section 5.1.1.2), the vector for solution is expanded ($n = n_1 + n_2$) to include the coefficients from both numerator and denominator polynomials:

$$u = (a_1 + a_2 X + a_3 Y + a_4 Z + a_5 X^2 + \dots) / (1 + b_1 X + b_2 Y + b_3 Z + b_4 X^2 + \dots), \quad (50)$$

with a $n \times 1$ vector of coefficients for solution $\mathbf{c} = \begin{bmatrix} \mathbf{c}_a^T & \mathbf{c}_b^T \end{bmatrix}^T = \begin{bmatrix} a_1 & \dots & a_{n_1} & b_1 & \dots & b_{n_2} \end{bmatrix}^T$.

Assume an a priori estimate for \mathbf{c} is available, and represented as $\mathbf{c}_0 = \begin{bmatrix} \mathbf{c}_{a_0}^T & \mathbf{c}_{b_0}^T \end{bmatrix}^T$. A correction $\Delta \mathbf{c}$ relative to the a priori estimate is solved for based on the following first-order Taylor series expansion:

$$u_i = (\mathbf{b}_{a_i} \mathbf{c}_a / (1 + \mathbf{b}_{b_i} \mathbf{c}_b)) \cong (\mathbf{b}_{a_i} \mathbf{c}_{a_0} / (1 + \mathbf{b}_{b_i} \mathbf{c}_{b_0})) + \frac{\partial}{\partial \mathbf{c}} \left[\mathbf{b}_{a_i} \mathbf{c}_a / (1 + \mathbf{b}_{b_i} \mathbf{c}_b) \right] \Delta \mathbf{c}, \quad (51)$$

where

$$\mathbf{b}_{a_i} = \begin{bmatrix} 1 & X_i & Y_i & Z_i & X_i^2 & \dots \end{bmatrix}, \text{ a } 1 \times n_1 \text{ row vector}$$

$$\mathbf{b}_{b_i} = \begin{bmatrix} X_i & Y_i & Z_i & X_i^2 & \dots \end{bmatrix}, \text{ a } 1 \times n_2 \text{ row vector}$$

Defining the scalar $\Delta u_i = u_i - (\mathbf{b}_{a_i} \mathbf{c}_{a_0} / (1 + \mathbf{b}_{b_i} \mathbf{c}_{b_0}))$, and the $1 \times n$ partial derivative matrix

$$\mathbf{b}_i = \frac{\partial}{\partial \mathbf{c}} \left[\mathbf{b}_{a_i} \mathbf{c}_a / (1 + \mathbf{b}_{b_i} \mathbf{c}_b) \right], \text{ evaluated at the operating point } \mathbf{c}_0 = \begin{bmatrix} \mathbf{c}_{a_0}^T & \mathbf{c}_{b_0}^T \end{bmatrix}^T, \text{ we have}$$

$\Delta u_i = \mathbf{b}_i \Delta \mathbf{c}$. Considering Δu_i as a measurement Δm_i , the basic measurement equation becomes:

$$\Delta m_i = \mathbf{b}_i \Delta \mathbf{c} + \varepsilon_i, \quad (52)$$

where ε_i is the associated error, the $1 \times (n_1 + n_2)$, or equivalently $1 \times n$, row vector $\mathbf{b}_i = [s_{a_i} \mathbf{b}_{a_i} \quad s_{b_i} \mathbf{b}_{b_i}]$, and scalars s_{a_i} and s_{b_i} are equal to: $s_{a_i} = (1 + \mathbf{b}_{b_i} \mathbf{c}_{b_0})^{-1}$ and $s_{b_i} = -(\mathbf{b}_{a_i} \mathbf{c}_{a_0})(1 + \mathbf{b}_{b_i} \mathbf{c}_{b_0})^{-2}$.

Define the $m \times 1$ (delta) measurement vector $\Delta \mathbf{m} = [\Delta m_1 \quad \dots \quad \Delta m_m]^T$ and $m \times n$ partial derivative matrix $\mathbf{B} = [\mathbf{b}_1^T \quad \dots \quad \mathbf{b}_m^T]^T$. The weighted least squares solution for the corrections $\Delta \mathbf{c}$ to the a priori coefficients is the solution to the normal equations:

$$(\mathbf{B}^T \mathbf{W} \mathbf{B}) \Delta \mathbf{c} = \mathbf{B}^T \mathbf{W} \Delta \mathbf{m}, \text{ with equal weights } \mathbf{W} = \mathbf{I}_{m \times m}. \quad (53)$$

Symbolically, the solution can be represented as:

$$\Delta \mathbf{c} = \mathbf{D}(\mathbf{c}_0) \Delta \mathbf{m}, \text{ where } \mathbf{D}(\mathbf{c}_0) = (\mathbf{B}^T \mathbf{W} \mathbf{B})^{-1} \mathbf{B}^T \mathbf{W} \quad (54)$$

The image measurements-to-coefficients mapping matrix \mathbf{D} is a function of the a priori coefficients, represented as $\mathbf{D}(\mathbf{c}_0)$, due to the inclusion of \mathbf{c}_0 in the computation of \mathbf{b}_i .

The solution $\Delta \mathbf{c}$ minimizes the quadratic cost function:

$$(\Delta \mathbf{m} - \mathbf{B} \Delta \mathbf{c})^T \mathbf{W} (\Delta \mathbf{m} - \mathbf{B} \Delta \mathbf{c}). \quad (55)$$

Once solved for, the corrections are added to the a priori coefficients to form a new set of a priori coefficients, i.e., $\mathbf{c}_0 \rightarrow \mathbf{c}_0 + \Delta \mathbf{c}$, and the solution performed again at the new operating point. When convergence has been reached, the solution process is finished with solution \mathbf{c}_0 ; otherwise, another iteration is performed. The check for convergence is typically based on the relative change of the cost function (Equation 55) from one iteration to the next.

Similar to the Quasi-linear-1 approach, it is also recommended that a priori constraints on the coefficient corrections $\Delta \mathbf{c}$ for solution be included for stability. The procedure is identical to that presented in Equations 48 and 49. Also, as in the Quasi-linear-1 approach, zero checks for the denominator should be performed and corrective action taken if detected, and fit statistics generated. Finally, the initial a priori estimate for the coefficients \mathbf{c}_0 should be reasonably accurate in order for the solution process to converge to the appropriate solution. Quasi-linear-1 approach (section 5.1.1.2) may be implemented to provide this estimate (although the non-identity weights of Equation 46 need not be implemented). That is, the initial a priori estimate \mathbf{c}_0 used in the Quasi-linear-2 approach is set to the solution \mathbf{c} from the Quasi-linear-1 approach.

5.1.1.4 Recommendations

(Dowman and Dolloff, 2000) further describes the automatic solution process and the Linear approach (numerator-only polynomial), and include fit accuracy results. In addition, (Tao and Hu, December 2001) essentially describe the same solution technique as presented in the Quasi-linear-1 approach for a rational polynomial (section 5.1.1.2), and include fit accuracy results.

The Quasi-linear-1 approach has numerous features. These features include: (1) the Linear approach (numerator-only polynomial) as a sub-case, and (2) no requirement for an a priori estimate of the coefficients for solution. Also, the potential negative impact of the Quasi-linear-1 approach's reliance on the measurement data ($\mathbf{c} = \mathbf{D}(\mathbf{m})\mathbf{m}$) is mitigated due to the deterministic (noise free) nature of these measurements. They are from the ground point-image point correspondence generated using the original sensor model and its image support data. They are not subjected to the addition of any mensuration error, such as operator image measurement error.

5.1.2 Ground-to-image function grid

Generation of the RSM ground-to-image grid is relatively straightforward. The original sensor model's adjustable ground-to-image function is used to generate the grid's image point coordinate values. For each Z (height) plane, an evenly spaced horizontal grid is utilized, and the corresponding image coordinates computed. The only other processing required is to determine the grid's domain and step sizes. The latter can be done either manually or automatically, based on the fit error associated with a candidate grid and the interpolation scheme used in $grid(\mathbf{x}, R)$. Fit error is relative to the original sensor model's ground-to-image relationship that is provided in an evaluation grid. Also, if required for fit accuracy and/or band-width limitations per image section, the image may be divided into sections with a grid per section - see similar processing for the ground-to-image polynomial, section 5.1.1. Note that a particularly efficient grid can be generated by selecting the RSM ground coordinate system as Rectangular, and identical to the local, rotated tangent plane coordinate system described in Section 3.1.3.

5.2 Adjustable parameters and error covariance

5.2.1 Error covariance generation

An optimal solution for a single or multiple ground (object) points was presented in Equation 21, and is representative of all optimal geopositioning and triangulation techniques. The following presents the solution (δ_x) using RSM and the corresponding solution ($\delta_x^\#$) using the original sensor model:

$$\begin{aligned}\delta_x &= [\mathbf{C}_{x_0}^{-1} + \mathbf{B}^T (\boldsymbol{\Sigma}_M + \mathbf{B}_R \mathbf{C}_R \mathbf{B}_R^T)^{-1} \mathbf{B}]^{-1} \mathbf{B}^T (\boldsymbol{\Sigma}_M + \mathbf{B}_R \mathbf{C}_R \mathbf{B}_R^T)^{-1} (\mathbf{m} - \mathbf{m}_0) \\ \delta_x^\# &= [\mathbf{C}_{x_0}^{-1} + \mathbf{B}^{\#T} (\boldsymbol{\Sigma}_M + \mathbf{B}_S \mathbf{C}_S \mathbf{B}_S^T)^{-1} \mathbf{B}^\#]^{-1} \mathbf{B}^{\#T} (\boldsymbol{\Sigma}_M + \mathbf{B}_S \mathbf{C}_S \mathbf{B}_S^T)^{-1} (\mathbf{m} - \mathbf{m}_0^\#)\end{aligned}\quad (56)$$

The above solution for ground point(s) δ_x , based on RSM, was explicitly described in section 4.1.1. (Actually δ_x is a correction to an a priori estimate, i.e., $\mathbf{x} = \mathbf{x}_0 + \delta_x$.) The corresponding solution for $\delta_x^\#$, based on the original sensor model, is completely analogous, with the appropriate substitution of original sensor model quantities for RSM quantities. Specifically, substitute the original sensor model error covariance (\mathbf{C}_S) instead of the RSM error covariance (\mathbf{C}_R), the partial derivative of the image measurements with respect to the original sensor model adjustable parameters (\mathbf{B}_S) instead of the partial derivatives of the image measurements with respect to the RSM adjustable parameters (\mathbf{B}_R), the predicted image measurements based on the original sensor model ($\mathbf{m}_0^\#$) instead of based on the RSM (\mathbf{m}_0), and the partial derivative of the image measurements with respect to the ground point based on the original sensor model ($\mathbf{B}^\#$) instead of based on the RSM (\mathbf{B}).

For the RSM based solution, the RSM (adjustable) ground-to-image function is used to compute both the predicted measurements and the partial derivatives of the image measurements with respect to the ground point. Because the RSM ground-to-image function represents the original sensor model's ground-to-image function so well (e.g., rms fit error less than 0.05 pixels), both $\mathbf{m}_0 \cong \mathbf{m}_0^\#$ and $\mathbf{B} \cong \mathbf{B}^\#$. Thus, the only relevant difference in the formulas for δ_x and $\delta_x^\#$ are the use of $\mathbf{B}_R \mathbf{C}_R \mathbf{B}_R^T$ versus $\mathbf{B}_S \mathbf{C}_S \mathbf{B}_S^T$, i.e., the difference in the projection of sensor model (support data) error covariance to image space. (Recall that \mathbf{B}_R is the partial derivative of image measurements with respect to δ_R , \mathbf{B}_S is the partial derivative of image measurements with respect to δ_S .) Thus, the solution using RSM will closely match the solution using the original sensor model, when:

$$\mathbf{B}_R \mathbf{C}_R \mathbf{B}_R^T \cong \mathbf{B}_S \mathbf{C}_S \mathbf{B}_S^T \quad (57)$$

Thus, \mathbf{C}_R must be generated such that Equation 57 is satisfied. Since \mathbf{B}_R can not be inverted in general, and because Equation 57 is to hold at arbitrary ground point positions \mathbf{x} within the image footprints, the generation of \mathbf{C}_R is accomplished as follows:

$$\begin{aligned} \mathbf{C}_R &= (\mathbf{B}_R^{*+})(\mathbf{B}_S^* \mathbf{C}_S \mathbf{B}_S^{*T})(\mathbf{B}_R^{*+})^T, \text{ where the pseudo-inverse of } \mathbf{B}_R^* \text{ equals} \\ \mathbf{B}_R^{*+} &= (\mathbf{B}_R^{*T} \mathbf{B}_R^*)^{-1} \mathbf{B}_R^{*T}. \text{ Thus, we also have} \\ \mathbf{C}_R &= (\mathbf{B}_R^{*T} \mathbf{B}_R^*)^{-1} \mathbf{B}_R^{*T} (\mathbf{B}_S^* \mathbf{C}_S \mathbf{B}_S^{*T}) \mathbf{B}_R^* (\mathbf{B}_R^{*T} \mathbf{B}_R^*)^{-T}. \end{aligned} \quad (58)$$

The superscript * on the partial derivative matrices \mathbf{B}_R and \mathbf{B}_S indicate that the partial derivatives correspond to a common grid of ground point positions, varying both

horizontally and vertically, within the image footprints. This is analogous to solving for a multi-ground point vector \mathbf{x} in Equation 56. The footprints correspond to all (correlated) images whose support data errors are represented by the original sensor model's \mathbf{C}_S .

The number and dispersion (pattern) of the ground points in the grid is such that the number of rows in \mathbf{B}_R^* is greater than or equal to the number of columns in \mathbf{B}_R^* , and that the subsequent matrix is full rank, required for the computation of its pseudo-inverse \mathbf{B}_R^{*+} . The grid should also capture any variation in the partial derivatives \mathbf{B}_S , as well as \mathbf{B}_R , over the footprints. In addition, the number of RSM adjustable parameters per image is typically less than or equal to the number of original sensor model adjustable parameters per image. This not only facilitates \mathbf{B}_R^* being full rank, but is a necessary condition for a positive definite \mathbf{C}_R . Also, it is assumed that the a priori sensor support data errors are not so large as to render the partial derivative computations invalid.

In general, Equation 58 correspond to multiple (p) images. Assuming n original sensor model adjustable parameters per image i ($i = 1, \dots, p$) contained in δ_{S_i} , m RSM adjustable parameters per image i contained in δ_{R_i} , and q ground points in image i 's ground point grid, then \mathbf{C}_S is a $pn \times pn$ multi-image original sensor model adjustable parameter error covariance matrix, and \mathbf{C}_R is a $pm \times pm$ multi-image RSM adjustable parameter error covariance matrix. In addition, define $\mathbf{B}_{S_i}^*$ as the $2q \times n$ matrix of partial derivatives of image i measurements with respect to δ_{S_i} applicable over the image i ground point grid, and $\mathbf{B}_{R_i}^*$ as the $2q \times m$ matrix of partial derivatives of image i measurements with respect to δ_{R_i} applicable over the image i ground point grid. In particular, if \mathbf{i}_{ik} is the two-dimensional image measurement corresponding to ground point k ($k \leq q$) in image i 's ground point grid, $\partial \mathbf{i}_{ik} / \partial \delta_{S_i}$ corresponds to rows $2k - 1$ and $2k$ of $\mathbf{B}_{S_i}^*$, and $\partial \mathbf{i}_{ik} / \partial \delta_{R_i}$ to rows $2k - 1$ and $2k$ of $\mathbf{B}_{R_i}^*$. Also, the (full) rank of $\mathbf{B}_{R_i}^*$ equals m , i.e., the number of rows is greater than or equal to the number of columns ($2q \geq m$), and the number of linearly independent rows is equal to the number of RSM adjustable parameters (m). In addition, if \mathbf{C}_R is to be positive definite, the number of RSM adjustable parameters can not exceed the number of original sensor model adjustable parameters ($m \leq n$)

Correspondingly, components of Equation 58 are further detailed as follows:

$$\mathbf{C}_R = \begin{bmatrix} \mathbf{C}_{R_{11}} & \cdot & \cdot & \mathbf{C}_{R_{1p}} \\ \cdot & \cdot & \mathbf{C}_{R_{ij}} & \cdot \\ \cdot & \cdot & \cdot & \cdot \\ \cdot & \cdot & \cdot & \mathbf{C}_{R_{pp}} \end{bmatrix} = \mathbf{\Omega} \begin{bmatrix} \mathbf{C}_{S_{11}} & \cdot & \cdot & \mathbf{C}_{S_{1p}} \\ \cdot & \cdot & \mathbf{C}_{S_{ij}} & \cdot \\ \cdot & \cdot & \cdot & \cdot \\ \cdot & \cdot & \cdot & \mathbf{C}_{S_{pp}} \end{bmatrix} \mathbf{\Omega}^T, \text{ where}$$

$$\mathbf{\Omega} = \begin{bmatrix} (\mathbf{B}_{R_1}^{*T} \mathbf{B}_{R_1}^*)^{-1} \mathbf{B}_{R_1}^{*T} \mathbf{B}_{S_1}^* & 0 & \cdot & \cdot & 0 \\ 0 & \cdot & \cdot & \cdot & \cdot \\ \cdot & \cdot & (\mathbf{B}_{R_i}^{*T} \mathbf{B}_{R_i}^*)^{-1} \mathbf{B}_{R_i}^{*T} \mathbf{B}_{S_i}^* & \cdot & \cdot \\ \cdot & \cdot & \cdot & \cdot & 0 \\ 0 & \cdot & \cdot & 0 & (\mathbf{B}_{R_p}^{*T} \mathbf{B}_{R_p}^*)^{-1} \mathbf{B}_{R_p}^{*T} \mathbf{B}_{S_p}^* \end{bmatrix}, \text{ or } (59)$$

$$\mathbf{C}_{R_{ij}} = \mathbf{\Phi}_i \mathbf{C}_{S_{ij}} \mathbf{\Phi}_j^T, \text{ where}$$

$$\mathbf{\Phi}_i \equiv (\mathbf{B}_{R_i}^{*T} \mathbf{B}_{R_i}^*)^{-1} \mathbf{B}_{R_i}^{*T} \mathbf{B}_{S_i}^* = \mathbf{B}_{R_i}^{*+} \mathbf{B}_{S_i}^*$$

For the direct approach to specification of the RSM error covariance (see section 3.2.1), the entire \mathbf{C}_R is generated. It is then supplied in the RSM support data for each image i within the correlated group of p images. For the indirect approach to specification of the RSM error covariance (see section 3.2.2), only the mapping matrix $\mathbf{\Phi}_i$ is generated for an image i . Both $\mathbf{\Phi}_i$ and the data defining $\mathbf{C}_{S_{ij}}$ are then provided in image i 's RSM support data. Note that, in support of both \mathbf{C}_R and $\mathbf{\Phi}_i$ generation, the required partial derivatives are generated using both the original sensor model and the RSM. Also, both \mathbf{C}_S and the data defining $\mathbf{C}_{S_{ij}}$ are provided by the original sensor model (and its image support data). Finally, as a reminder, when in support of the direct approach to specification of the RSM error covariance, Equations 58 and 59 are actually applicable to a variable number and variable definition of both original adjustable parameters and RSM adjustable parameters across the p images. Specifically, Equation 59 is still applicable as written, however the dimensions of all the matrices are image dependent. For example, if image $i=1$ has m_1 RSM adjustable parameters and image $i=2$ has m_2 , $\mathbf{\delta}_{R_1}$ is $m_1 \times 1$, $\mathbf{B}_{R_1}^*$ is $2q \times m_1$, $\mathbf{\delta}_{R_2}$ is $m_2 \times 1$, $\mathbf{B}_{R_2}^*$ is $2q \times m_2$, and $\mathbf{C}_{R_{12}}$ is $m_1 \times m_2$. (The number of ground points q in an image's ground point grid may also vary with image, i.e., $q \rightarrow q_i$.)

The solution of Equation 57 can also be generalized by solving for \mathbf{C}_R such that the matrix norm difference of Equation 60 is minimized:

$$\left\| \mathbf{B}_R^* \mathbf{C}_R \mathbf{B}_R^{*T} - \mathbf{B}_S^* \mathbf{C}_S \mathbf{B}_S^{*T} \right\|_F \quad (60)$$

The particular norm is the Frobenius norm which is the square root of the sum of the matrix elements squared. The solution to this minimization problem is provided by (Rao and Mitra, 1971):

$$\mathbf{C}_R = \mathbf{B}_R^{*++} (\mathbf{B}_S^* \mathbf{C}_S \mathbf{B}_S^{*T}) \mathbf{B}_R^{*++T}, \quad (61)$$

The superscript $^{++}$ is used to indicate the Moore-Penrose Generalized Inverse. The Moore-Penrose Generalized Inverse of a matrix is based on the Singular Value Decomposition of the matrix.

When \mathbf{B}_R^* is full rank, \mathbf{B}_R^{*++} becomes the pseudo-inverse \mathbf{B}_R^{*+} , and Equation 61 is equivalent to Equation 58. Thus, the solution for \mathbf{C}_R of Equation 61 is only required for the pathological case when \mathbf{B}_R^* is not full rank. Note also that, when \mathbf{B}_R^* is full rank, the solution of Equation 58 minimizes the Frobenius norm as well. The remainder of this section assume that \mathbf{B}_R^* is full rank, and that Equation 58, and more specifically, Equation 59, is applicable.

5.2.2 Adjustment vector selection

For a given adjustment vector δ_R (definition), \mathbf{C}_R is computed such that its projection to image space closely approximates the projection of \mathbf{C}_S to image space. In particular, the Frobenius norm metric (Equation 60) is minimized. In addition, this metric can be used to select an optimal δ_R . More specifically, it can be used to select an optimal δ_{R_i} definition for each image i , i.e., which members of the RSM choice set $\tilde{\delta R}$ are applicable. In particular, a δ_R can be selected such that its corresponding minimum Frobenius norm value is also minimal compared to the minimum Frobenius norm values computed for other δ_R candidates. The candidates can be selected manually, or can be selected automatically using an algorithm which selects combinations of δ_R components from a list of possible candidates.

In addition, the selection process may be augmented with a positive definite constraint on the δ_R and corresponding \mathbf{C}_R candidates. That is, for a candidate δ_R , the corresponding \mathbf{C}_R must also be a positive definite matrix, which is required for triangulation applications. (There is also an alternative generation technique for \mathbf{C}_R that insures that \mathbf{C}_R is positive definite regardless the δ_R definition. However, it is typically less accurate (larger Frobenius norm value) than the technique previously presented, and as such, is not presented here.) Note that in Equation 59, since \mathbf{C}_S is assumed positive definite, \mathbf{C}_R will be positive definite if the total number of RSM adjustable parameters is less than or equal to the total number of original parameters and $\mathbf{\Omega}$ is full rank (see Horn and Johnson, 1994). This occurs when, for each image i , the number of RSM adjustable

parameters is less than or equal to the number of original adjustable parameters ($m \leq n$) and the mapping matrix Φ_i is full rank (m).

In practice, δ_R selection is typically done off-line and on a per sensor basis. For a given sensor, the resulting selection becomes the default RSM adjustable parameters (δ_R definition) for any image from that sensor. Whenever a (multi-image) error covariance is generated later that involves one or more images from the sensor, the default RSM adjustable parameters are used in Equation 59 for those images.

The normalized Frobenius norm is the actual metric used in the off-line selection process for ease of interpretation. (Normalization also allows a different generation grid to be used for each candidate, if so desired.) For each δ_R candidate, the metric is evaluated on a per image basis across a set of representative images (support data) for the sensor. In particular, for each image i in the set, the following is computed:

$$\left\| \mathbf{B}_{R_i}^* \mathbf{C}_{R_i} \mathbf{B}_{R_i}^{*T} - \mathbf{B}_{S_i}^* \mathbf{C}_{S_i} \mathbf{B}_{S_i}^{*T} \right\|_F / \left\| \mathbf{B}_{S_i}^* \mathbf{C}_{S_i} \mathbf{B}_{S_i}^{*T} \right\|_F \quad (62)$$

Of course, \mathbf{C}_{R_i} is computed prior to computation of the metric, using Equation 59. The same ground point grid can be used for both \mathbf{C}_{R_i} generation and metric evaluation. A $5 \times 5 \times 3$ grid in $X - Y - Z$ is typical. The δ_R candidate that minimizes the rms of the above metric taken over all images i in the set and that also yields a positive definite \mathbf{C}_{R_i} ($m \leq n$ and Φ_i full rank) for each image i is typically selected.

A δ_R (definition) that corresponds to an image-space adjustment (see section 3.1.3) works well for most sensors that have a field-of-view that is not excessively large and are not at a low altitude. The actual number of members from the choice set is typically either 6 or 12 per image, and typically one or two less than the number of corresponding original sensor model adjustable parameters. The actual adjustable parameter definitions corresponding to the 6 member set are $\{\delta u_0 \ \delta u_x \ \delta u_y \ \delta v_0 \ \delta v_x \ \delta v_y\}$, and for the 12 member set $\{\delta u_0 \ \delta u_x \ \delta u_y \ \delta u_{xx} \ \delta u_{xy} \ \delta u_{yy} \ \delta v_0 \ \delta v_x \ \delta v_y \ \delta v_{xx} \ \delta v_{xy} \ \delta v_{yy}\}$. Sensors requiring a δ_R (definition) that corresponds to a ground-space adjustment (see section 3.1.3), typically use a 6 member set, such as $\{\delta x_o \ \delta y_o \ \delta \alpha \ \delta \beta \ \delta \kappa \ \delta s\}$.

In some situations, where the original sensor model adjustable parameters (errors) are highly correlated or their effect across a (small) image footprint very similar, significantly less RSM adjustable parameters may be selected than described above.

5.3 Time and illumination models

The time-of-image model and illumination model are generated in a straightforward manner using the original sensor model. The illumination model also requires redundant,

equal weight fitting of the two angle polynomials to the illumination direction information.

6.0 RSM development status and performance summary

6.1 Development status

An RSM prototype has been built at BAE Systems and has undergone testing using both simulated data (Dowman and Dolloff, 2000) and actual data. The majority of testing with actual data was sponsored by the National Imagery and Mapping Agency (NIMA). In particular there were two studies, one for commercial satellite imagery and one for tactical imagery, both completed in 2001.

The following summarizes current (November 2003) RSM development status. The contents of the RSM support data groups have been defined. Detailed draft formats for their inclusion as NITF Tagged Record Extensions (TRE's) have been generated and submitted to the NITF board for approval - see (NIMA 1997, 1999) for a general description of the NITF. In addition, two RSM software modules are currently under development at BAE Systems. The RSM Generator automatically generates the appropriate set of RSM image support data from a set of original sensor model image support data. The RSM Exploiter automatically provides all sensor model functionality associated with a set of RSM image support data. For example, for a given ground point, it provides the corresponding image point and all associated partial derivatives. For a given image point and height, it provides the corresponding ground point. It also supplies the multi-image direct error covariance and/or (fully assembled) multi-image indirect error covariance. Both of these software modules include an Application Program Interface (API). Use of the RSM Generator and/or RSM Exploiter mitigates RSM complexity.

6.2 Performance Summary

Full RSM testing using the prototype and actual data has been performed using six different sensors to-date, including low altitude frame, space-borne pushbroom, and SAR. Full testing includes optimal multi-image, multi-ground point geopositioning, as well as triangulation. Both require RSM's full functionality – adjustable ground-to-image functions and multi-image error covariance. During the testing, both the ground-to-image polynomial and grid, both the image-space and ground-space adjustable parameters, and the direct error covariance method were all tested. In addition to full RSM testing, testing of the RSM ground-to-image polynomial and grid functions were tested for an additional five sensors. Typically, not enough images were available for these additional sensors at the time in order to perform full RSM testing.

For each of the eleven sensors tested, RSM ground-to-image fit accuracy was always 0.05 pixels (rms) or better. Testing of the polynomial was more extensive than that for the grid, and it was selected as the ground-to-image function for most sensors.

Polynomial fit accuracy ranged between 0.001 and 0.01 pixels (rms), with a maximum fit error typically three to four times larger than its rms counterpart. A third order rational polynomial was typically selected. When the RSM ground-to-image function was an interpolated grid, fit accuracy ranged between 0.001 and 0.05 pixels (rms), and was dependent on specified grid density, interpolation order, and coordinate system representation. A grid size of $20 \times 20 \times 10$ (X, Y, Z) or less and separable tri-quadratic interpolation were typical. (Separable tri-cubic interpolation was not tested.) All results are relative to a single image section (polynomial or grid) covering the entire image.

Geopositioning results obtained during full RSM testing are most conveniently and usually most appropriately reported as a percentage of error propagation results. For a given triangulation or geopositioning scenario (e.g., a 4 overlapping image, 5 ground point, simultaneous geopositioning solution), two optimal solutions were performed. One used the original sensor model and its image support data, and is termed the “original solution”. The other used the RSM and its image support data, and is termed the “RSM solution”. The RSM image support data was generated from the original sensor model and its image support data prior to both solutions. All other factors affecting the two solutions were identical (e.g., image measurements). The results of the two solutions were then compared, including both the best estimate of all ground point positions as well as estimates of their accuracy via the a posteriori solution error covariance, i.e., error propagation. Note that the error propagation was summarized using CE and LE for both absolute and relative accuracy. CE is 0.9p horizontal position error and LE is 0.9p vertical position error. Both are computed from the a posteriori solution error covariance and assume a mean zero, Gaussian distribution of errors. CE is the radius of a circle such that 90% of the probability is inside, and LE is the length of a linear segment such that 90% of the probability is within +/- the length.

Differences between the original and RSM solutions were computed as an absolute value. These differences were then normalized by the appropriate error propagation results from the original solution. If there were more than one ground point solved for simultaneously, the normalized differences were computed for each ground point (and ground point pair for relative differences) and then averaged. Typical comparison results were on the order of 1% for all aspects of the solution. For example, if for a given ground point, the horizontal error propagation (CE) from the original solution was 20 meters, then the absolute value of the difference in the two solutions’ estimate of horizontal ground point position was approximately $0.01 * 20 = 0.2$ meter or less, and the absolute value of the difference in their error propagation (CE) was also approximately $0.01 * 20 = 0.2$ meters or less. If one considers the difference in the solutions’ horizontal position as an additional error source relative to the original solution and attributable to the RSM representation, it is negligible. This is described in more detail below.

6.2.1 RSM representation error

One of the charters for RSM is that the RSM solution closely match all aspects of the original solution. This brings up the somewhat subjective question of “how close is close enough?” If we attribute solution differences solely to RSM, the differences are “RSM

representation error” and can be considered an additional error source relative to the original solution. For example, if for a given scenario the original solution’s CE is 20 meters, and the RSM solution’s horizontal position differs from the original by 1 meter 90% of the time, the expanded CE associated with the RSM solution would be approximately the root-sum-square of 20 meters and 1 meters, i.e., $\text{rss}(20,1) = 20.03$ meters, a negligible increase. The root-sum-square is applicable due to the addition of two uncorrelated errors. The following further characterizes this change analytically, first for LE and then for CE.

An analytic representation was derived that maps the percentage increase in LE as a function of the average normalized vertical position difference between the two solutions. It accounts for the 0.9p probability levels, the fact that normalized differences are absolute values of differences, and equates average value to probabilistic expectation. Figure 13 presents the results. In particular, a 2.5% average normalized vertical position difference increases LE by 0.1%, and a 7.5% average normalized vertical position difference increases LE by 1.2%. The mapping of average normalized horizontal position differences to a % increase in CE is even more favorable (smaller increase) than the corresponding mapping for LE. Based on these results, normalized horizontal position and vertical position differences of 5% or less are considered negligible, and normalized differences of 15% or less are considered acceptable. (This assumes that the original CE and LE are not excessively small to begin with. For example, a 0.2 meter representation error is negligible in most applications, yet if the original CE were 1 meter, the normalized difference would be 20%.) Although somewhat more subjective, the same tolerances described above for solution horizontal and vertical position differences, are assumed applicable to solution error propagation (CE and LE) differences as well.

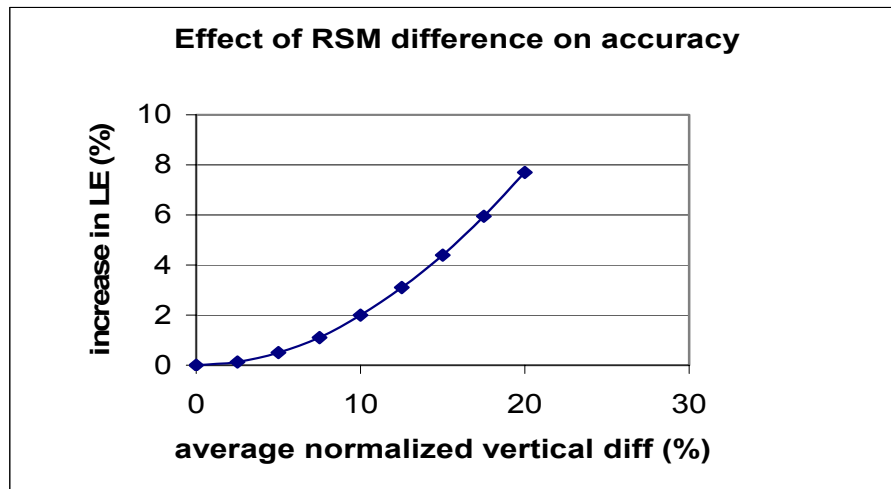


Figure 13. The effects of RSM representation error on vertical solution accuracy.

6.2.2 NIMA-sponsored RSM Commercial Imagery Study

6.2.2.1 SPOT Results

Table 5 presents typical results based on a set of 5 partially overlapping SPOT images. Image selection and footprint overlap was “by opportunity”, and resultant image geometry relatively poor. A typical elevation angle was 80 degrees (90 degrees corresponding to nadir geometry), and a typical convergence angle between image pairs was 20 degrees. Various geopositioning solution scenarios were addressed: monoscopic (rows 1-6 of Table 5), stereo (rows 7-12), and multi-image (rows 13-16). An original solution and a corresponding RSM solution were performed for each case.

Monoscopic solutions (with DEM) were performed with either 1 or 6 ground points solved for simultaneously. Stereo solutions were performed with either 1 or 5 ground points solved for simultaneously. A “multi-image” solution using all 5 SPOT images was performed with 14 ground points solved for simultaneously. The SPOT image support data used was a priori (unadjusted) support data.

Another set of geopositioning solutions were also performed based on SPOT adjusted image support data. This adjusted image support data was the output of a previous original solution triangulation, which utilized all 5 images, 22 tie points, and 26 control points. For a particular geopositioning solution scenario, the original solution used the SPOT adjusted image support data, and the RSM solution used RSM image support data generated from the SPOT adjusted image support data. These solutions are indicated by “adj” in the support data column (“Sprt Data”) in Table 5. Both the SPOT adjusted image support data and corresponding RSM image support data included a full error covariance relative to the appropriate adjustable parameters for all images. There was significant correlation between adjustable parameters corresponding to the same image, as well as between adjustable parameters corresponding to different images

Table 5 has one final entry corresponding to triangulation. The previously discussed original solution triangulation was also performed as an RSM solution triangulation. The latter adjusted the RSM support data that was previously generated from the SPOT a priori (unadjusted) support data. The results of the original and RSM triangulation solutions were compared by comparing the solution position and error propagation results for all 22 tie points. The triangulation comparison results are contained in the last two rows of Table 5.

Note that all results in Table 5 are normalized as discussed previously. (When based on unadjusted support data, the original solution’s CE and LE were on the order of hundreds of meters due to poor geometry and large support data error covariance.) Also, both absolute and relative statistics are presented in the table, indicated by “abs” and “rel”, respectively, in the “statistics” column. Absolute statistics refer to a ground point’s horizontal position solution and vertical position solution and their corresponding error propagation (accuracy estimates) CE and LE, respectively. Relative statistics refer to the relative results between a pair of ground points solved for simultaneously. (A small relative position error or corresponding accuracy estimate would indicate highly, positively correlated solution position errors between the two ground points that nearly cancel out.) Note also that table results are actually in terms of maximum normalized

difference between the original and RSM solutions, presented to the nearest one-tenth of one percent. For a given geopositioning or triangulation solution, the absolute statistics presented refer to the largest normalized difference among all points (tie points if a triangulation) solved for. Relative statistics refer to the largest normalized difference among all possible point pairs involving ground points in the solution. Thus, results are some what conservative relative to the use of average normalized differences.

An example of how to interpret Table 5 is as follows. Rows 9-10 (of the rows containing numeric or “n/a” data) correspond to a stereo (two-image) geopositioning solution for 5 ground points using unadjusted support data. Absolute statistics are presented in row 9. There is a 0.2% maximum normalized difference in the original and RSM solutions’ horizontal position estimate, a 0.4% maximum normalized difference in the original and RSM solutions’ vertical position estimate, a 0.1% maximum normalized difference in the original and RSM solutions’ horizontal error propagation (CE), and a 0.2% maximum normalized difference in the original and RSM solutions’ vertical error propagation (LE). Row 10 presents corresponding relative statistics. As detailed in these rows and the remainder of Table 5, differences between the RSM and original solutions are negligible for all scenarios.

Case	Sprt Data	# pts	statistics	% norm hor diff	% norm ver diff	% norm CE diff	% norm LE diff
Geopos							
mono		1	abs	0	0	0	0
			rel	n/a	n/a	n/a	n/a
mono		6	abs	0	0	0.1	0.1
			rel	0	0	0.1	0.1
mono	adj	6	abs	0.1	0	0.1	0
			rel	0	0	0.1	0
stereo		1	abs	0	0	0	0
			rel	n/a	n/a	n/a	n/a
stereo		5	abs	0.2	0.4	0.1	0.2
			rel	0.3	0.1	0.9	0.7
stereo	adj	5	abs	0.2	0.2	0.2	0.2
			rel	0.2	0.2	0.2	0.1
multi img		14	abs	0.1	0.3	0.1	0.1
			rel	0.4	0.4	0.5	0.6
multi img	adj	14	abs	0.5	0.4	0.2	0.2
			rel	0.6	0.6	0.2	0.2
Triang							
baseline		22 tp 26 c	abs	1.5	2.3	0.2	0.2
			rel	2.0	2.7	0.3	0.3

Table 5. SPOT RSM - original solution maximum normalized differences (%).

The SPOT original sensor model included seven adjustable parameters per image, three for position, three for attitude, and one for focal length. Corresponding a priori accuracy (one sigma) was appropriately large: 300 meters for all position components, 0.0009 radians for all attitude (orientation) components, and 0.0005 meters for focal length. The images were approximately 6k×6k in size with a 10 meter ground sample distance. A priori support data errors were uncorrelated between images. There were a total of 6 RSM image-space adjustable parameters per image (identical to those specified in Equation 12). Also, the RSM ground-to-image function was a third order rational polynomial that covered the entire image. No denominator zeros were present in any SPOT case, nor in any other cases involving the six sensors fully tested to-date.

6.2.2.2 Sensitivity to adjustment magnitude

The SPOT a priori uncertainty associated with the above ge positioning and triangulation scenarios was appropriately large. However, when artificially set to very large uncertainty (corresponding position component a priori accuracy of 3000 meters, one sigma), normalized differences are approximately 15 % for some aspects of the triangulation solution comparison due to the larger support data adjustment. This effect corresponds to an operational scenario where the RSM a priori image support data is being generated by an up-stream process using the original sensor model's a priori image support data that reflects very large uncertainty. The resultant RSM a priori image support data and the original sensor model's a priori image support data are then adjusted later by a down-stream user via their corresponding triangulation solutions. (The original triangulation is performed hypothetically for comparison purposes only.) Consequently, the operating point that was used by the up-stream RSM generation process is modified significantly by the subsequent adjustment of both the original and RSM image support data. However, the RSM a priori error covariance is not regenerated using the new operating point.

Specifically, the operating point affects the partial derivatives (\mathbf{B}_S and \mathbf{B}_R) used in the generation of the RSM error covariance \mathbf{C}_R from the original a priori error covariance \mathbf{C}_S (see section 5.2, and Equations 57-59). \mathbf{C}_R is generated from \mathbf{C}_S at an initial operating point corresponding to the a priori support data, and then both are utilized later as the a priori error covariance in the first and subsequent iterations of their respective triangulation solution processes (see section 4.1.2). Following the first iteration, both the original and RSM support data are adjusted and their corresponding partial derivatives (\mathbf{B}_S and \mathbf{B}_R) change. However, \mathbf{C}_R is not regenerated from \mathbf{C}_S at this new operating point; hence, the two a priori covariances become somewhat "misaligned" for the start of the second (and subsequent) iterations. The degree of misalignment is dictated by the amount of support data adjustment.

Experimental results to-date indicate that when partial derivatives start to change by approximately 1 % due to changes in the operating point, RSM triangulation solutions

can start to disagree with their original triangulation solution counterparts by a non-negligible and possibly unacceptable amount. For a space-borne sensor, a 1% change occurs when adjustments to its support data are equivalent to a ground space adjustment on the order of one thousand meters. For an air-borne sensor, on the order of one hundred meters. Of course these ground space adjustment values are approximate, and are dependent on the specific imaging geometry. Also, the sensitivity of the RSM triangulation solution to changes in the partial derivatives diminishes with improved imaging geometry, ground point distribution, and control point accuracy, i.e., as the solution scenario becomes more stable. Thus, the 1% number is conservative.

6.2.2.3 SPOT-IKONOS Results

Another experiment was performed based on a different set of 4 SPOT images with reasonable image geometry. A typical elevation angle was 65 degrees, and a typical convergence angle between image pairs was 40 degrees. In addition, for this case, the support data was modified to simulate Ikonos level support data uncertainty. That is, the SPOT original sensor model was utilized, but the support data, including a priori accuracy (one sigma), were modified to be consistent with Ikonos. This was necessary since the original sensor model for Ikonos was unavailable. Support data a priori accuracy was appreciably better than for SPOT: 3 meters for all position components, 0.00001 radians for all attitude components, and 0.00005 meters for focal length. The position and attitude accuracies were based on those detailed in (Zhou and Li, 2000). However, focal length (interior orientation) accuracy was not provided, so it was set to one-tenth the value used for SPOT. The form of the RSM adjustable ground-to-image function remained the same as for the SPOT experiment.

In order to simulate Ikonos support data uncertainty, a relative orientation involving all four images was first performed using the original sensor model, and then the resultant, adjusted image support data was perturbed using random numbers consistent with Ikonos a priori accuracy and uncorrelated support data errors. Synthetic control points were also generated consistent with the relative orientation and perturbed with random numbers consistent with absolute accuracies of CE=4 meters and LE=3 meters. These errors were generated independently between points. Finally, a 1 meter ground sample distance (and corresponding 60k×60k image size) was emulated by artificially setting the a priori mensuration uncertainty for the measured image coordinates associated with all ground points from a 1 pixel error down to 0.1 pixel error (one sigma). Although, this reduction represents a mis-modeling, it has no appreciable effect on the study as we are comparing two different solutions, both with the same exact mis-modeling.

Table 6 presents the results for this “SPOT-IKONOS” sensor. Note that in this case, results are presented un-normalized, i.e., average absolute differences between the two solutions, and expressed in meters, rounded to the nearest one-tenth. This was done for ease of interpretation and because some of the original solutions yielded very small CE and LE error propagation results. Table 7 presents the original solution error propagation results, averaged over all ground points in the original solution or over all ground point pairs in the original solution, as appropriate. Notice the improved geopositioning

accuracy when more images are involved in the solution, and the improved accuracy when triangulated (adjusted) images are involved in the solution.

Case	Sprt Data	# pts	statistics	hor diff	ver diff	CE diff	LE diff
Geopos							
mono		8	abs	0	0	0	0
			rel	0	0	0	0
stereo		8	abs	0.1	0.1	0	0
			rel	0	0	0	0
multi img		8	abs	0	0.1	0	0
			rel	0	0	0	0
mono	adj	8	abs	0	0	0	0
			rel	0	0	0	0
stereo	adj	8	abs	0	0	0	0
			rel	0	0	0	0
multi img	adj	8	abs	0	0	0	0
			rel	0	0	0	0
Triang							
baseline		23 tp 24 c	abs	0.1	0.1	0	0
			rel	0.1	0.1	0	0

Table 6. SPOT-IKONOS RSM - original sensor model average differences (meters).

Case	Sprt Data	# pts	abs CE	abs LE	rel CE	rel LE
Geopos						
mono		8	21.7	38.7	15.2	54.7
stereo		8	14.1	25.2	2.4	5.0
multi img		8	9.8	17.5	1.7	3.3
mono	adj	8	10.7	38.1	15.0	53.9
stereo	adj	8	2.0	3.7	2.3	4.8
multi img	adj	8	1.6	2.6	1.7	3.2
Triang						
baseline		23 tp 24 c	1.9	3.3	2.4	4.5

Table 7. SPOT-IKONOS original sensor model average error propagation results (meters).

As can be seen by Table 6, “SPOT-IKONOS” comparison results are even better than the comparison results for SPOT. In general, the less uncertain the original sensor model image support data, the smaller the differences between the original and RSM solutions, particularly when multiple images are utilized and multiple ground points are solved for simultaneously. In other words, the more challenging cases occur when the original solution support data is inaccurate, and there are multiple images and multiple ground points in the solution.

Also, as mentioned previously, both the SPOT and SPOT-IKONOS cases involved seven adjustable parameters per image for the original sensor model, and six adjustable parameters per image for the RSM. Similar experiments were performed using 13 adjustable parameters per image for the original sensor model (velocity and attitude rates were added), and 12 image space adjustable parameters per image for the RSM (identical to those specified in Equation 10). Comparison results were similar to those of the initial experiments.

In summary, geopositioning solutions based on RSM are virtually identical to solutions based on the original sensor model. Triangulation solutions are also virtually identical when support data adjustments are of reasonable magnitude.

7.0 Bibliography

Baltsavias, E.P., and D. Stallman, 1992, Metric information from SPOT images and the role of polynomial mapping functions, *International Archives of Photogrammetry and Remote Sensing*, 29(B4):358-364.

Bar-Shalom, Y., and T. E. Fortmann, 1988, *Tracking and Data Association*, Academic Press.

Di, K., and R. Ma, R. Li, 2001, Defining 3-D shorelines from high resolution IKONOS satellite imagery with rational functions, *Proceedings of 2001 ASPRS Annual Convention (CD ROM)*, 23-27 April, St. Louis, Missouri, unpaginated.

Di K., and R. Ma, R. Li, January 2003, Rational Functions and Potential for Rigorous Sensor Model Recovery, *Photogrammetric Engineering and Remote Sensing*, Vol. 69.

Dial, G., 2000, Ikonos satellite mapping accuracy, *Proceedings of 2000 ASPRS Annual Convention*, 22-26 May, Washington, D.C., unpaginated (CD-ROM).

Dowman, I., and J.T. Dolloff, 2000, An Evaluation of Rational Functions for Photogrammetric Restitution, *International Archives of Photogrammetry and Remote Sensing*, Vol. XXXIII, Part B3, Amsterdam 2000.

Fraser, C.S., and H.B. Hanley, January 2003, Bias Compensation in Rational Functions for Ikonos Satellite Imagery, *Photogrammetric Engineering and Remote Sensing*, Vol. 69.

Fraser, C.S., and H.B. Hanley, T.Yamakawa, 2001, Sub-meter geopositioning with IKONOS Geo Imagery, *Proceedings of Joint ISPRS Workshop "High Resolution Mapping from Space 2001,"* 19-21 September, Hannover, Germany, pp. 61-68 (CD ROM).

Gelb, 1974, *Applied Optimal Estimation*, M.I.T. Press.

Greve, C.W., and C.W. Molander, D.K. Gordon, 1992, Image processing on open systems, *Photogrammetric Engineering and Remote Sensing*, 58(1):85-89.

Grodecki, J., 2001, Ikonos stereo feature extraction-RPC approach, *Proceedings of 2001 ASPRS Annual Convention (CD ROM)*, 23-27, April, St. Louis, Missouri, unpaginated.

Grodecki, J., and G. Dial, January 2003, Block Adjustment of High-Resolution Satellite Images Described by Rational Polynomials, *Photogrammetric Engineering and Remote Sensing*, Vol. 69.

Gugan, D. and I. Dowman, 1988, Topographic Mapping from SPOT imagery, *Photogrammetric Engineering and Remote Sensing*, 54(10):1409-1414.

Horn, R.A., and C.R. Johnson, 1994, *Matrix Analysis*, Cambridge University Press, page 399.

Konecny, G., and P. Lohmann, H. Engel, E. Kruck, 1987, Evaluation of SPOT Imagery on analytic photogrammetric instruments, *Photogrammetric Engineering and Remote Sensing*, 53(9):1223-1230.

Kratky, V., 1989, On line aspects of stereophotogrammetric processing of SPOT images, *Photogrammetric Engineering and Remote Sensing*, 55(3):311-316.

Madani, M., 1999, Real-Time Sensor-Independent Positioning by Rational Functions, *proceedings of ISPRS Workshop 'Direct versus indirect methods of sensor orientation'*, Barcelona, November 25-25, 1999, pages 64-75.

McGlone, C., 1996, Sensor modeling in image registration, *Digital Photogrammetry: An Addendum* (C.W. Greve, editor), American Society for Photogrammetry and Remote Sensing, Bethesda, Maryland, pp. 115-123.

Mikhail, E. M., 1976, *Observations and Least Squares*, New York, NY: University Press

Mikhail, E.M., and J.S. Bethel, J.C. McGlone, 2001, *Introduction to Modern Photogrammetry*, John Wiley & Sons.

Newman, D.J., 1978, Approximation with Rational Functions, Regional Conference Series in Mathematics No. 41, American Mathematical Society, Providence, Rhode Island, 52 p.

NIMA National Imagery Transmission Format Version 2.1 [MIL-STD-2500B], August 1997.

NIMA The Compendium of controlled Extensions (CE) for the National Imagery Transmission Format (NITF), Version 2.0 [STDI-0002], March 1999.

OGC, 1999, The Open GIS™ Abstract Specification, Volume 7: The Earth Imagery Case (99-107.doc), <http://www.opengis.org/techno/specs.htm>.

Paderes, Jr, F.C., and E.M. Mikhail, J.A. Fagerman, 1989, Batch and on-line evaluation of stereo SPOT imagery, Proceedings of the ASPRS-ACSM Convention, 02-07 April, Baltimore, Maryland, pp. 31-40.

Papoulis, A., 1991, Probability, Random Variables, and Stochastic Processes, McGraw-Hill.

Press, W.H., and S.A. Teukolsky, W.T. Vetterling, B.P. Flannery, 2002, Numerical Recipes in C, Second Edition, Cambridge University Press

Rao, C.R., and S.K. Mitra, 1971, Generalized Inverse of Matrices and its Applications, John Wiley & Sons.

Sorenson, H., 1980, Parameter Estimation, Marcel Dekker.

Tao, C.V., and Y. Hu, December 2001, A Comprehensive Study of the Rational Function Model for Photogrammetric Processing, Photogrammetric Engineering and Remote Sensing, Vol. 67.

Tao, C.V., and Y. Hu, 2001, The rational function model: A tool for processing high-resolution imagery, Earth Observation Magazine (EOM), 10(1):13-16.

Tao., C.V., and Y. Hu, July 2002, 3D Reconstruction Methods Based on the Rational Function Model, Photogrammetric Engineering and Remote Sensing, Vol. 68.

Tao., C.V., and Y. Hu, July 2002, Updating Solutions of the Rational Function Model Using Additional Control Information, Photogrammetric Engineering and Remote Sensing, Vol. 68.

Toutin, T., January 2003, Error Tracking in Ikonos Geometric Processing Using a 3D Parametric Model, Photogrammetric Engineering and Remote Sensing, Vol. 69.

Yang, X., 2000, Accuracy of rational function approximation in photogrammetry, Proceedings of 2000 ASPRS Annual Convention (CD ROM), 22-26, May, Washington D.C., unpaginated.

Zhang, Z.,R., and R. Deriche, O. Faugeras, Q.T. Luong, 1995, A robust technique for matching two uncalibrated images through the recovery of the unknown epipolar geometry, Artificial Intelligence, 78(1-2):87-119.

Zhou, G., and R. Li, September 2000, Accuracy Evaluation of Ground Points from IKONOS High-Resolution Satellite Imagery, Photogrammetric Engineering & Remote Sensing, Vol. 66, No. 9.